AD-A078 682 TRW DEFENSE AND SPACE SYSTEMS GROUP REDONDO BEACH CA F/G 20/3
FINITE ELEMENT APPLICATION TO TRANSIENT SCATTERING PROBLEMS.(U)
OCT 79 A SANKAR , T C TONG F49620-78-C-0049
UNCLASSIFIED TRW-79-002-AFOSR AFOSR-TR-79-1302 NL

1 OF 2
AD
A078682

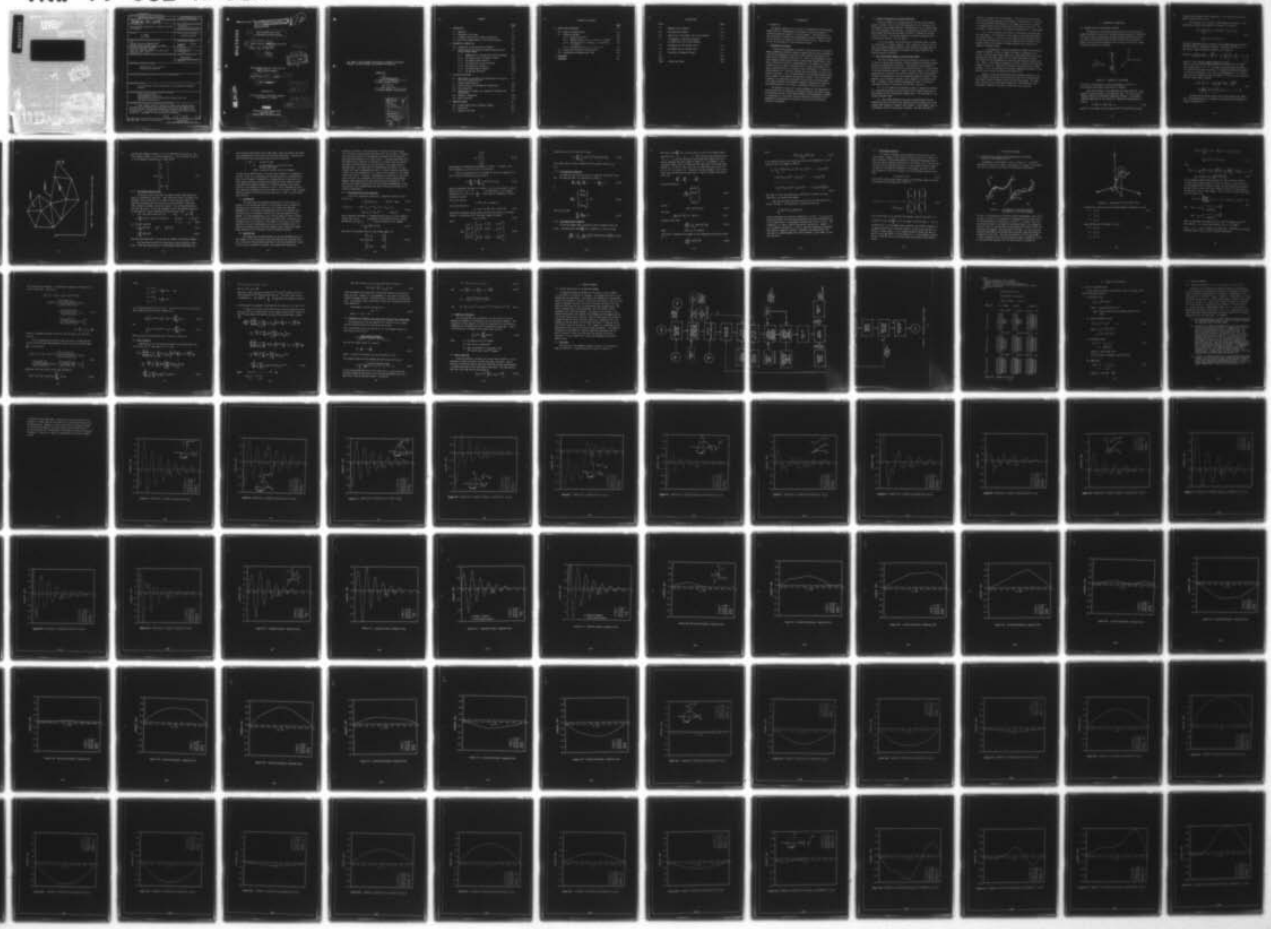

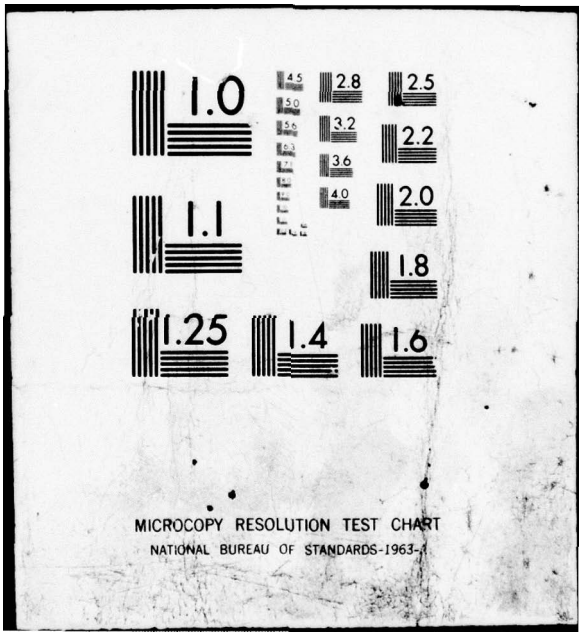
1.0
1.1
1.25
1.4
1.6
1.8
2.0
2.2
2.5
2.8
3.2
3.6
4.0
4.5
5.0
5.6
MICROCOPY RESOLUTION TEST CHART
NATIONAL BUREAU OF STANDARDS-1963-A

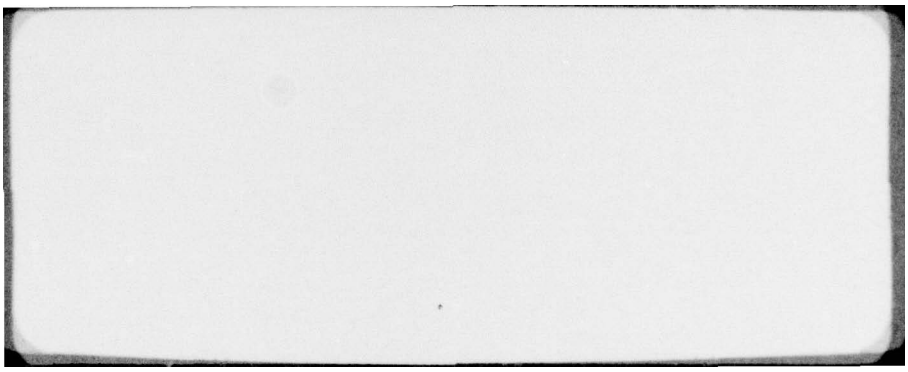

UNCLASSIFIED

SECURITY CLASSIFICATION OF THIS PAGE (When Data Entered)

REPORT DOCUMENTATION PAGE	READ INSTRUCTIONS BEFORE COMPLETING FORM
1. REPORT NUMBER: AFOSR-TR- 79-1302	2. GOVT ACCESSION NO.: ---
	3. RECIPIENT'S CATALOG NUMBER: ---
4. TITLE (and Subtitle): FINITE ELEMENT APPLICATION TO TRANSIENT SCATTERING PROBLEMS	5. TYPE OF REPORT & PERIOD COVERED: Final Report JAN 1978 to October 1979
	6. PERFORMING ORG. REPORT NUMBER
7. AUTHOR(s): A. Sankar, T.C. Tong	8. CONTRACT OR GRANT NUMBER(s): F 49620-78-C-0049
9. PERFORMING ORGANIZATION NAME AND ADDRESS: TRW, DEFENSE AND SPACE SYSTEMS GROUP, One Space Park, Redondo Beach, CA 90278	10. PROGRAM ELEMENT, PROJECT, TASK AREA & WORK UNIT NUMBERS: 61102F 2301/A3
11. CONTROLLING OFFICE NAME AND ADDRESS: Director of Physics, AFOSR, Attn: NP, Bldg 410, BOLLING AIR FORCE BASE, Washington D.C. 20332	12. REPORT DATE: 31 October 1979
	13. NUMBER OF PAGES: 122
14. MONITORING AGENCY NAME & ADDRESS (if different from Controlling Office)	15. SECURITY CLASS. (of this report): UNCLASSIFIED
	15a. DECLASSIFICATION/DOWNGRADING SCHEDULE

16. DISTRIBUTION STATEMENT (of this Report)

Approved for public release; distribution unlimited.

17. DISTRIBUTION STATEMENT (of the abstract entered in Block 20, if different from Report)

---

18. SUPPLEMENTARY NOTES

To be published in IEEE Journal and to be presented at IEEE/APS meeting

19. KEY WORDS (Continue on reverse side if necessary and identify by block number)

Finite Element Method
Electromagnetic Scattering
Current Distribution on Arbitrarily-Oriented Thin Wire
Time Domain Calculations

20. ABSTRACT (Continue on reverse side if necessary and identify by block number)

Finite element method is applied to compute the induced current distributions on arbitrarily-oriented thin wire in the time domain due to arbitrary pulses. The required mathematical equations and computer code are developed. The predictions by this method compare very well with other techniques. Advantages of this approach are mentioned.

79 12 18 31

DD FORM 1 JAN 73 1473 EDITION OF 1 NOV 65 IS OBSOLETE

UNCLASSIFIED

SECURITY CLASSIFICATION OF THIS PAGE (When Data Entered)

12

(6) FINITE ELEMENT APPLICATION TO TRANSIENT SCATTERING PROBLEMS

(9) FINAL TECHNICAL REPORT, AFOSR-TRW-79-002
Jan 78 - Oct 79

(12) 131

By

(10) A. Sankar
T.C. Tong

Work Performed Under Air Force Contract

(15) No. F49620-78-C-0049

(14) TRW-79-002-AFOSR

(11) 31 October 1979

(16) 2301

(17) A3

Prepared for:

Air Force Office of Scientific Research
Washington, D.C. 20332

(18) AFOSR

(19) TR-79-1302

TRW

Defense and Space Systems Group
One Space Park
Redondo Beach, California 90278

THIS REPORT "FINITE ELEMENT APPLICATION TO TRANSIENT SCATTERING PROBLEMS" HAS BEEN REVIEWED AND APPROVED FOR SUBMITTAL.

APPROVED BY:

A. Sankar, Project Manager

D. Jortner, Manager, V&H Laboratory

CONTENTS

CONTENTS (Continued)

ILLUSTRATIONS

1. INTRODUCTION

1.0 OBJECTIVE

The primary objective of this study is to develop the Finite Element Method (FEM) for electromagnetic techniques to solve the problem of transient scattering directly in the time domain. The techniques will then be applied to compute the time-dependent currents induced on curved thin wires due to an arbitrary incident plan wave pulse. Special cases of this are straight thin wires and Gaussian pulse.

1.1 Relevance of the Study

Transient electromagnetic response of structures such as strategic weapon systems and strategic command, communication and control systems to a nuclear electromagnetic pulse are of great concern from the point of view of their vulnerability and survival. Again, the importance of transient response cannot be overstated in radar target identification, electronic warfare and electronic countermeasures. For example, the impulse response can give a useful characterization of each radar target since such a response contains all necessary radar information in a compact and understandable form. Strategic systems should be designed to survive the nuclear transients. Thus, an understanding of the response becomes mandatory to impact on and improve the designs of systems. Since the systems, in general, are complicated structures, they can only be solved numerically; hence efficient and economical numerical techniques are required. The method developed in this study is expected to offer such a tool.

The approach is based on a unique technique for the computation of currents and fields on arbitrary structures excited by arbitrary sources. This technique called "Finite Element Method for Electromagnetics (FEMEM)" is predicated on a variational principle governing the physics of the problem and an approximation procedure to carry out the variational expression integration.

1.2 A General Discussion of Transient Solutions

There are essentially two approaches for solving linear electromagnetic problems. One is an indirect approach in which the physics of the problem is abstracted either by a differential or by an integral equation with frequency as the variable. The equations are solved in the frequency domain and then the time domain solution is obtained by inverse Fourier transform. In the other approach, the governing equations are formulated and solved in the time domain.

In the time domain, the problem can be formulated either in terms of differential or integral equation. From a numerical solution point of view, the integral equation approach offers definite advantages over the differential equation approach with respect to solution stability and imposing boundary conditions.

1.3 The Finite Element Method in the Transient Domain

The finite element method has been successfully applied to a host of static or steady state problems, including eigenvalue problems throughout the many engineering disciplines. The extension of the method to transient problems may be credited to Wilson and Nickell[1] in their study of the heat conduction equation. Most of the early papers in this area are concerned with solutions to the diffusion equation in one form or another. Although the wave equation has been considered generally by Oden[2] there appears to be no specific solutions to this equation for transient problems. In general, three different approaches are used in solving the time domain problem in conjunction with the FEM. They are:

(1) In this method, the transient solution is obtained by developing a recurrence relation with the ordinary finite element equations for the problem and then time-stepping progressively. This technique will be further discussed later.

(2) This method depends on the idea of incorporating the time dimension directly into the finite element analysis as another one of the unknown nodal degrees of freedom of the systems. In this manner, time is discretized, as well as the spatial variables. Here the time span of

interest is divided into finite elements. Thus, the initial value problem is converted to a boundary value problem. Solutions for all intervals of time are obtained simultaneously, with nodes on each wire or surface t = constant defining the configuration of the system at that time. The increase in problem size due to the added time dimension is a disadvantage.

(3) In this approach, the solution is obtained by the mode superposition method. This technique is also known as the normal mode method or as modal analysis. The basis of this method is that the modal matrix of the eigenvalue problem can be used to diagonalize the problem and thus decouple the multiple degrees of freedom problem to give several one-degrees of freedom problem.

One advantage of the mode superposition method over the direct integration methods is that it reduces the number of equations to be solved. Since the lower normal modes play a more significant role in the response than the higher modes, only the lower modes need to be used. This method has the disadvantage of requiring the eigenvalue problem solution. Again, if the number of degrees of freedom is large, the eigenvalue problem is difficult. Superposition method is applicable only to linear problems. Thus, it transpires that the modal superposition method is less general than the other two methods mentioned earlier.

However, it must be mentioned that the advantages inherent in the finite element formulations can be profitably used in all three methods. This report primarily concerns itself with the first method. The subsequent sections discuss the problem formulation, FEM methodology, code development, numerical solutions, discusssions, and conclusion.

2. MATHEMATICAL FORMULATION

2.0 FORMULATION OF THE VARIATIONAL INTEGRAL

The application of the FEM technique requires that we select the proper variational principle for the posed problem, express the functional involved in terms of approximate assumed current distribution functions which satisfy the boundary conditions and minimize this functional to obtain a set of governing equations which is then solved for the unknown current distributions at the nodes.

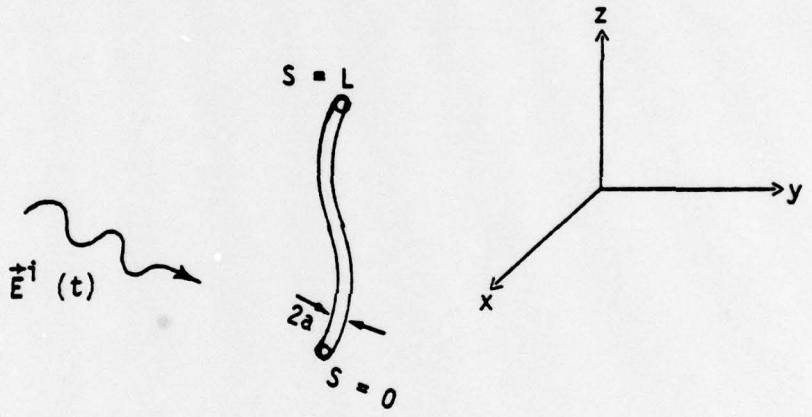

Figure 2-1. Geometry of the Problem

The wire is illuminated by a plane electromagnetic pulse $\vec{E}^i$ (t) with arbitrary polarization and angle of incidence.

Here the relations will be developed for general validity. Then, these will be specialized to the problem at hand. Let $\vec{J}$ $(\vec{r},t)$ be the induced current on the perfectly conducting structure. The boundary condition applicable at the surface of a perfectly conducting body is given by

$$\hat{n} \times \vec{E}^t = \hat{n} \times (\vec{E}^s + \vec{E}^i) = 0 \qquad (2\text{-}1)$$

where $\hat{n}$ is unit normal to the surface and $\vec{E}^t$, $\vec{E}^i$ and $\vec{E}^s$ are the total,

incident and scattered fields, respectively. This implies that the tangential electric field is zero.

The variational form functional $L(\vec{J})$ governing the physics of the problem and containing the quantity of interest $\vec{J}$ is given by

$$L(\vec{J}) = \int_S \int_{S'} \vec{J}(\vec{r},t) \cdot \overline{\overline{K}}(\vec{r},\vec{r}';t) \cdot \vec{J}(r';t)\, dr\, dr' - 2\int_S \vec{J}(\vec{r},t) \cdot \vec{E}^i(\vec{r},t)\, dr \tag{2-2}$$

where $\int_S$ and $\int_{S'}$ denote Cauchy principal value integrations over the structure and dr and dr' differential elements. The Kernel $\overline{\overline{K}}(\vec{r},\vec{r}',t)$ is a complicated integro-differential operator and is given by

$$\overline{\overline{K}}(\vec{r},\vec{r}';t) \equiv \frac{1}{4\pi}\left\{ \frac{\mu_o}{R}\hat{s}\cdot\hat{s}'\frac{\partial}{\partial\tau} + \eta_o \frac{\hat{s}\cdot\vec{R}}{R^2}\vec{\nabla}' + \frac{1}{\varepsilon_o}\frac{\hat{s}\cdot\vec{R}}{R^3}\int_0^\tau dt\, \vec{\nabla}'\cdot\right\}_\tau, \quad \tau = t - \frac{R}{c} \tag{2-3}$$

where $\hat{s}$, $\hat{s}'$ are the unit tangent vectors at $\vec{r}$ and $\vec{r}'$ and μ_o, ε_o and η_o are free space permeability, permittivity and impedance, respectively; $\vec{R} = \vec{r} - \vec{r}'$, the vector distance between the observation point $\vec{r}$ and the source point $\vec{r}'$; $\vec{\nabla}'\cdot$ denotes the divergence operation in the source coordinates; $\tau = t - \frac{R}{c}$ is the retarded time. It is easily seen that the variation of $L(\vec{J})$ with respect to $\vec{J}$ leads to the time domain electric field integral equation

$$\delta L(\vec{J}) = \hat{s}\cdot\vec{E}^i(\vec{r},t) - \frac{1}{4\pi}\int_S \left\{\frac{\mu_o}{R}\hat{s}\cdot\hat{s}'\frac{\partial}{\partial\tau} + \eta_o\frac{\hat{s}\cdot\vec{R}}{R^2}\vec{\nabla}\right. + \frac{1}{\varepsilon_o}\frac{\hat{s}\cdot\vec{R}}{R^3}\int_0^\tau dt\, \vec{\nabla}'\cdot\Big\}_\tau \vec{J}(\vec{r}',t)\, dr' = 0, \quad \tau = t - \frac{R}{c} \tag{2-4}$$

Now that the variational form is set for the problem, the remainder of the FEM technique is a procedure for rendering L(J) stationary by using an expression for J.

2.1 Solution of the Variational Integral Equation by the Finite Element Method

The FEM is primarily a numerical procedure for solving complex problems. The method was originally used in the field of structural mechanics; but since its roots belong in mathematics as a class of approximation procedure, it can be applied to a wider variety of problems in other areas. In the FEM, the region of interest is divided into sub-domains or finite elements, with some functional representation of the solution being adopted over the elements so that the parameters of the representation become unknowns of the problems. Usually the element parameters are the nodal values and their derivatives at the nodes. Although the region of the problem is discretized into elements, the whole domain remains as a continuum because of the imposed restriction on the continuity across element interfaces. The mathematical procedure of solving (2-2) by the FEM is discussed in the following sections.

2.1.1 Segmentation in the Space and Time Coordinates

Examination of Eq (2-2) shows that the source current at $\bar{r}$ delayed by a time $|\bar{r} - \bar{r}'|/c$ is affecting the current at the observation point $\bar{r}$. Because of this retardation effect, Eq (2-2) can be solved as an initial-valued problem by using a time marching procedure. This phenomenon can best be visualized by considering the space-time diagram as shown in Figure 2-2.

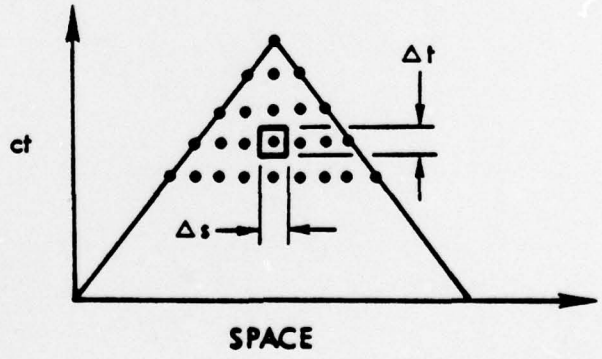

Figure 2-2. The Space-Time Diagram

In the space-time diagram each dot represents a space-time point; the solid lines are the characteristics of the wave equations and they separate the past and the future. To divide the current into the space and time coordinates, we expand the current in space and time as

$$\vec{J}(r',t) = \sum_{i=1}^{N_s} \sum_{j=1}^{\infty} \vec{J}_{ij}(\vec{r}' - \vec{r}_i, t' - t_j)\, U(\vec{r}' - \vec{r}_i)\, U(t' - t_j) \tag{2-5}$$

where
$$U(\vec{r}' - \vec{r}_i) = \begin{cases} 1 & \text{if } |\vec{r}' - \vec{r}_i| \le \frac{\Delta_s}{2} \\ 0 & \text{otherwise} \end{cases} \tag{2-6}$$

$$U(t' - t_j) = \begin{cases} 1 & \text{if } |t' - t_j| \le \frac{\Delta_t}{2} \\ 0 & \text{otherwise} \end{cases}$$

with Δ_s and Δ_t as the spatial and temporal increments and J_{ij} represents the current value within the space segment i and time interval j. Therefore if one postulates that the incident field and all surface current on S are known or equal to zero for all time less than, say t_o, then the retarded time effect allows us to start the solution at time t_o and to view the integral equation as an initial-valued problem in a "marching on" procedure in time.

2.1.2 The Subdivision of the Spatial Region (A Generalized Approach)

The region R is subdivided into discrete sub-regions or elements, each of the same general form, as shown in Figure 2-3, with the boundaries of each element being plane or curvilinear faces, and with the adjacent boundaries of any pair of elements being coincident. Commonly used elements for surfaces are triangular or polygonal form. At similar positions in each element, a number of points are identified as nodes. They are generally at the vertices of the elements, and at positions such as the center of an edge, the centroid of a face or the centroid of the element volume.

Let us denote the nodal values of the solution ϕ at the p^{th} node as ϕ_p. Let the number of elements into which region R is subdivided be N^t,

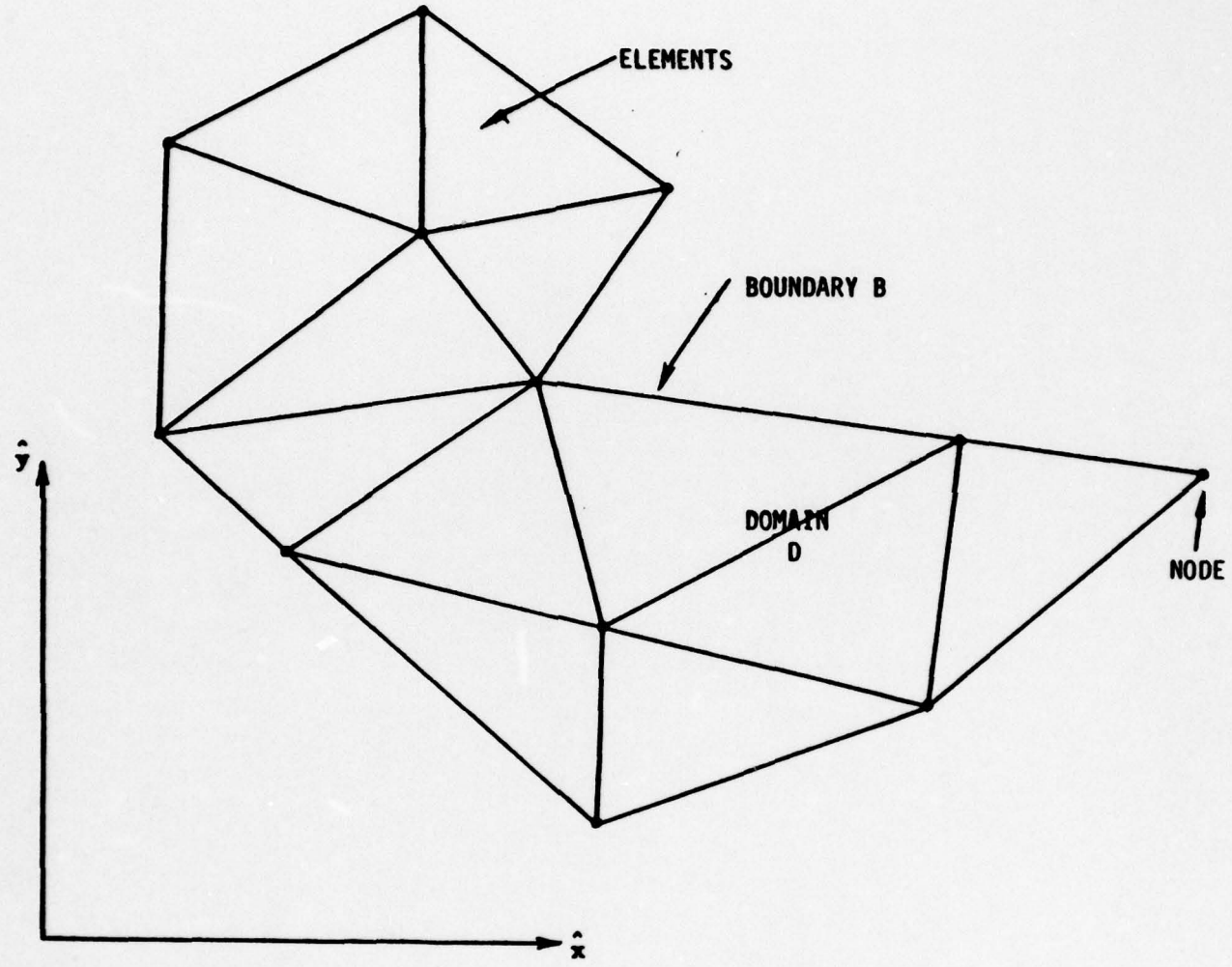

Figure 2-3. Subdivision of the Region into Finite Elements

and the total number of nodes in R = D + B (Boundary) be n_d and n_b. The Total number of nodes in a single element be n_s. Then the nodal values of ϕ can be generally expressed as a column vector

$$\{\phi\} = \begin{bmatrix} \phi_1 \\ \phi_2 \\ \vdots \\ \phi_{n_d} \\ \vdots \\ \phi_{n_d + n_b} \end{bmatrix} . \tag{2-7}$$

2.1.3 The Element Shape Function

To solve Eq (2-2) by the FEM, one needs to define some shape functions or interpolation functions. These functions allow us to express the solution ϕ at any position of R in terms of only the nodal values $\{\phi\}$. Therefore, we assume that the solution ϕ can be described in functional forms, element by element, across the region, i.e., can be defined piecewise over the region. Within each element, it will be supposed that ϕ can be described by a linear combination of functions $N_1^e, N_2^e, \ldots N_k^e, \ldots N_s^e$, and nodal values $\phi_1^e, \phi_2^e, \ldots, \phi_k^e \ldots \phi_s^e$, thus

$$\phi = \sum_e N_1^e \phi_1^e + N_2^e \phi_2^e + N_3^e \phi_3^e + \ldots N_k^e \phi_k^e + \ldots + N_s^e \phi_s^e, \quad s = 1,2, \ldots N_s \tag{2-8}$$

or, in matrix notation

$$\phi = \sum_e (N_1^e \; N_2^e \ldots N_k^e \ldots N_s^e) \{\phi^e\} \tag{2-9}$$

$$= \sum_e (N^e) \{\phi^e\} . \tag{2-10}$$

Note that the superscript e is used here to identify a particular element.

The shape functions (N^e) are restricted to being functions of positions. Since the true solution ϕ is prescribed as being continuous and

with continuous derivatives (up to some order) across the region, the piecewise representation (2-10) should have the same properties. Therefore the shape functions are restricted by the following conditions:

1. $N_j^e = 1$ at the j^{th} node
2. $= 0$ outside element e, with the j^{th} node as one of its nodes
3. $= N(\bar{r})$, a position function within the elements.

In choosing the shape function, one has to pay attention to convergence in the FEM. Since it is recognized that the FEM solution to a problem with a given size of element is necessarily an approximation to the exact solution, there must be an assurance that successive finite element solutions using smaller and smaller elements will converge smoothly to the exact solution as the element size tends to a point. While comprehensive conditions ensuring convergence are not yet known for all types of linear problems, there are certain criteria that must be observed in order to obtain convergent solutions:

(1) Completeness

This means that the piecewise representation (2-10) within the element of the variable/derivative in a key integral must be capable of representing any continuous function as the element size decreases. Mathematically, the piecewise representation calls for a complete set of functions such as a polynomial function with infinite number of terms. However, in a FEM representation, only a finite number of terms is taken. But as pointed out by Melosh [5] and by Zienkiewicz [6], a monotonic convergence can still be obtained if the number of terms used in the representation allow the variable/derivative up to and including order t to take up any constant value within the element, where t being the highest-order derivative of the variable in the variational functional.

(2) Compatibility

This means that the representation of the variable/derivative in a key integral of (2-4) must tend to the same continuity as the exact solution, across the inter-element boundaries, as the size decreases to a point. If for a given variational functional, the highest-order derivative

involved is of order n, the derivatives of order up to and including (n-1) are known as the principal derivatives of that variable. Presuming that the exact solution of the dependent variables are continuous with continuous derivatives up to at least order n. One weak requirement that the compatibility criterion is satisfied is to require that the variable and their principal derivatives are continuous in the shape function representation. This means that the highest-order derivative in a key integral will have a representation that is at worst piecewise continuous, in which case the representation will tend to be continuous as the element reduces to a point. In general, completeness and compatibility are sufficient conditions for convergence in variational finite element methods. However, these conditions are very strong and can be relaxed [7]. In practice, the shape functions will not be an exact representation of the true solution, but an approximate one, and the solution obtained will be similarly approximate.

2.1.4 The Subdivision of the Functional

Since (2-2) represents essentially a quadratic function, we can write it as

$$\Phi = \int_D F(u_1, u_2, u_3 \ldots, u_d)\, dD \quad , \text{ where} \tag{2-11}$$

$$F(u_1, u_2, u_3 \ldots, u_d) = a_{11}\, u_1^2 + a_{12}\, u_1\, u_2 + a_{13}\, u_1\, u_2 + a_{21}\, u_2\, u_1 + a_{22}\, u_2^2 + \ldots + a_{dd}\, u_d^2, \tag{2-12}$$

and D represents the domain of integration which can be a line, surface or volume, and $u_1, u_2, u_3 \ldots, u_d$ represent the solution ϕ and its various derivatives, ϕ_x, ϕ_{xy}, ϕ_y . . . . In matrix notation (2-11) becomes

$$\Phi = \int_D \{u\}^T [A]\, \{u\}\, dD \tag{2-13}$$

where [A] is a dxd matrix and {u} a dxl column vector, or

$$[A] = \begin{bmatrix} a_{11} & a_{12} & \ldots & a_{1d} \\ a_{21} & a_{22} & & a_{2d} \\ \vdots & & & \\ a_{d1} & a_{d2} & \ldots & a_{dd} \end{bmatrix} , \tag{2-14}$$

$$\{u\} = \begin{bmatrix} u_1 \\ u_2 \\ \vdots \\ u_d \end{bmatrix} \tag{2-15}$$

and superscript T denotes the transpose of a matrix. In general, the matrix elements a_{ij} are functions of the position.

If ϕ^e is the contribution of an element to the total integration in (2-13), then this equation can be written as

$$\phi = \sum_{e=1}^{\ell} \phi^e = \sum_{e=1}^{\ell} \int_{D_e} \{u\}^T [A] \{u\} \, dD_e \tag{2-16}$$

where D_e represents the domain of element e, let us now consider a typical term u_r in $\{u\}$ $r = 0, 1, 2, \ldots$. By definition, u_r is a spatial derivative of ϕ, that is $u_r = \dfrac{\partial \phi}{\partial \xi^r} = D_r \phi$, where ξ^r represents a spatial variable of concern.

From (2-10) we have

$$u = (N^e) \{\phi^e\} \text{ in element e.}$$

Thus within element e

$$u_r = D_r \phi = (D_r N^e) \{\phi^e\} = (U_r{}^e) \{\phi^e\} \tag{2-17}$$

where $(U_r{}^e)$ represents the row vector for the r-derivative of the shape function. So applying (2-17) for every element, we obtain

$$\{u\} = (U) \{\phi^e\} \tag{2-18}$$

where

$$[U] = \begin{Bmatrix} U_1{}^e \\ U_2{}^e \\ \vdots \\ U_d{}^e \end{Bmatrix} = \begin{bmatrix} D_1 N_1{}^e & D_1 N_2{}^e & \ldots & D_1 N_s{}^e \\ D_2 N_1{}^e & D_2 N_2{}^e & \ldots & D_2 N_s{}^e \\ \vdots & \vdots & & \vdots \\ D_d N_1{}^e & D_d N_2{}^e & \ldots & D_d N_s{}^e \end{bmatrix}. \tag{2-19}$$

Substitution of (2-18) into (2-13) yields

$$\Phi = \sum_{e=1}^{\ell} \int_{D_e} \{\phi^e\}^T [U]^T [A] [U] \{\phi^e\} \, dD_e \qquad (2\text{-}20)$$

which shows that Φ is now a function of the n_d nodal values $\phi_1, \phi_2, \ldots \phi_{n_d}$.

2.1.5 The Stationary Condition

In order to solve (2-20) we have to invoke the variational principle. The condition that Φ is stationary is given by

$$\frac{\partial \Phi}{\partial \phi_1} = \frac{\partial \Phi}{\partial \phi_2} = \frac{\partial \Phi}{\partial \phi_3} = \ldots = \frac{\partial \Phi}{\partial \phi_{n_d}} = 0 \quad , \qquad (2\text{-}21)$$

or

$$\frac{\partial \Phi}{\partial \{\phi\}} = \begin{Bmatrix} \partial\Phi/\partial\phi_1 \\ \partial\Phi/\partial\phi_2 \\ \vdots \\ \partial\Phi/\partial\phi_{n_d} \end{Bmatrix} = \{0\} \quad . \qquad (2\text{-}22)$$

From (2-16) we get

$$\sum_{e=1}^{\ell} \frac{\partial \Phi^e}{\partial \{\phi\}} = 0 \qquad (2\text{-}23)$$

2.1.6 The Element Matrix Equation

To get the element matrix equation we have to combine (2-23) and (2-20). Considering the term $\frac{\partial \Phi^e}{\partial \{\phi\}}$ for an element e in (2-20), we get

$$\frac{\partial \Phi^e}{\partial \{\phi^e\}} = \int_{D_e} \frac{\partial}{\partial \{\phi^e\}} \left[\{\phi^e\}^T [U]^T [A] [U] \{\phi^e\} \right] dD_e . \qquad (2\text{-}24)$$

Note that a term $\frac{\partial \phi^e}{\partial \phi_p}$ will be zero unless p is one of the element nodes identified by 1, 2, . . . k, . . , s. Also note that the node identifiers 1, 2, 3, . . , s are not the same as the system node numbers which are used to represent the total number of nodes in D. For example, if the triangular element e has its three vertices identified in the system node numbers as 7, 9, and 5, then we can let its node identifiers (now s = 3) as 1 ↔ 7, 2 ↔ 9 and 3 ↔ 5. Therefore, the only elements in the column vector that are non-zero are those that, in terms of element node identifiers, are

$$\frac{\partial \phi^e}{\partial \phi_1} \ , \ \frac{\partial \phi^e}{\partial \phi_2} \ , \ . \ . \ . \ \frac{\partial \phi^e}{\partial \phi_s} \ .$$

So (2-22) reduces to

$$\frac{\partial \phi^e}{\partial \{\phi^e\}} = \begin{Bmatrix} \partial\Phi/\partial\phi_1{}^e \\ \partial\Phi/\partial\phi_2{}^e \\ \vdots \\ \partial\Phi/\partial\phi_s{}^e \end{Bmatrix} . \qquad (2\text{-}25)$$

Letting

$$[B] = [U]^T [A] [U] \ , \qquad (2\text{-}26)$$

and using

$$\frac{\partial}{\partial \{Y\}} \{Y\}^T [Q] \{Y\} = 2[Q] \{Y\} \ , \qquad (2\text{-}27)$$

we obtain from (2-24)

$$\frac{\partial \phi^e}{\partial \{\phi^e\}} = \int_{D_e} 2[A^1] \{\phi^e\} \, dD_e \qquad (2\text{-}28)$$

where $[A^1]$ is a s x s matrix .

Since $\{\phi^e\}$ is constant with respect to the integration we can write (2-28) as

$$\frac{\partial \phi^e}{\partial \{\phi^e\}} = [A^{1e}] \{\phi^e\} \qquad (2\text{-}29)$$

where

$$[A^{1e}] = \int_{D_e} 2[A^{1e}]\, dD_e \tag{2-30}$$

If we substitute (2-19) into (2-24) and carry out the mathematics, we will obtain for the ij^{th} element of $[B^e]$ as

$$\begin{aligned} b_{ij} = \int_{D_e} 2 \Big[& D_1 N_i^e \left(a_{11} D_1 N_j^e + a_{12} D_2 N_j^e + \ldots + a_{1d} D_d N_j^e\right) \\ & + D_2 N_i^e \left(a_{21} D_1 N_j^e + a_{22} D_2 N_j^e + \ldots + a_{2d} D_d N_j^e\right) \\ & + \ldots\ldots\ldots\ldots\ldots + \\ & + D_d N_i^e \left(a_{d1} D_1 N_j^e + a_{d2} D_2 N_j^e + \ldots + a_{dd} D_d N_j^e\right) \Big] dD_e \,. \end{aligned} \tag{2-31}$$

Note that in (2-31) the subscripts on the N^e are in terms of the node identifiers, not system node numbers.

Note that the shape functions are explicitly defined functions of spatial variables. The integrand of a particular term, say

$$\int_{D_e} 2(D_2 N_i^e)\, a_{21} (D_1 N_j^e)\, dD_e \,,$$

could be evaluated as an explicit function of x, y and z. If a_{ij} are constant coefficients, the prescribed integration over the defined domain D_e of the element would, in consequence, evaluate the term as a scalar. The integration, if simple, could be carried out analytically. However, if a_{ij} are complex functions of x, y and z, then the integration would generally require a numerical solution. Therefore, the computational time involved in a problem depends very much on whether a_{ij} are simple or complex functions.

2.1.7 The Boundary Condition

It is known in boundary-value problems that the solution is not unique unless it meets all the required boundary conditions. However, in the variational finite element methods, if the specified boundary conditions are natural boundary conditions for the problem, then it can be shown that the class of admissible functions is not required to satisfy these. In order to illustrate the treatment of the boundary condition in the matrix equation (2-29) let us assume a Dirichlet boundary condition such that

$$\phi = g(x,y,z) \text{ on } B. \tag{2-32}$$

Using (2-32), the n_b nodal values $(\phi_p)_B$ for the boundary nodes on B can be calculated yielding n_b equations of the form

$$(0\ ,\ 0\ ,\ 0\ ,\ \ldots\ 0\ ,\ \underset{\substack{\uparrow \\ p^{th}\ \text{Position}}}{1}\ ,\ 0\ ,\ \ldots\ 0) \begin{Bmatrix} \phi_1 \\ \phi_2 \\ \phi_p \\ \vdots \\ \phi_{n_b} \end{Bmatrix} = \begin{Bmatrix} g \\ g \\ g \\ \\ g \end{Bmatrix}, \tag{2-33}$$

which implies that if ϕ_p satisfies the boundary condition and hence it is a constant value, then $\frac{\partial \phi^e}{\partial \phi_p} = 0$ for an element containing node p. Thus to include the B.C. in the element matrix equation, the simplest procedure is to replace the p^{th} row of the matrix $[A^{1e}]$ in (2-29) by the row matrix of (2-33). In other words, if p is a boundary-condition node, put zeros in the p^{th} row of the $[A^{1e}]$ in (2-29) except for a 1 in the diagonal position and put in the p^{th} row of the driving vector the boundary value given by (2-32).

3. THIN WIRE SCATTERING

3.0 APPLICATION OF THE FEM TO THE SCATTERING OF AN ARBITRARY PULSE BY A THIN CONDUCTING WIRE

The geometry of the problem is given in Figure 3-1. A perfectly conducting curved wire of length L and radius a is located in free space with one of its ends at the origin of the Cartesian coordinates.

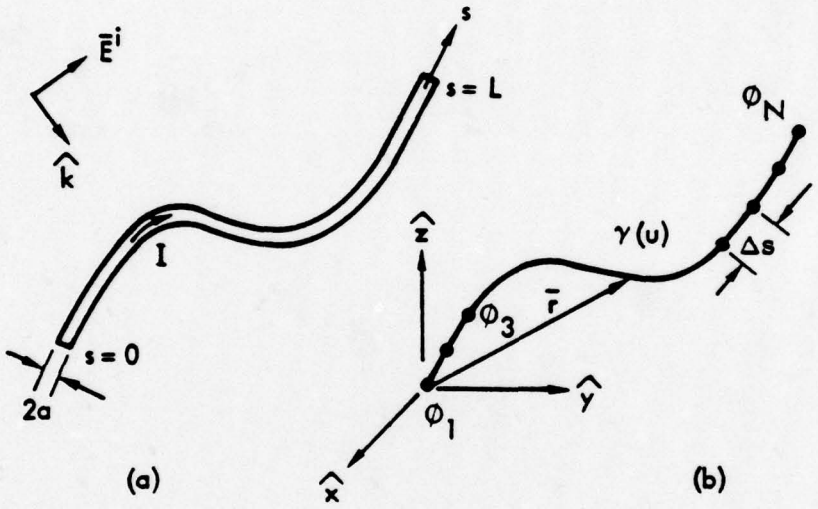

Figure 3-1. (a) Geometry of Thin-Wire Scatterer
(b) Subdivision into Finite Elements

The wire is illuminated by an arbitrary plane electromagnetic pulse, $\vec{E}^i(t)$. As shown in Figure 3-2 the direction of propagation and the polarization of the incident pulse is defined by a triad (Θ, ϕ, η) where Θ and ϕ are the ordinary angles in the spherical coordinates made by the propagation vector $\hat{k}$, and η is the polarization angle between the electric vector and the plane of incidence. Since the wire is thin ($\frac{a}{\lambda} << 1$), we can use the thin-wire approximation and assume that the current flows only along the orientation of the wire. The surface integration in (2.2) now becomes a linear integration along the wire whose arc length is denoted by s, and so the variational equation (2-2) for the thin-wire is reduced to:

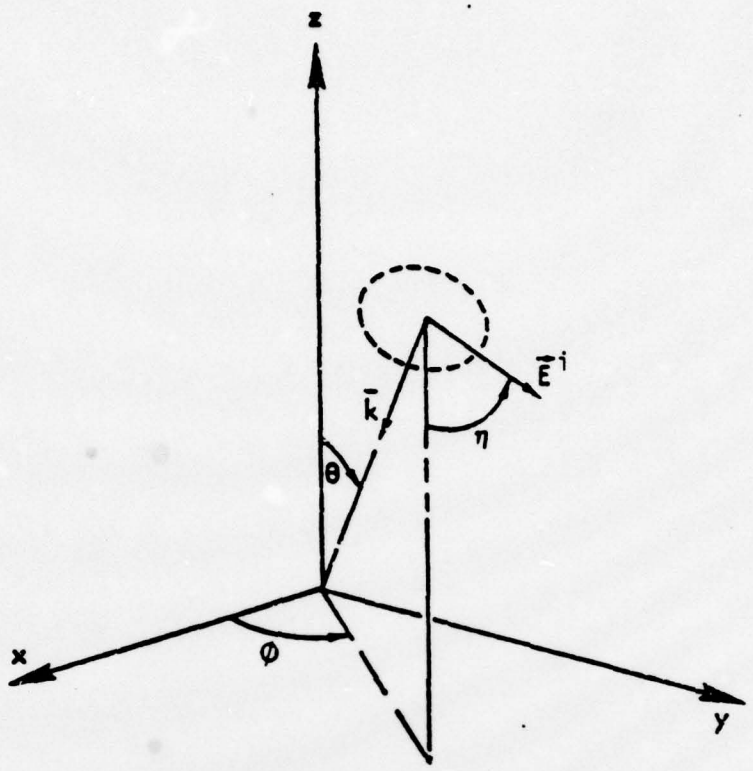

Figure 3-2. Orientation of the Incident Pulse.

To define the curved wire the following parametric equations are used:

$$x = f_x(u) \tag{3-1}$$

$$y = f_y(u)$$

$$z = f_z(u)$$

whose derivatives with respect to u are:

$$\dot{x} = g_x(u) \tag{3-2}$$

$$\dot{y} = g_y(u)$$

$$\dot{z} = g_z(u)$$

$$F(J_s,t) = \int_L \int_{L'} I_s(s,t) \cdot \overline{\overline{K}}(s,s',\tau) \cdot I_s(s',\tau)\, ds'ds$$

$$-2\int_L I_s(s,t) \cdot \vec{E}^{\,i}(s,t)\, ds \qquad (3\text{-}3)$$

where

$$\overline{\overline{K}}(s,s',\tau) = \frac{1}{4\pi}\left\{\frac{\mu_o}{R}\ \hat{s}\cdot\hat{s}'\frac{\partial}{\partial\tau} + \frac{\eta_o \hat{s}\cdot\vec{R}}{R^2}\frac{\partial}{\partial s'} + \frac{1}{\varepsilon_o}\ \frac{\hat{s}\cdot\vec{R}}{R^3}\int_{-\infty}^{\tau} dt\ \frac{\partial}{\partial s'}\right\},\ \tau = t - \frac{R}{c}$$

$$\text{and } R = |\bar{r}(s)-\bar{r}'(s)| = \sqrt{(r - r')^2 + a^2}\ . \qquad (3\text{-}4)$$

$\bar{r}(s)$ is position vector from the origin to a point with arc length s.
To convert the integral equation we first divide the curved wire into N_s uniform segments with N^n number of nodes, and then express the current at any point lying inside a particular segment in terms of a shape function and the nodal values of that segment. Thus from (2-4) we have, after dropping the subscript s

$$I^i(s',t') = \sum_{i=1}^{N_s}\sum_{j=1}^{\infty} I_{ij}\,(s' - s_i,\ t' - t_j)\ U(s' - s_i)\ U(t' - t_j) \qquad (3\text{-}5)$$

with $$U(s' - s_i) = \begin{cases} 1 & \text{if } |s' - s_i| \le \frac{\Delta s}{2} \\ 0 & \text{otherwise} \end{cases}$$

$$U(t' - t_j) = \begin{cases} 1 & \text{if } |t' - t_j| \le \frac{\Delta t}{2} \\ 0 & \text{otherwise} \end{cases},$$

where I_{ij} represents the shape function at the i^{th} segment and the j^{th} time interval. For a given time interval, say $|t' - t_k| \le \frac{\Delta t}{2}$, $I_{ij}(s' - s_i,\ t' - t_j)$ is a function of space only. Therefore we can express the shape function I_{ij} in terms of spatial coordinates.

3.1 Spatial Shape Function

For the curved thin wire problem, we can represent the shape function by a polynomial of s. Thus, for $|t' - t_j| \leq \frac{\Delta t}{2}$

$$I_{ij}(s' - s_i,\ t' - t_j) = N_1 + N_2 s + N_3 s^2 + \ldots + N_k s^{k-1}. \quad (3\text{-}6)$$

The coefficients N_k's are to be determined by the continuity requirement across element boundaries. Since the variational equation (2-2) involves first spatial derivative, it is necessary to use a polynomial of at least second order in order to meet the completeness and compatibility requirements for convergence. Thus we let

$$I_{ij}(s' - s_i,\ t' - t_j) = N_1 + N_2 s + N_3 s^2. \quad (3\text{-}7)$$

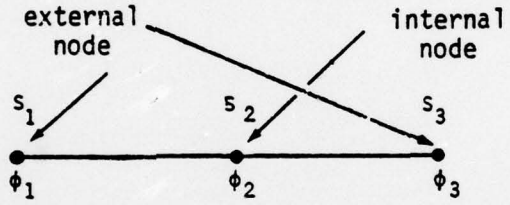

Figure 3-3. An Element with an Internal Node.

In order to determine N_1, N_2 and N_3 uniquely, we have to pick an internal node in an element as shown in Figure 3-3, and require that

$$\begin{aligned} \phi_1 &= N_1 + N_2 s_1 + N_3 s_1^2 \\ \phi_2 &= N_1 + N_2 s_2 + N_3 s_2^2 \\ \phi_3 &= N_1 + N_2 s_3 + N_3 s_3^2 \quad , \end{aligned} \quad (3\text{-}8)$$

or $$\phi_i = N_1 + N_2 s_i + N_3 s_i^2 \quad , \quad i = 1, 2, 3$$

where ϕ_i is the nodal value of current at the i^{th} node.

We can write (3-8) in matrix notation as

$$\begin{pmatrix} N_1 \\ N_2 \\ N_3 \end{pmatrix} = \begin{pmatrix} 1 & s_1 & s_1^2 \\ 1 & s_2 & s_2^2 \\ 1 & s_3 & s_3^2 \end{pmatrix}^{-1} \begin{pmatrix} \phi_1 \\ \phi_2 \\ \phi_3 \end{pmatrix} . \tag{3-9}$$

After some matrix algebra manipulation we get

$$\begin{pmatrix} N_1 \\ N_2 \\ N_3 \end{pmatrix} = \left|\frac{1}{S}\right| \begin{pmatrix} s_2 s_3 (s_3 - s_2) & s_1 s_3 (s_1 - s_3) & s_1 s_2 (s_2 - s_1) \\ (s_2 - s_3)(s_2 + s_3) & (s_3 - s_1)(s_3 + s_1) & (s_2 - s_3)(s_2 + s_3) \\ (s_3 - s_2) & (s_1 - s_3) & (s_1 - s_2) \end{pmatrix} \begin{pmatrix} \phi_1 \\ \phi_2 \\ \phi_3 \end{pmatrix} \tag{3-10}$$

where $|S| = (s_3 - s_2)\,(s_3 - s_1)\,(s_2 - s_1)$. (3-11)

From Eq (3-7) through (3-11) we obtain for an element connecting the i^{th} and the $(i+1)^{th}$ nodes

$$I_{ij}(s'-s_i,\ t'-t_j) = \frac{(s_m - s')(s_{i+1} - s')}{(s_m - s_i)(s_{i+1} - s_i)}\,\phi_i + \frac{(s_i - s')(s_{i+1} - s')}{(s_i - s_m)(s_{i+1} - s_m)}\,\phi_m + \frac{(s_i - s')(s_m - s')}{(s_i - s_{i+1})(s_m - s_{i+1})}\,\phi_{i+1} \tag{3-12}$$

$$s_i \le s' \le s_{i+1} ,$$

where the subscript m denotes the internal node. Although the internal node can be placed at any position within the particular element, it is usually located at the midpoint of that element.

3.2 Time Derivative and Integration Interpolation

Since the kernel of the variational integral equation (2-2) contains also first time derivative, it is necessary to do temporal interpolation

over adjacent time intervals. A second-order Lagrangian interpolation is usually sufficient. Thus we let

$$I_{ij}(s'-s_i,\ t'-t_j) = I_{ij}(s'-s_i)\ U\ (t'-t_j)$$

$$= I_{ij}(s'-s_i)\left[\frac{(t'-t_j)(t'-t_{j+1})}{(t_j-t_{j-1})(t_{j+1}-t_{j-1})}\ \phi_{i,j-1}\right.$$

$$+\frac{(t'-t_{j-1})(t'-t_{j+1})}{(t_{j-1}-t_j)(t_{j+1}-t_j)}\ \phi_{i,j} \qquad (3\text{-}13)$$

$$\left.+\frac{(t'-t_{j-1})(t'-t_j)}{(t_{j-1}-t_{j+1})(t_j-t_{j+1})}\ \phi_{i,j+1}\right]$$

$$t_j - \frac{\Delta t}{2} \le t' \le t_j + \frac{\Delta t}{2}\ ,$$

where ϕ_{ij} represents the nodal current at the i^{th} node at the j^{th} time interval.

To avoid extrapolation into the future, we have to interpolate the current at the j^{th} time step backwards to the j-1 and j-2 time steps when $\frac{R}{c\Delta t} < 0.5$ such that

$$I_{ij}(s'-s_i,\ t'-t_j) = I_{ij}(s'-s_i)\left[\frac{(t'-t_{j-1})(t'-t_j)}{(t_{j-1}-t_{j-2})(t_j-t_{j-2})}\ \phi_{i,j-2}\right.$$

$$\left.+\frac{(t'-t_{j-2})(t'-t_j)}{(t_{j-2}-t_{j-1})(t_j-t_{j-1})}\ \phi_{i,j-1}+\frac{(t'-t_{j-2})(t'-t_{j-1})}{(t_{j-2}-t_j)(t_{j-1}-t_j)}\ \phi_{i,j}\right]. \qquad (3\text{-}14)$$

Equations (3-13) and (3-14) can be simply written as

$$I_{ij}(s'-s_i,t'-t_j) = I_{ij}(s'-s_i)\sum_{n=n_1}^{n_2} T_n\ \phi_{in} \qquad (3\text{-}15)$$

where

$$\left.\begin{aligned} n_1 &= j-1 \\ n_2 &= j+1 \end{aligned}\right\} \quad \text{if } \frac{R}{c\Delta t} \geq 0.5 \quad , \text{ and}$$

$$\left.\begin{aligned} n_1 &= j-2 \\ n_2 &= j \end{aligned}\right\} \quad \text{if } \frac{R}{c\Delta t} < 0.5 \quad .$$

T_n is either given by (3-13) or (3-14). From (3-13) and (3-14) we can also derive temporal derivative and integration as

$$\frac{\partial}{\partial t'}\left[I_{ij}\, U\,(t'-t_j)\right] = I_{ij}(s'-s_i)\sum_{n=n_1}^{n_2} Q_n\, \phi_{in} \quad , \tag{3-16}$$

and

$$\int_{\Delta t} I_{ij}\, U\,(t'-t_j)dt' = I_{ij}(s'-s_i)\sum_{n=n_1}^{n_2} D_n\, \phi_{in} \tag{3-17}$$

where Q_n and D_n can be obtained easily from (3-13) and (3-14).

3.3 Matrix Equation

Substitution of all the pertinent equations as derived above into (2-2) yields the ν^{th} time step (i.e., $t = \nu\Delta t$).

$$F(\bar{J}) = \sum_{i=1}^{N_s}\sum_{j=1}^{N_s}\int_{\Delta s_i}\int_{\Delta s_j}\sum_{\ell_i} N_{\ell_i}\,\phi_{\ell_i n}\left[\frac{\mu_o}{R}\,\hat{s}\cdot\hat{s}'\sum_n Q_n + \eta_o\,\frac{(\hat{s}\cdot\bar{R})}{R^2}\,\frac{\partial}{\partial s'}\right.$$

$$\left. + \frac{1}{\varepsilon_o}\,\frac{\hat{s}\cdot\bar{R}}{R^3}\int_o^\tau \sum_n D_n dt\right]\left[\sum_{\ell_j} N_{\ell_j}\,\phi_{\ell_j n}\right] ds'ds$$

$$- 2\sum_{i=1}^{N_s}\int_{\Delta s_i}\sum_{\ell_i} N_{\ell_i}\,\phi_{\ell_i}\,E_s^{\,i}\,(s_i,t_\nu)\,ds \tag{3-18}$$

for $s_i \le s \le s_{i+1}$, $s_j \le s' \le s_{j+1}$

and $\left| t_\nu - \frac{R}{c} - t_k \right| \le \frac{\Delta t}{2}$.

Note that i and j are used to denote the i^{th} and j^{th} elements while k is used to denote the k^{th} retarded time interval. The actual time interval is denoted by ν. The summation $\sum_{\ell_i}$ and $\sum_n$ denote the summation process

over the spatial and temporal interpolations as given by (3-12) and (3-15).

To cast (3-18) into a matrix equation we invoke the stationary property of (3-18) by differentiating it with respect to each nodal current at the ν^{th} time interval and setting the resulting equations equal to zero. Thus

$$\frac{\partial F(\bar{J})}{\partial \phi_{pn}} = \sum_{i=1}^{N_s}\sum_{j=1}^{N_s} \int_{\Delta_i}\int_{\Delta_j} \sum_{\ell_i} N_{\ell_i}\,\delta_{\ell_i p}\left[\frac{\mu_o}{R}\,\hat{s}\cdot\hat{s}'\sum_n Q_n + \eta_o\,\frac{(\hat{s}\cdot\bar{R})}{R^2}\,\frac{\partial}{\partial s'}\right.$$

$$\left. + \frac{1}{\epsilon_o}\,\frac{\hat{s}\cdot\bar{R}}{R^3}\int_o^\tau \sum_n D_n dt\right]\left[\sum_{\ell_j} N_{\ell_j}\,\phi_{\ell_j n}\right] ds'ds$$

$$- \sum_{i=1}^{N_s}\sum_{j=1}^{N_s} \int_{\Delta_i}\int_{\Delta_j} \sum_{\ell_i} N_{\ell_i}\phi_{\ell_i n}\left[\frac{\mu_o}{R}\,\hat{s}\cdot\hat{s}'\sum_n Q_n + \eta_o\,\frac{(\hat{s}\cdot\bar{R}')}{R^2}\,\frac{\partial}{\partial s'}\right.$$

$$\left. + \frac{1}{\epsilon_o}\,\frac{(\hat{s}\cdot\bar{R}')}{R^3}\int_o^\tau \sum_n D_n dt\right]\sum_{\ell_j} N_{\ell_j}\,\delta_{\ell_j p}\; ds'ds$$

$$- 2\sum_{i=1}^{N_s}\int_{\Delta_i}\sum_{\ell_i} N_{\ell_i}\,E_s^i(s_i,t_\nu)\,\delta_{\ell_i p}\,ds = 0 \quad , \qquad (3\text{-}19)$$

where $p = 1, 2, \ldots\ldots\ldots, N^n$ and

$\delta_{ip} = 0$ if $i \ne p$

$= 1$ $i = p$.

The final form of (3-19) can be symbolically written as

$$[Z]\ (\phi_{iv}) = \left(E_s^i \mid_{t=t_v}\right) + (F) \quad , \tag{3-20}$$

where [Z] denotes the system matrix whose coefficients are functions of space and time. However its time dependence is the same for every time interval (assumed uniform). Therefore, matrix inversion is required only once. (F) denotes a known column vector containing information from previous computation.

The boundary condition imposed here is

$$\phi_{iv} = 0 \tag{3-21}$$

where $i = 1$ and $i = N^n$.

3.4 Computation of Tangents, arc Lengths and Distances for Curved Wires

The evaluations of the dot products $\hat{s}.\hat{s}'$ and $\hat{s}.\bar{R}$, the arc length s and the distance vector $\bar{R}$ are carried out as follows:

For a given smooth curve $\gamma(u)$ defined by (3-1) the tangent vector at a point $p(u_s)$ on the curve is

$$\hat{s} = \frac{g_x(u) + g_y(u) + g_z(u)}{\sqrt{g_x(u)^2 + g_y(u)^2 + g_z(u)^2}} \Bigg|_{u = u_s} \tag{3-22}$$

and the unit normal vector $\hat{n}$ is given by

$$\hat{n} = \frac{d\hat{s}}{du} \ , \ \rho = \left|\frac{d\hat{s}}{du}\right| \tag{3-23}$$

where ρ = radius of curvature and g(u) are given by (3-2).

The distance along the curve between two points $p(u_1)$ and $p(u_2)$ is

$$s = \int_{u_2}^{u_1} \sqrt{g_x^{\ 2}(u) + g_y^{\ 2}(u) + g_z^{\ 2}(u)} \quad du \tag{3-24}$$

To find the distance vector $\bar{R} = \bar{r} - \bar{r}' + a\hat{n}$ we let α_x, α_y and α_z be the direction cosines for the radial vector from the coordinate origin to a point p(u), then the position vector r is given by:

$$\bar{\bar{r}} = |\bar{r}| \ (\alpha_x \hat{x} + \alpha_y \hat{y} + \alpha_z \hat{z}) \tag{3-25}$$

and $$\alpha_x = \frac{f_x(u)}{|\bar{r}|} , \ \alpha_y = \frac{f_y(u)}{|\bar{r}|} , \ \alpha_z = \frac{f_z(u)}{|\bar{r}|} \tag{3-26}$$

$$|\bar{r}| = \sqrt{f_x^2(u) + f_y^2(u) + f_z^2(u)} = r$$

thus $$\bar{R} = (r\alpha_x - r'\alpha_x') \hat{x} + (r\alpha_y - r'\alpha_y') \hat{y} + (r\alpha_z - r'\alpha_z') \hat{z} + a\hat{n} \tag{3-27}$$

3.5 Numerical Integration

By using the FEM, the integration over the entire wire is now reduced to a summation of integration over the individual elements. The integration in each element is carried out numerically by replacing the integration by its Riemann sum with unit-weighting coefficient. That is, if we divide the i^{th} element into N subdivisions, we have

$$\int_{\Delta_i} f(s)ds = \sum_{j=1}^{N} f(s_j) \ \Delta s \tag{3-28}$$

where Δ_i = the domain of the i^{th} element

Δs = the size of a subdivision

s_j = the s coordinates of the center of the j^{th} subdivision of the i^{th} element.

3.6 Matrix Inversion

Since the problem is solved as an initial-value problem, it is not necessary to invert the matrix at each time step of solution. Matrix inversion is done only once at the first time step and the inverted matrix is stored to be used for the following-on time steps. Thus the solution after the first time step can be written as

$$(\phi_{iv}) = [Z]^{-1} \left[(E_s^i \mid_{t=t_v}) + (F) \right] \tag{3-29}$$

4. COMPUTER PROGRAM

4.0 A BRIEF DESCRIPTION OF THE COMPUTER PROGRAM

The computer program developed for this study is called "TWFEM". It is written in the Fortran IV language. The program consists of a main program and ten subroutines. The input to the programs are: the maximum value of the parametric variable for the wire, the radius of the wire, the number of elements into which the wire is divided, the size of the time step, the final time for the run, polarization and incident angles, the kind of incident pulse, pulse parameters, and a few control option parameters for running the program. The output of the program is the current distribution, the indident field strength and the segment excitation on each node at each time step. Most of these outputs are stored in a magnetic tape and can be saved for future use. Because of this, the program can use the results of the final time step in a previous run as the initial values for the new run. This capability is designed to save computational time by eliminating duplicated computation. The numerical integration is performed by a simple trapezoidal quadrature, and the matrix inversion is done only once using the gaussian elimination algorithm. To save computational time, many parameters are stored in common blocks.

4.1 Flow Chart

The structure of the computer program is given in a flow chart as shown in Figure 4-1. A sample print-out is given in Figure 4-2.

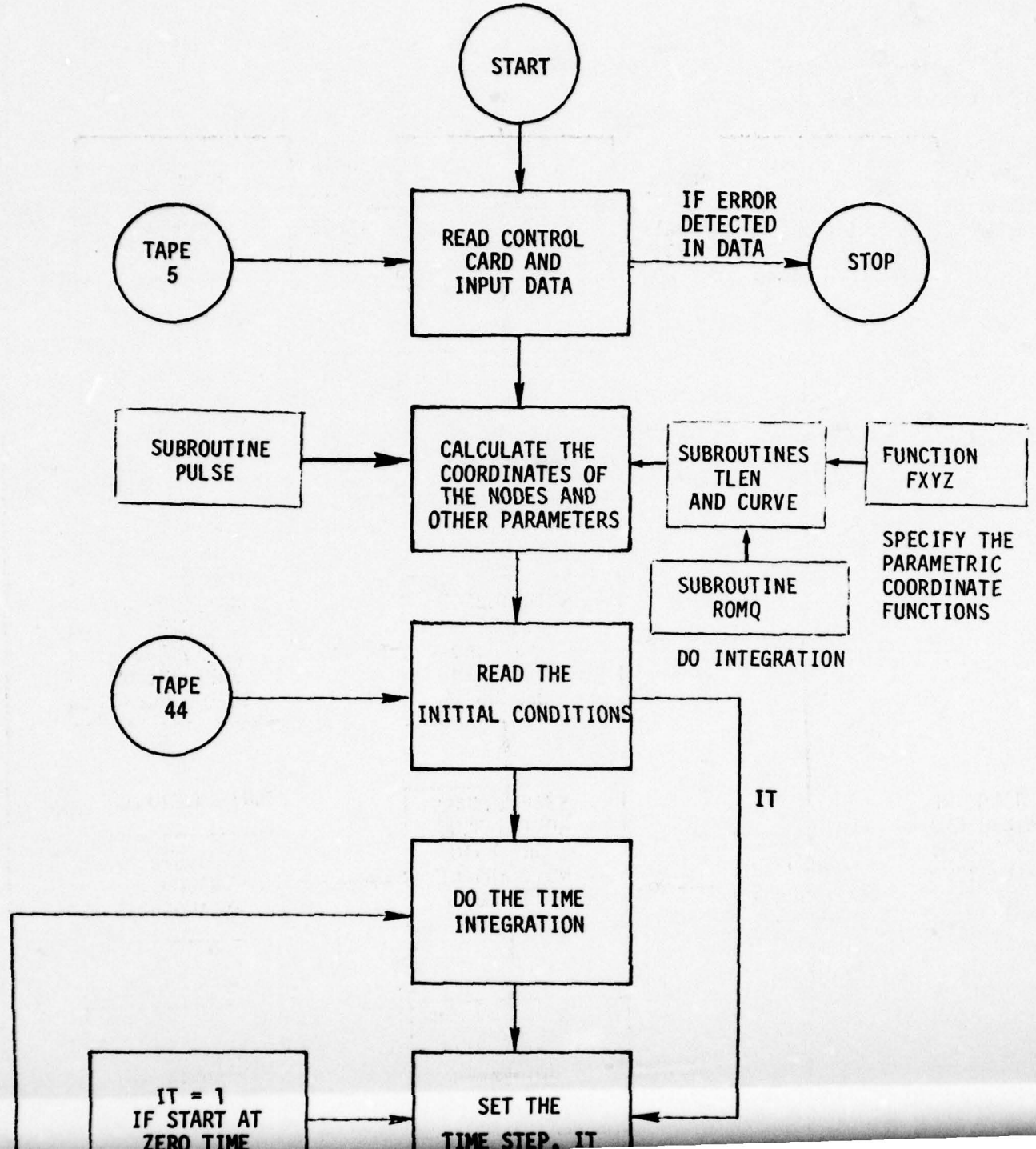
START
TAPE 5
READ CONTROL CARD AND INPUT DATA
IF ERROR DETECTED IN DATA
STOP
SUBROUTINE PULSE
CALCULATE THE COORDINATES OF THE NODES AND OTHER PARAMETERS
SUBROUTINES TLEN AND CURVE
FUNCTION FXYZ
SPECIFY THE PARAMETRIC COORDINATE FUNCTIONS
SUBROUTINE ROMQ
DO INTEGRATION
TAPE 44
READ THE INITIAL CONDITIONS
IT
DO THE TIME INTEGRATION
IT = 1 IF START AT ZERO TIME
SET THE TIME STEP, IT

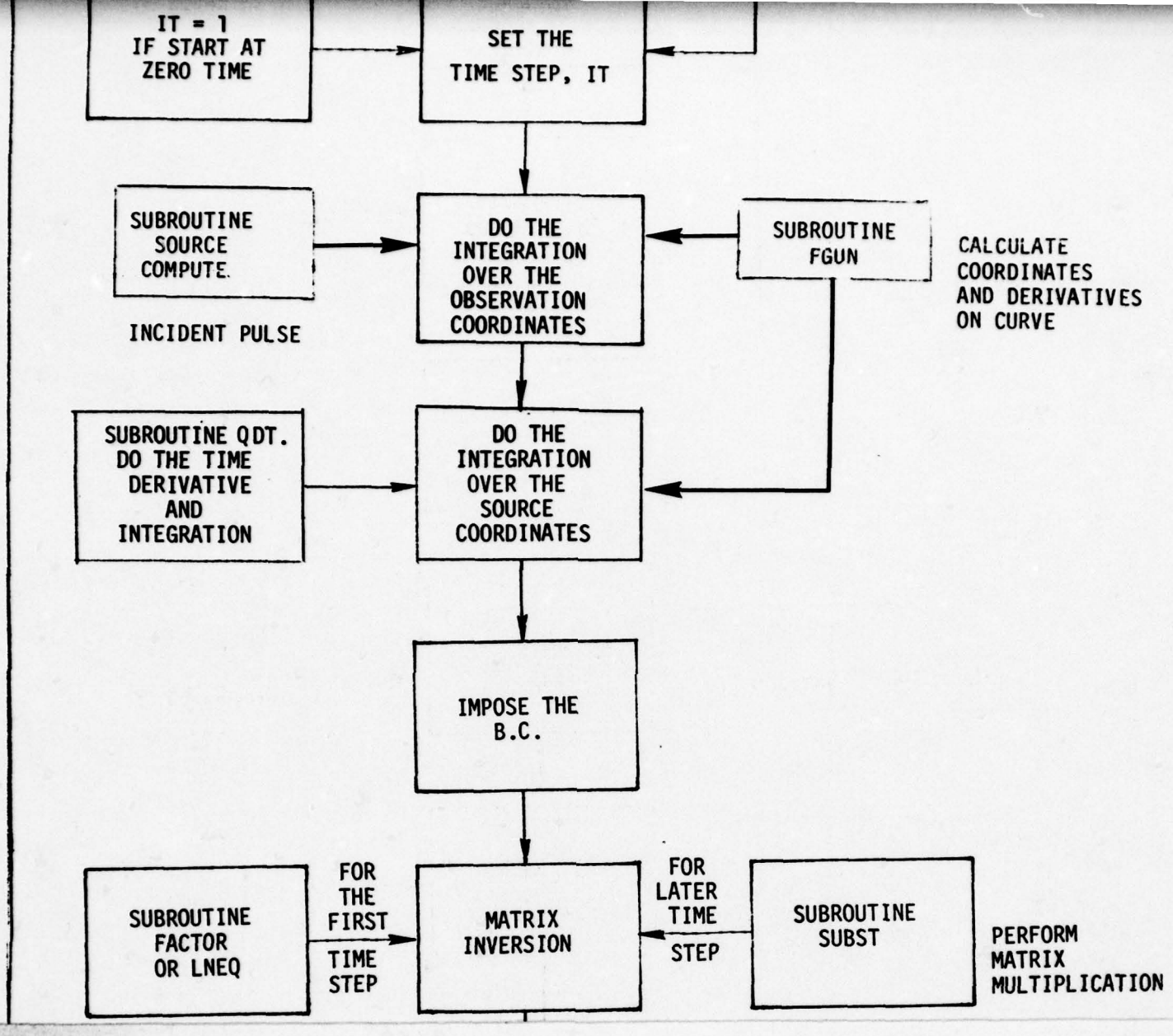
IT = 1
IF START AT
ZERO TIME
SET THE
TIME STEP, IT
SUBROUTINE
SOURCE
COMPUTE
INCIDENT PULSE
DO THE
INTEGRATION
OVER THE
OBSERVATION
COORDINATES
SUBROUTINE
FGUN
CALCULATE
COORDINATES
AND DERIVATIVES
ON CURVE
SUBROUTINE QDT.
DO THE TIME
DERIVATIVE
AND
INTEGRATION
DO THE
INTEGRATION
OVER THE
SOURCE
COORDINATES
IMPOSE THE
B.C.
SUBROUTINE
FACTOR
OR LNEQ
FOR
THE
FIRST
TIME
STEP
MATRIX
INVERSION
FOR
LATER
TIME
STEP
SUBROUTINE
SUBST
PERFORM
MATRIX
MULTIPLICATION

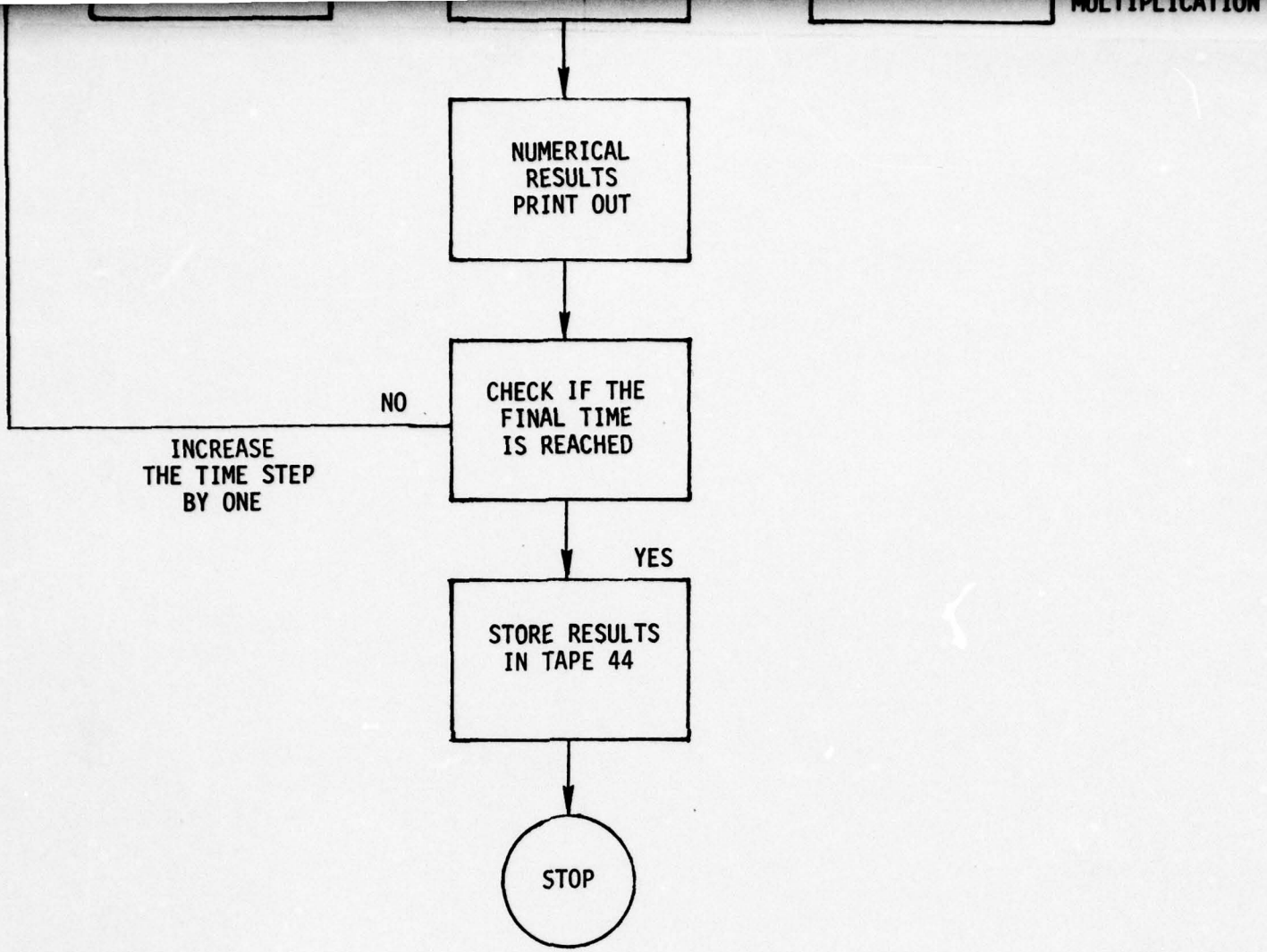

Figure 4-1. Flow Chart of Computer Program

```
$DATA
  TXL=3.1416,RAD=3.36E-3,THETA=0.,
  NZ=5,NZJ=5,DELT=.167,FTIME=25.,
  JCONT=0,INVT=0,PHI=0.,ETA=90.,PZERO=.159,
  PSP1=1.,PSP2=1.E-8,PSP3=.334E-9,PSP4=1.E-9,JCHO=3,
  NDIVP=100,JPART=1,
$END
```

RECTANGULAR PULSE

WIRE LENGTH = 4.995E-01

SHAPE FACTOR = 1.000E+01

NODE NO.	INC. FIELD	SOURCE	CURRENT(A)
	TIME STEP= 1 TIME= 8.350E-11 (SEC)		
1	0.000	0.000	0.000
2	0.000	0.000	-1.760E-08
3	0.000	0.000	-2.477E-07
4	0.000	0.000	-3.468E-06
5	-9.511E-01	-1.195E+01	-4.856E-05
6	-1.000E+00	-1.257E+01	-5.369E-05
7	-9.511E-01	-1.195E+01	-4.856E-05
8	0.000	0.000	-3.468E-06
9	0.000	0.000	-2.477E-07
10	0.000	0.000	-1.760E-08
11	0.000	0.000	0.000
	TIME STEP= 2 TIME= 2.505E-10 (SEC)		
1	0.000	0.000	0.000
2	0.000	-1.971E-02	-7.191E-06
3	-5.878E-01	-7.642E+00	-1.323E-04
4	-8.090E-01	-1.206E+01	-2.075E-04
5	-9.511E-01	-1.317E+01	-2.289E-04
6	-1.000E+00	-1.513E+01	-2.609E-04
7	-9.511E-01	-1.317E+01	-2.289E-04
8	-8.090E-01	-1.206E+01	-2.075E-04
9	-5.878E-01	-7.642E+00	-1.323E-04
10	0.000	-1.971E-02	-7.191E-06
11	0.000	0.000	0.000
	TIME STEP= 3 TIME= 4.175E-10 (SEC)		
1	0.000	0.000	0.000
2	-3.090E-01	-9.214E+00	-1.565E-04
3	-5.878E-01	-1.335E+01	-2.331E-04
4	-8.090E-01	-2.132E+01	-3.673E-04
5	-9.511E-01	-2.326E+01	-4.036E-04
6	-1.000E+00	-2.369E+01	-4.125E-04
7	-9.511E-01	-2.326E+01	-4.036E-04
8	-8.090E-01	-2.125E+01	-3.661E-04
9	-5.878E-01	-1.335E+01	-2.332E-04
10	-3.090E-01	-9.329E+00	-1.583E-04
11	0.000	0.000	0.000

Figure 4-2. Sample of print out.

5. RESULTS AND DISCUSSIONS

5.0 TYPES OF INCIDENT PULSES

In this study we consider four different types of incident pulses. They are defined as follows:

(a) Gaussian pulse

$$E^i(t) = e^{-p^2(t-t_{max})^2} \tag{5-1}$$

where p = spread parameter (sec^{-1})

t_{max} = time at which the pulse reaches maximum value (sec)

(b) Double exponential pulse

$$E^i(t) = e^{-\alpha t} - e^{-\beta t} \qquad t > 0 \tag{5-2}$$

where $\alpha = 4.0 \times 10^6$ (sec^{-1})

$\beta = 4.76 \times 10^8$ (sec^{-1})

(c) Rectangular pulse

$$E^i(t) = 1 \quad 0 \leq t \leq tp \tag{5-3}$$
$$= 0 \quad \text{otherwise}$$

where tp = pulse width (sec)

If tp is large, it becomes a unit step pulse.

(d) Ramp pulse

$$E^i(t) = t \quad 0 \leq t \leq t_r \tag{5-4}$$
$$= 1 \quad t_r \leq t$$

where t_r = rise time. (sec)

5.1 TRANSIENT CURRENTS

5.1.1 Semi-Circular Wire (x = 0, y = 0.159 cosu, z = 0.159 sinu)

Figures 5-1 to 5-6 present the induced currents as a function of time at the middle of a thin semi-circular wire illuminated by different types of pulses at various angles of incidence. The parameter of the pulses are $p = 9 \times 10^8$ sec^{-1}, t_{max} = 1 nsec, tp = 10 nsec and t_r = 10 nsec. The length of the wire is L = 0.5 M and the radius is given by the shape factor $\Omega = 2\ell n \left(\frac{L}{a}\right) = 10$. The wire is uniformly divided into 5 elements with eleven nodes (six external and five internal). The time step is Δt = 0.167 nsec which is approximately equal to $\Delta s/c$. The current is defined positive when it flow from s = o to s = L. Examinations of the plots reveal many interesting points of physics concerning the transient response of thin wire structures. For example:

(a) Even for curved wires, the current displays damped oscillations at a dominant frequency which is close to the lowest frequency of a straight wire of the same length.

(b) In general, the temporal development of the current along the wire is a very complicated thing. It depends on many factors, such as the wire length, the type of incident pulse, the angle of incidence as well as the shape of the wire. The build up of the current can be see as follows. First, the current starts to build up from the end of the wire where the incident field pulse hits initially. As time goes on, the other part of the wire is also illuminated and the current pulse begins to travel with the velocity of propagation towards the other end. When the current pulse reaches the other end the current pulse reverses its direction of propagation as the current cannot flow forward any farther. This phenomenon goes on and on until the current completely decays due to radiation loss. At any instant of time the current is a superposition of response due to direct excitation, reflections along wire and scattering from other parts of wire.

(c) As shown in Figures 5-2 and 5-3, it is observed that any sudden change in the incident pulse would induce some new charges and in turn alter the current distribution on the wire. In the case of the rectangular pulse whose pulse width is 10 nsec, this sudden change occurs at the end of the pulse (ct/L = 6).

(d) The reason that the second current peak is larger than the first peak in the gaussian pulse is attributed to its relatively large spread parameter which produces a very rapid rise and fall-off behavior.

(e) For non-symmetrical excitation as shown in Figures 5-4 to 5-6, the reflections from both ends are not equal and also arrive at an observation point at different times. Therefore, the current development is no longer dominated by the fundamental resonant frequency but contains higher harmonics as well.

5.1.2 Parabolic Wire ($x = o$, $y = 0.5u$, $z = 0.25u^2$)

Figures 5-7 to 5-12 show the transient currents at different positions along a parabolic wire of length $L = 0.574u$ and shape factor $\Omega = 10.01$ under illumination by a rectangular pulse ($tp = 5nsec$) and a double exponential pulse. The starting time is taken to be zero when the pulse first hits the higher end of the wire ($s = L$). As expected the response of the rectangular pulse has more ripples and roughness due to its discontinuities.

5.1.3 Helical Wire ($x = 0.25 \cos u$, $y = 0.25 \sin u$, $z = 0.25u$)

Figures 5-13 to 5-16 present the transient currents at different locations on a helical wire of length $L = 1.111M$ under a gaussian pulse ($p = 9 \times 10^8$ sec, $t_{max} = 1$ nsec). Again it is seen that currents display a more symmetrical oscillation pattern for points at region near the middle of the wire, where reflections from both ends are more equal, than those at positions close to the ends of the wire.

5.1.4 Straight Wires ($x = 0$, $y = 0$, $z = u$)

Figures 5-17 to 5-19 present transient currents on a thin straight wire illuminated by a gaussian pulse at three different angles of incidence. The wire is along the z axis and the incident wave is in the y-z plane ($\phi = 90°$ and $\eta = 0$). It is seen that the current exhibits strong oscillation at the lowest characteristic frequency of the wire. The comparison between the FEM results and those obtained by using the method of moments code[8] are also included in Figures 5-18 and 5-19. Extremely good agreement is obtained between these two different approaches.

5.2 CURRENT DISTRIBUTION ON THE ENTIRE WIRE

Figures 5-20 through 5-85 present the snap shot type current distributions on the straight wire, semi-circular, parabolic and helical wires for various types of incident pulses and angles of incidence as discussed earlier in the previous section. These plots clearly indicate the build-up mechanism for the transient currents on wire structures at each instant of time, say t = T, the current at a point on this wire is a complicated combination of three different excitation mechanisms evaluated in the appropriate retarded time frame. One source of excitation is of course the direct incident field, the second is due to reflections at ends of the wire and the third comes from scattering from other part of the wire. The field near the time of arrival of the incident wavefront is determined by its high-frequency content. However, at later times, long after the wavefront has traversed the scatterer, the induced currents set up oscillations at the natural frequencies of the wire. Since the wire is in free space, leakage of energy to infinity leads to damped oscillations, and the most weakly damped (probably the lowest mode) dominates the late time response. This implies that the long-time response of the wire is determined primarily by its overall size rather than its detailed shape. The opposite is true for the early-time response.

5.3 CONVERGENCE AND COMPUTATIONAL TIME

Figure 5-86 shows the convergence test for the current at the middle of a semi-circular thin wire of length L = 0.5 m and Ω = 10. The number of elements used in the test are 4, 5 and 6 which correspond to 9, 11 and 13 nodes. It is seen that the numerical results show a better convergence in early time than in late time. This is understandable because at late time the incident pulse has more or less died down and the driving source is merely due to the smaller residual current and charge flowing along the wire which are more sensitive to element size. Also in an iterated numerical solution, errors propagate and accumulate as time goes on. The step sizes used in this convergence test are chosen such that $\frac{c\Delta t}{\Delta s} = 1$, where Δt is the time step and Δs is the element size. The computational time for each run depends on the number of elements and

the number of time steps used. A typical run in this study uses five elements (11 nodes) and 150 time steps and it takes about 100 sec on the CDC 6600 machine. However, it must be noted that the computer program has not been optimized to take into account various factors such as structure symmetry for the broadside illumination and possible analytical integration. Once this is done, the computational time can be reduced further.

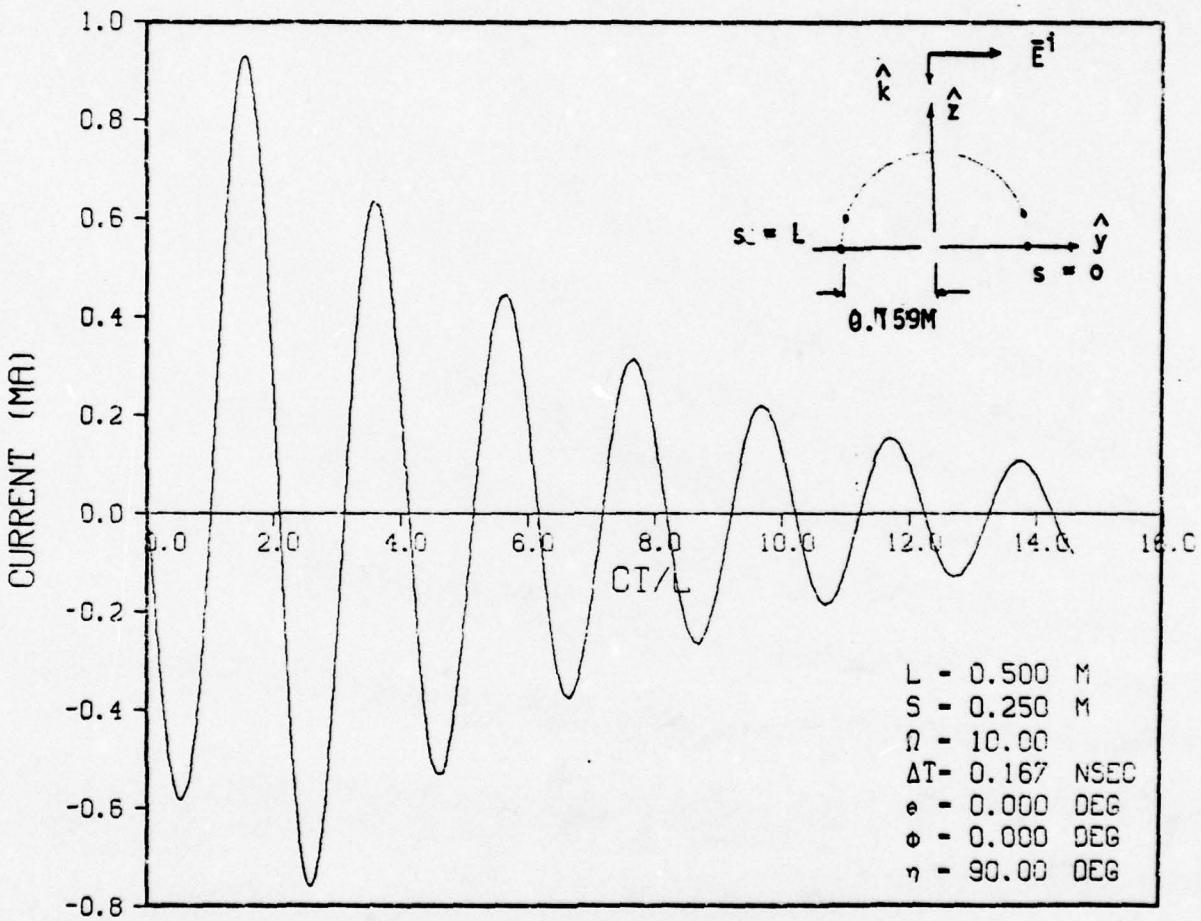

Figure 5-1. TRANSIENT CURRENT-GAUSSIAN PULSE

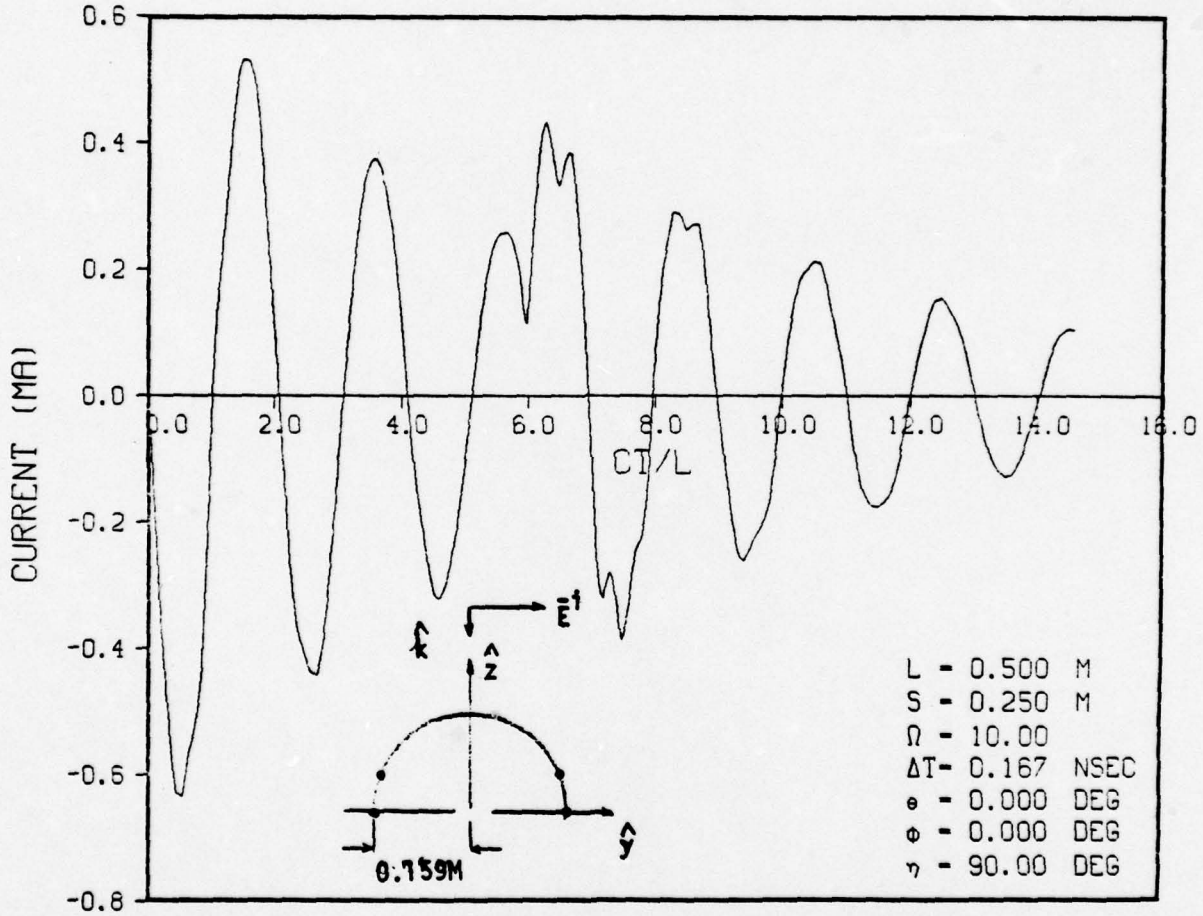

Figure 5-2. TRANSIENT CURRENT-RECTANGULAR PULSE

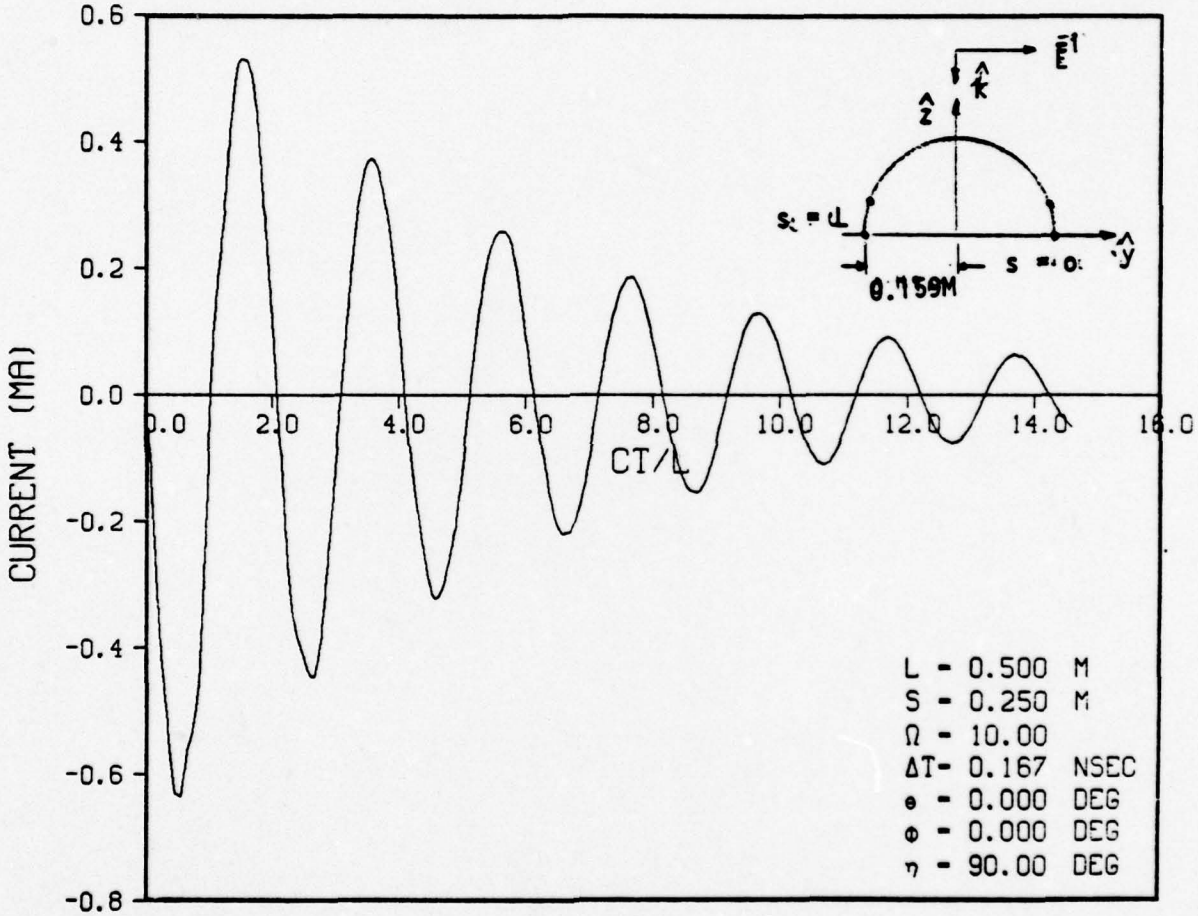

Figure 5-3. TRANSIENT CURRENT-UNIT STEP PULSE

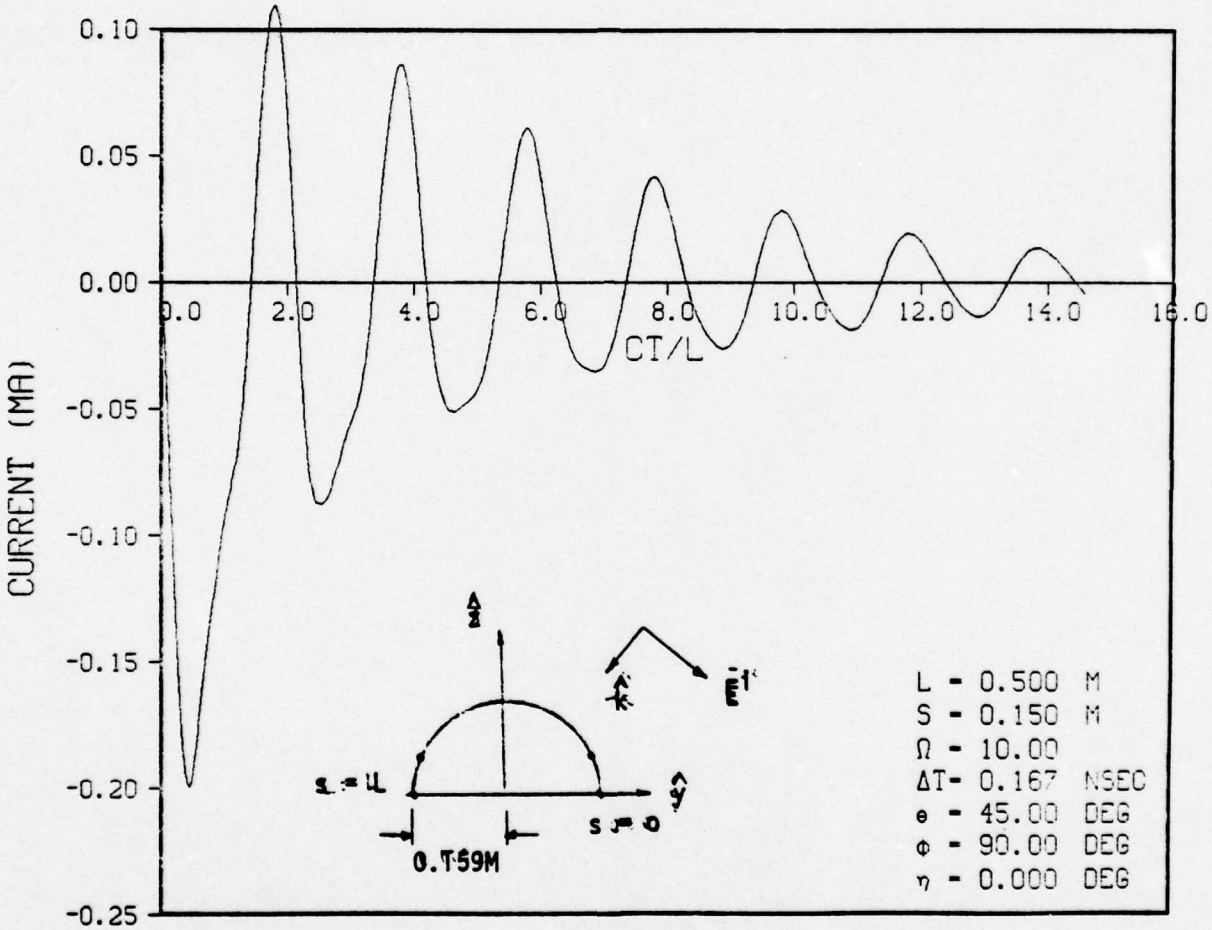

Figure 5-4. TRANSIENT CURRENT-DOUBLE EXPONENTIAL PULSE

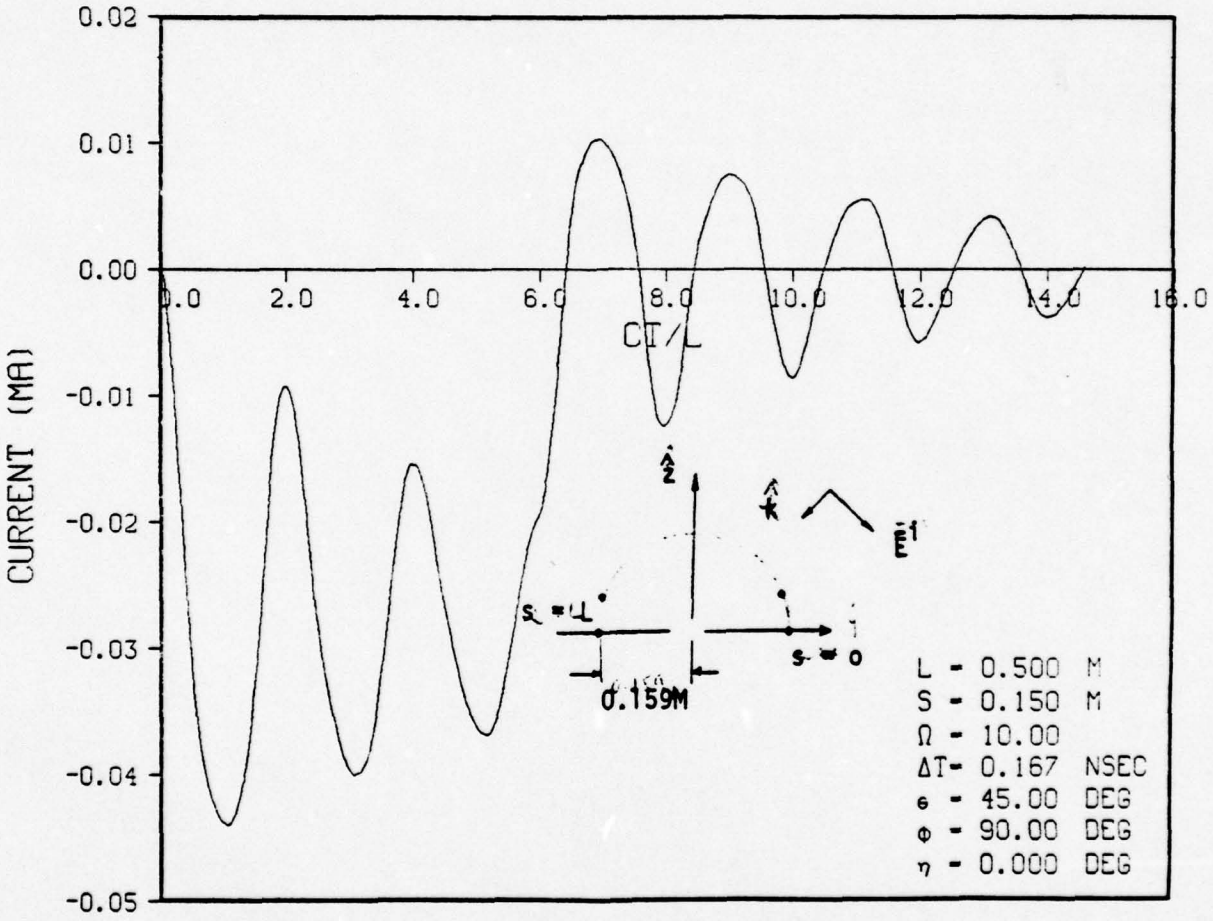

Figure 5-5. TRANSIENT CURRENT-RAMP PULSE

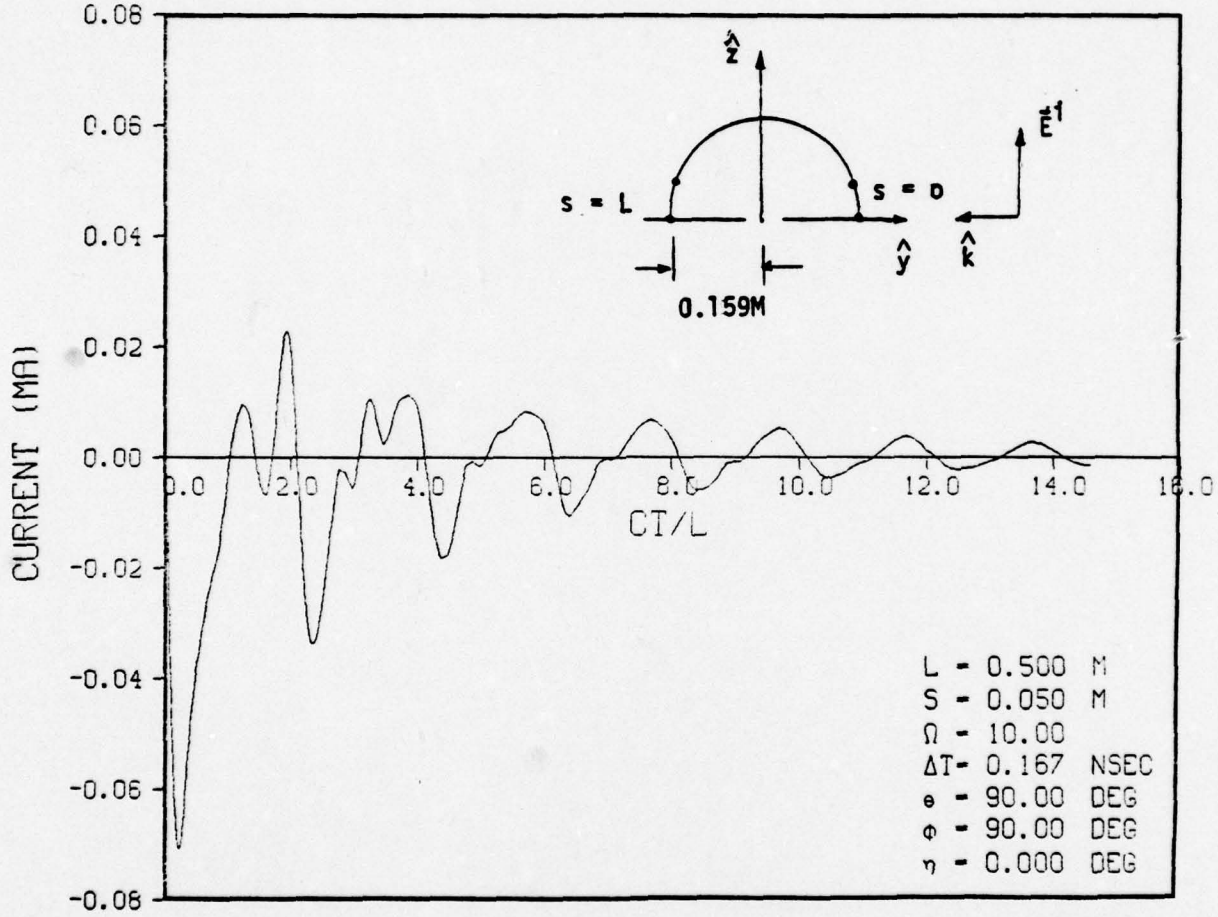

Figure 5-6. TRANSIENT CURRENT-DOUBLE EXPONENTIAL PULSE

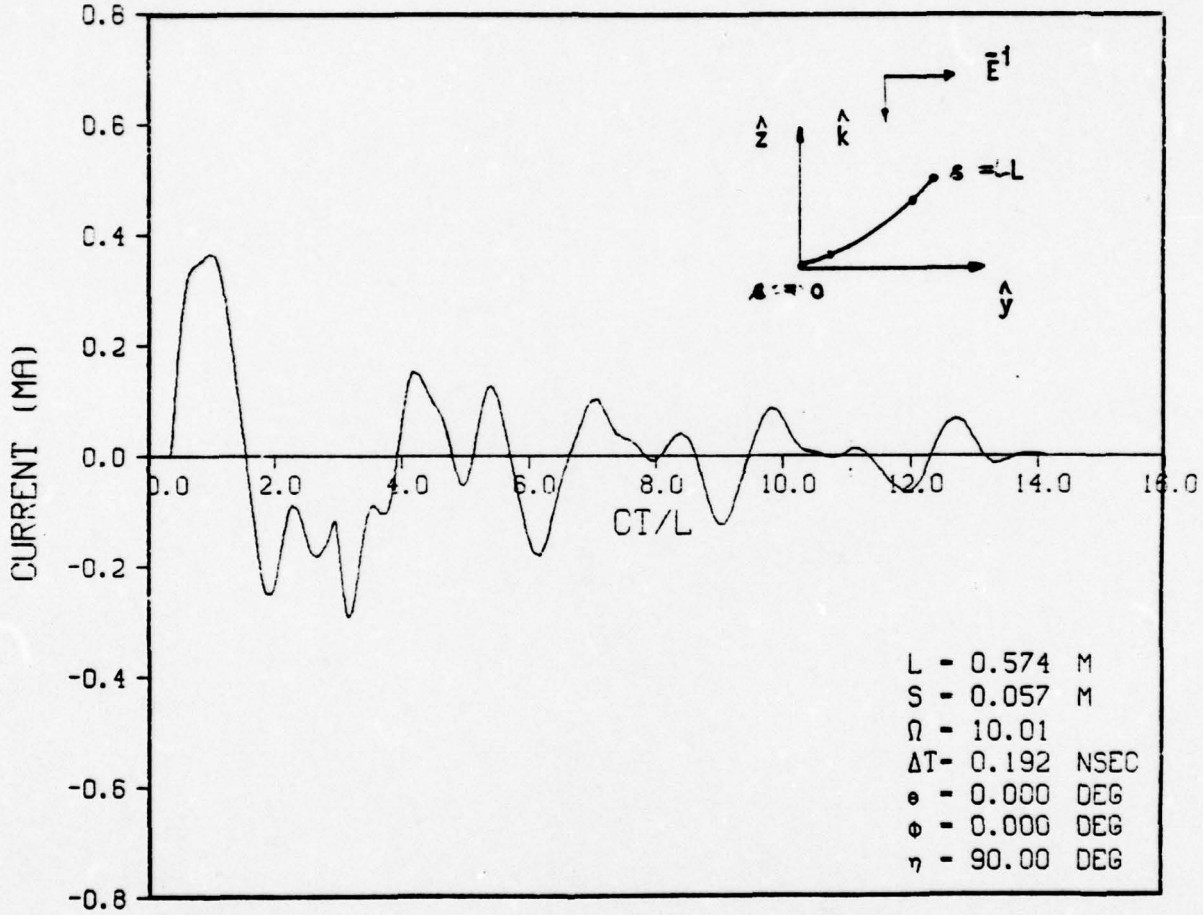

Figure 5-7. TRANSIENT CURRENT-RECTANGULAR PULSE

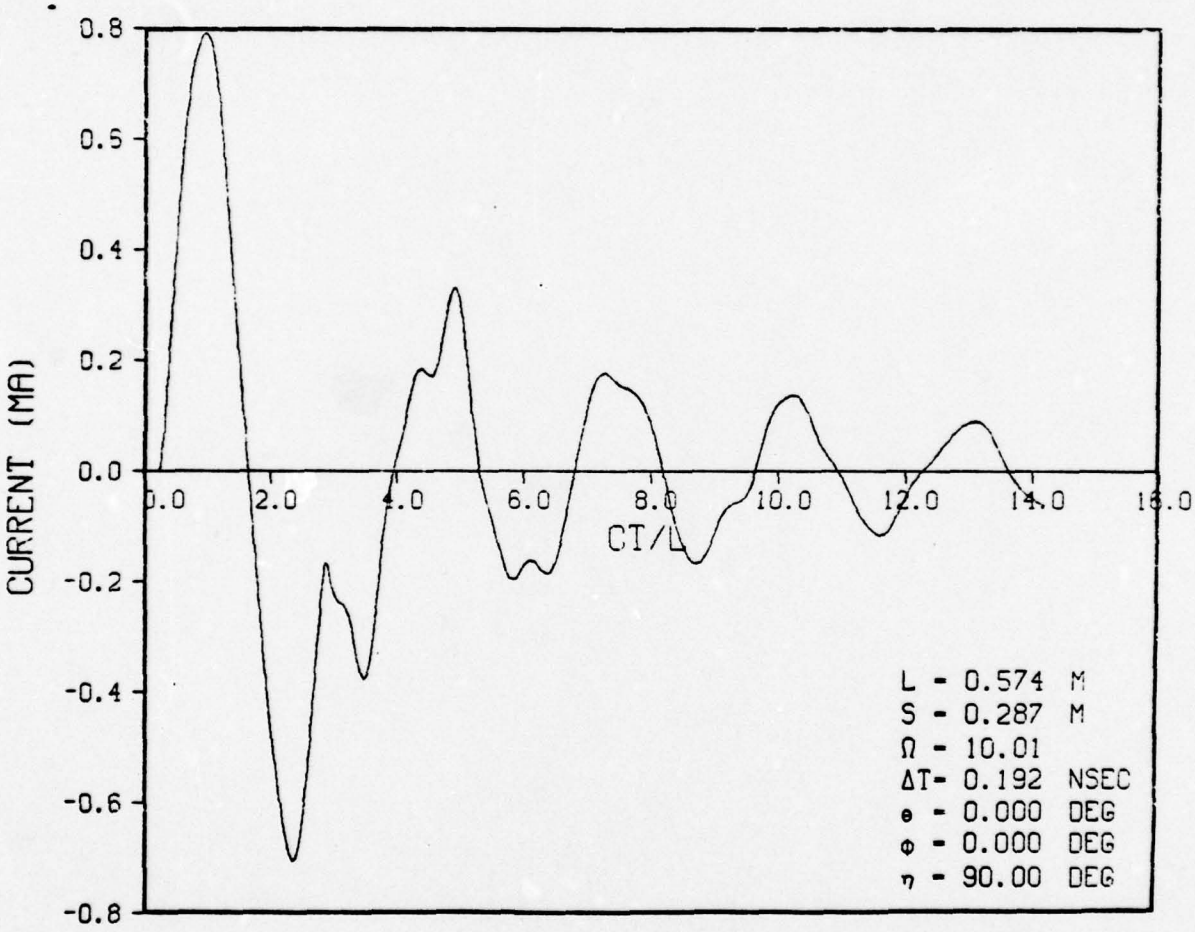

Figure 5-8. TRANSIENT CURRENT-RECTANGULAR PULSE

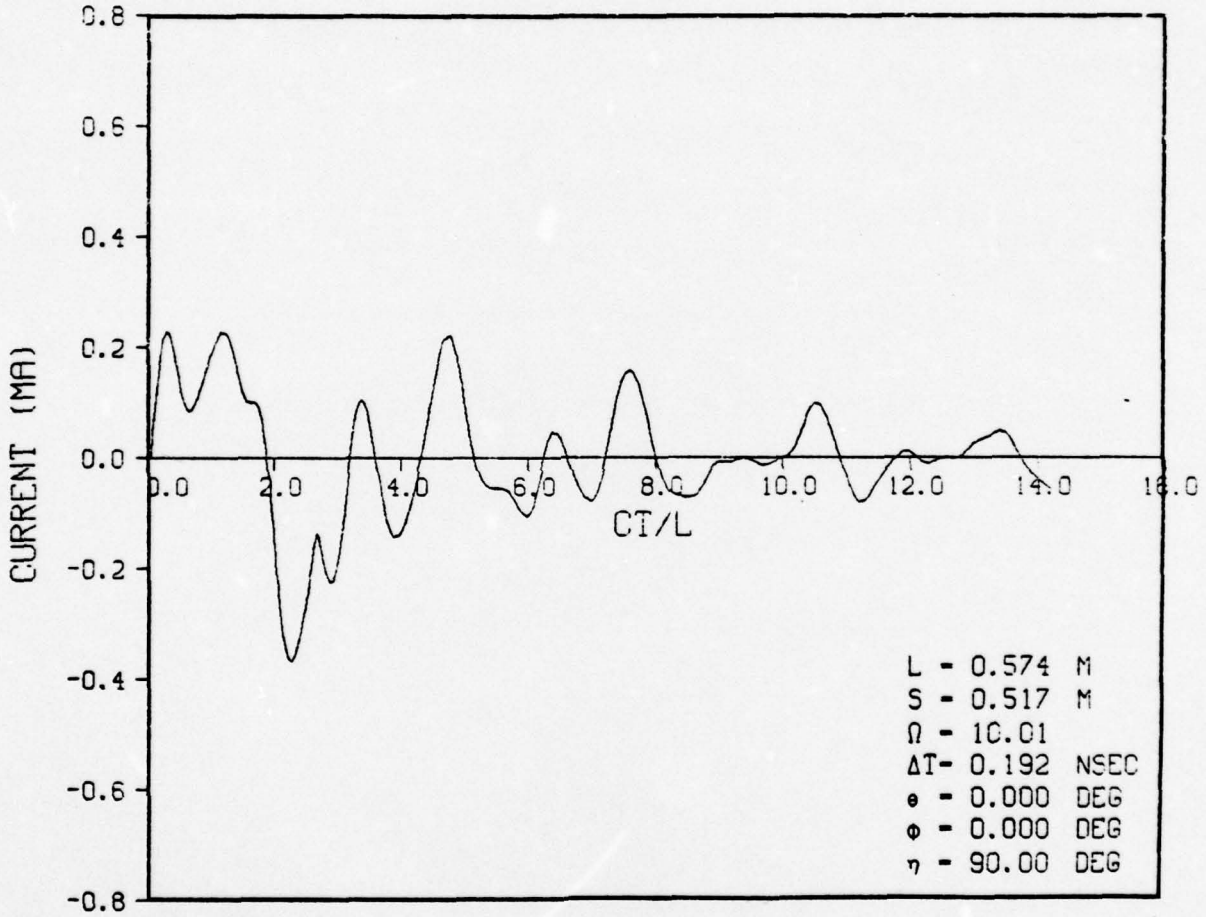

Figure 5-9. TRANSIENT CURRENT-RECTANGULAR PULSE

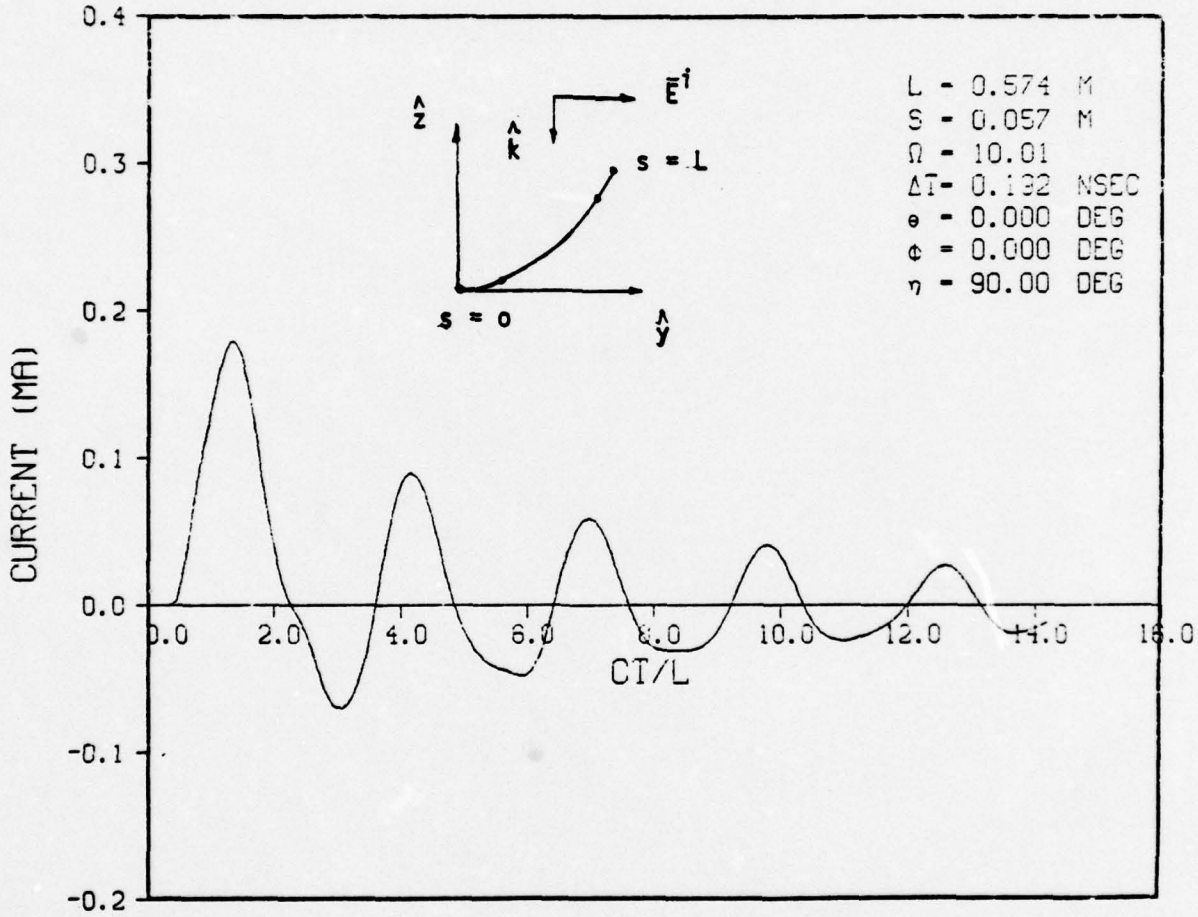

Figure 5-10. TRANSIENT CURRENT-DOUBLE EXPONENTIAL PULSE

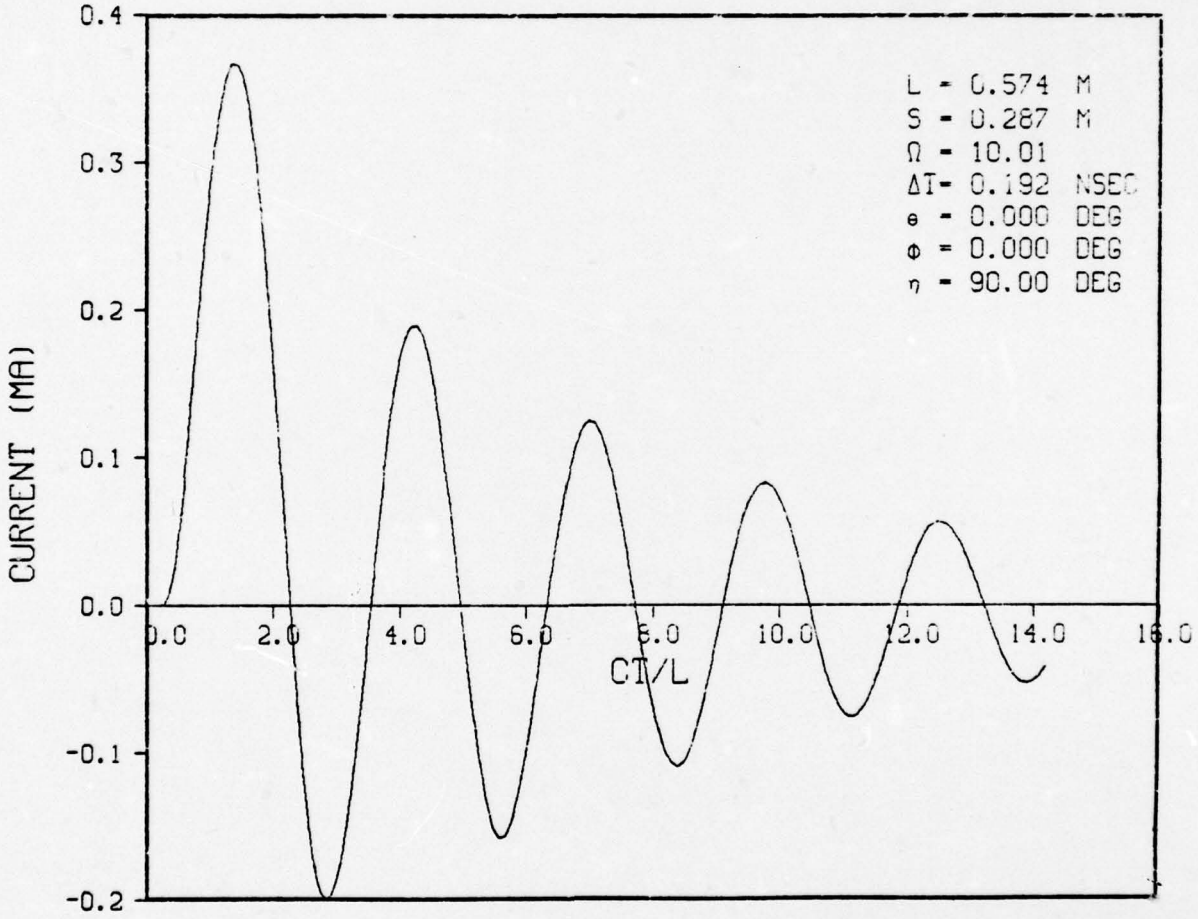

Figure 5-11. TRANSIENT CURRENT-DOUBLE EXPONENTIAL PULSE

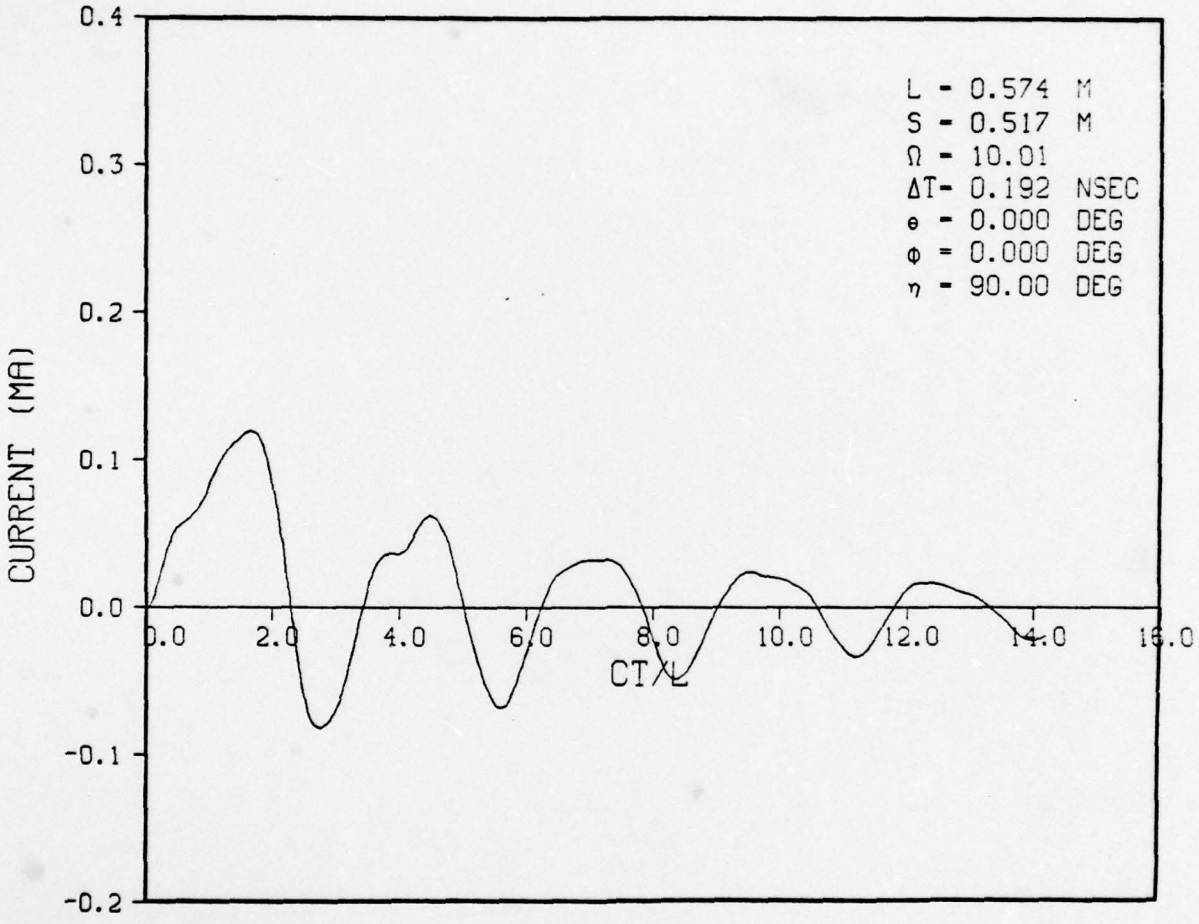

Figure 5-12. TRANSIENT CURRENT-DOUBLE EXPONENTIAL PULSE

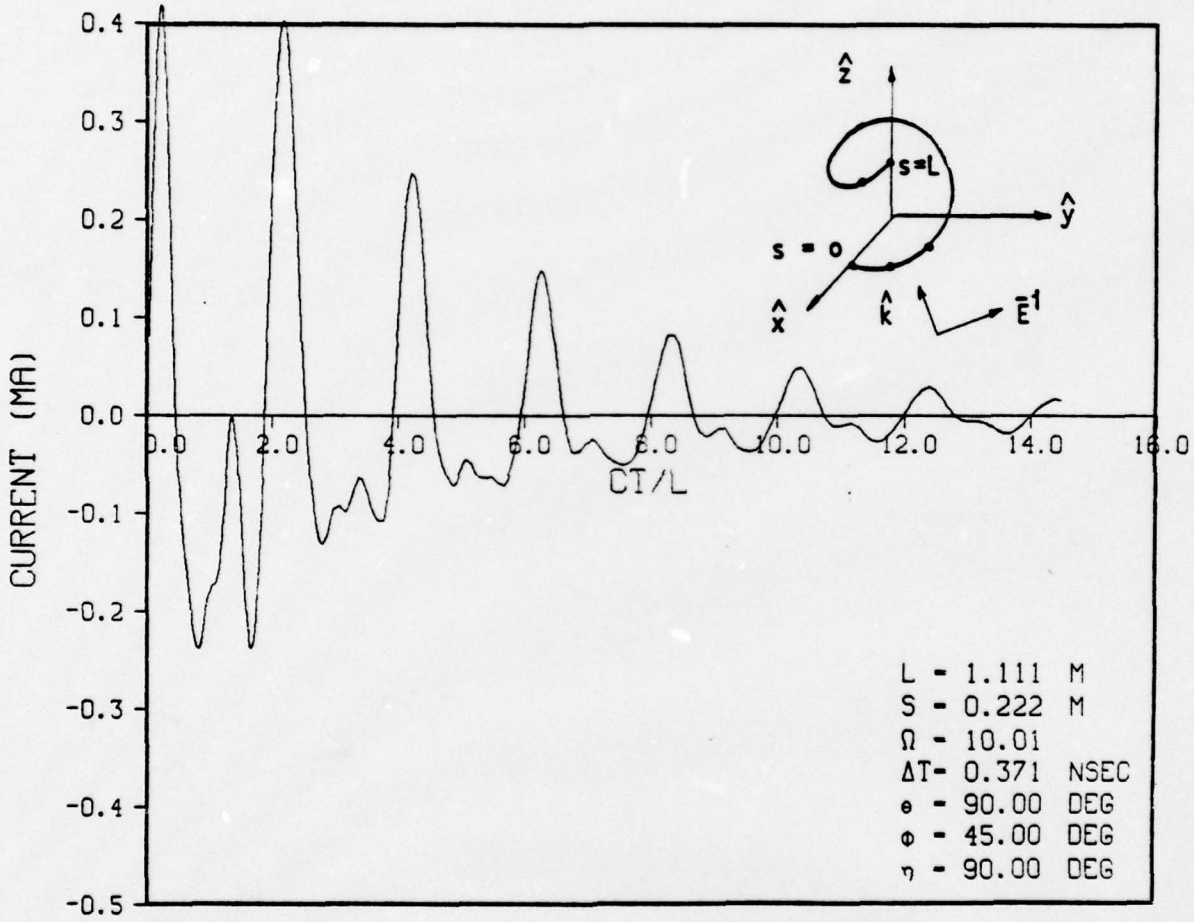

Figure 5-13. TRANSIENT CURRENT-GAUSSIAN PULSE

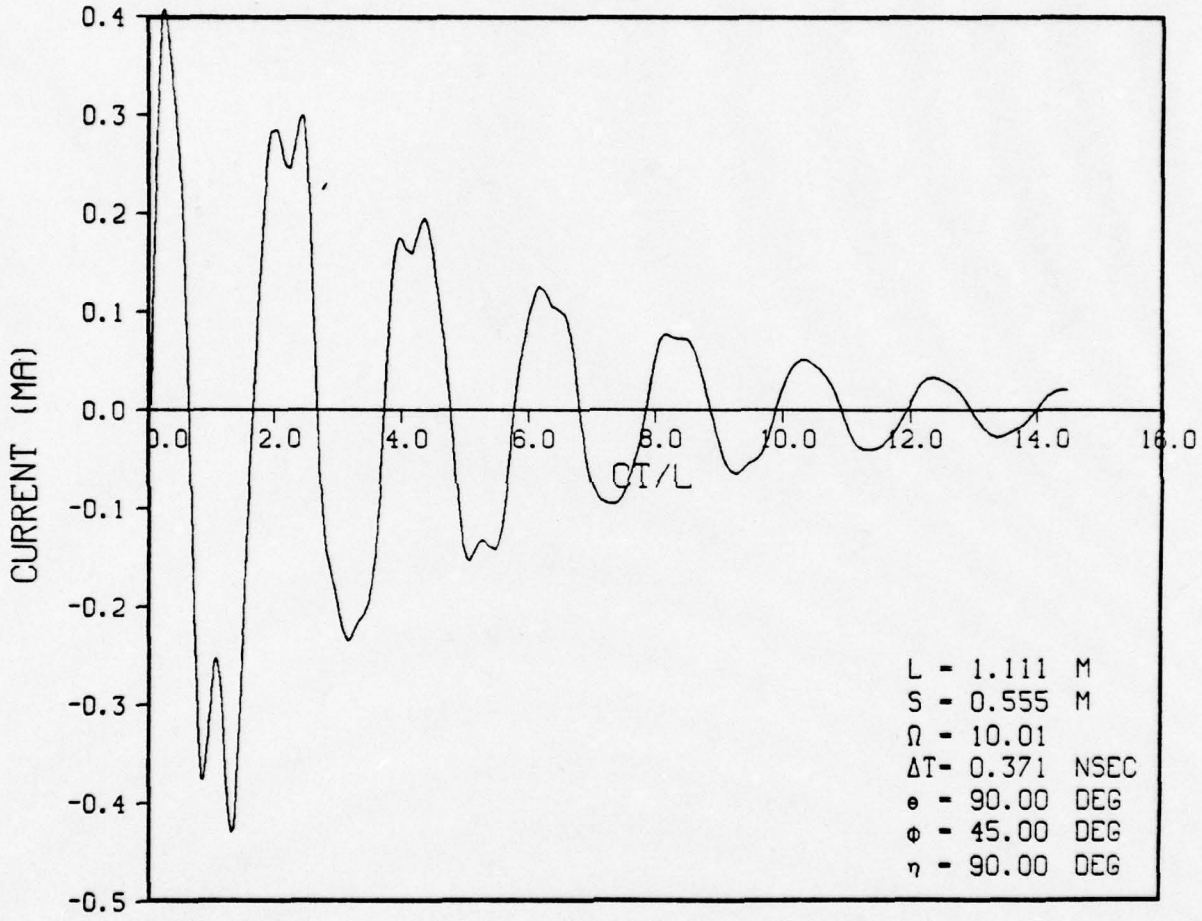

Figure 5-14. TRANSIENT CURRENT-GAUSSIAN PULSE

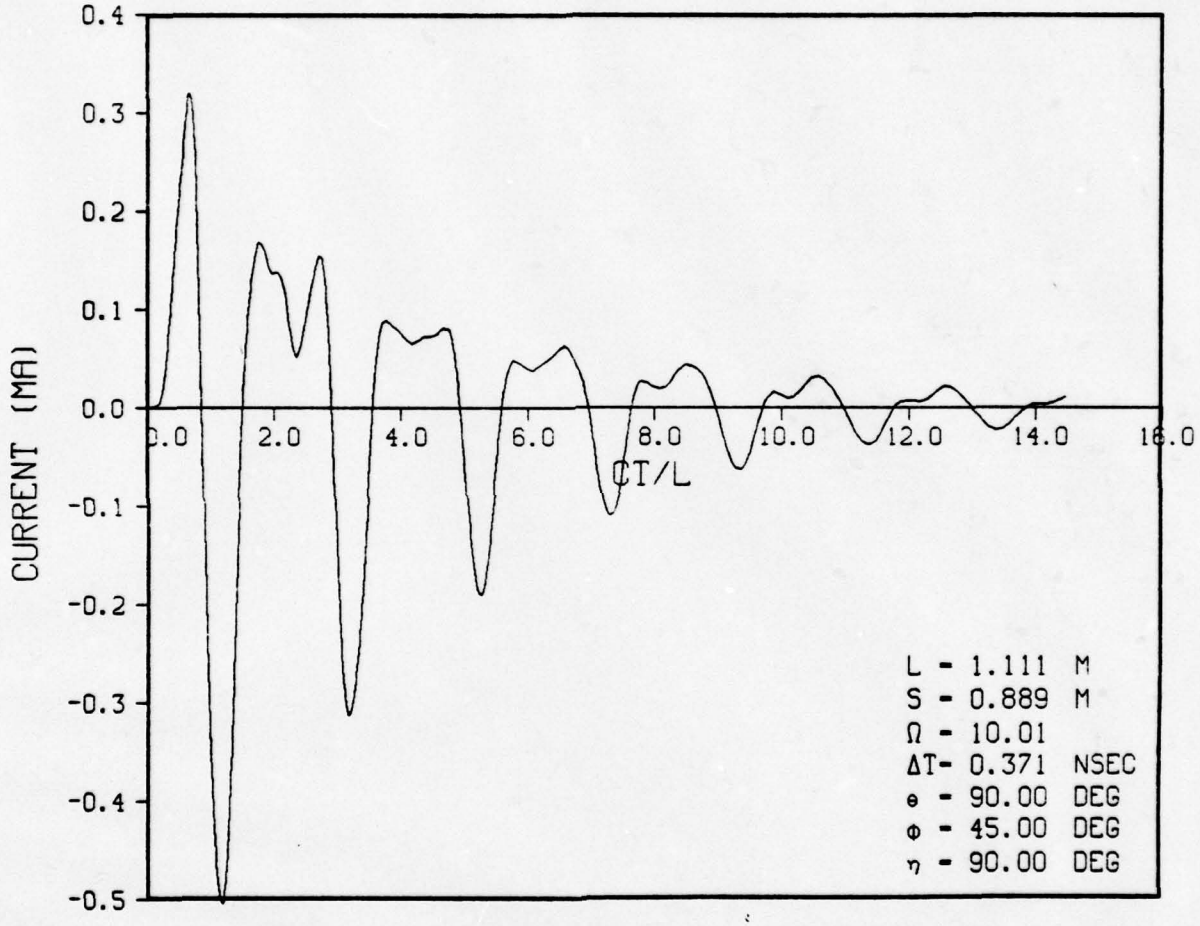

Figure 5-15. TRANSIENT CURRENT-GAUSSIAN PULSE

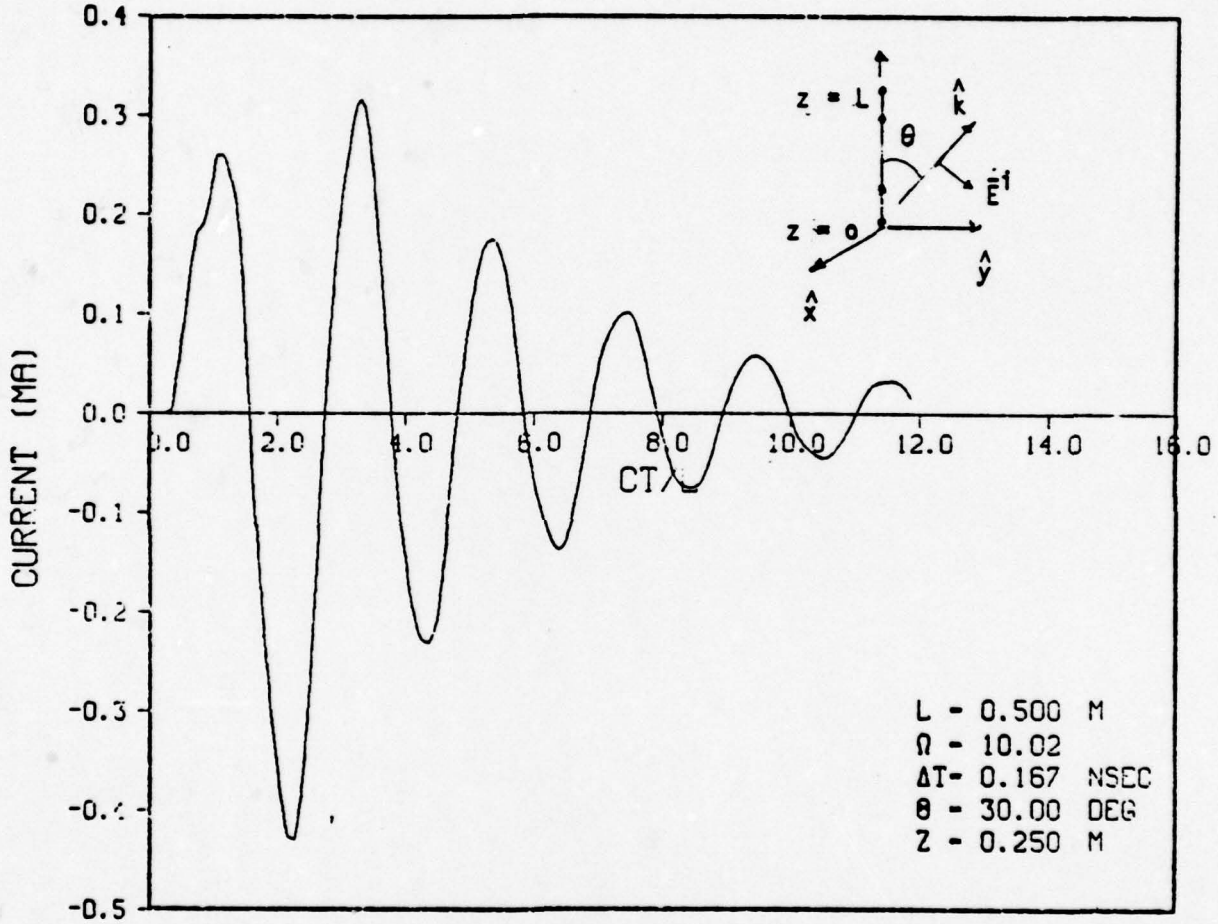

Figure 5-16. Transient Current — Gaussian Pulse

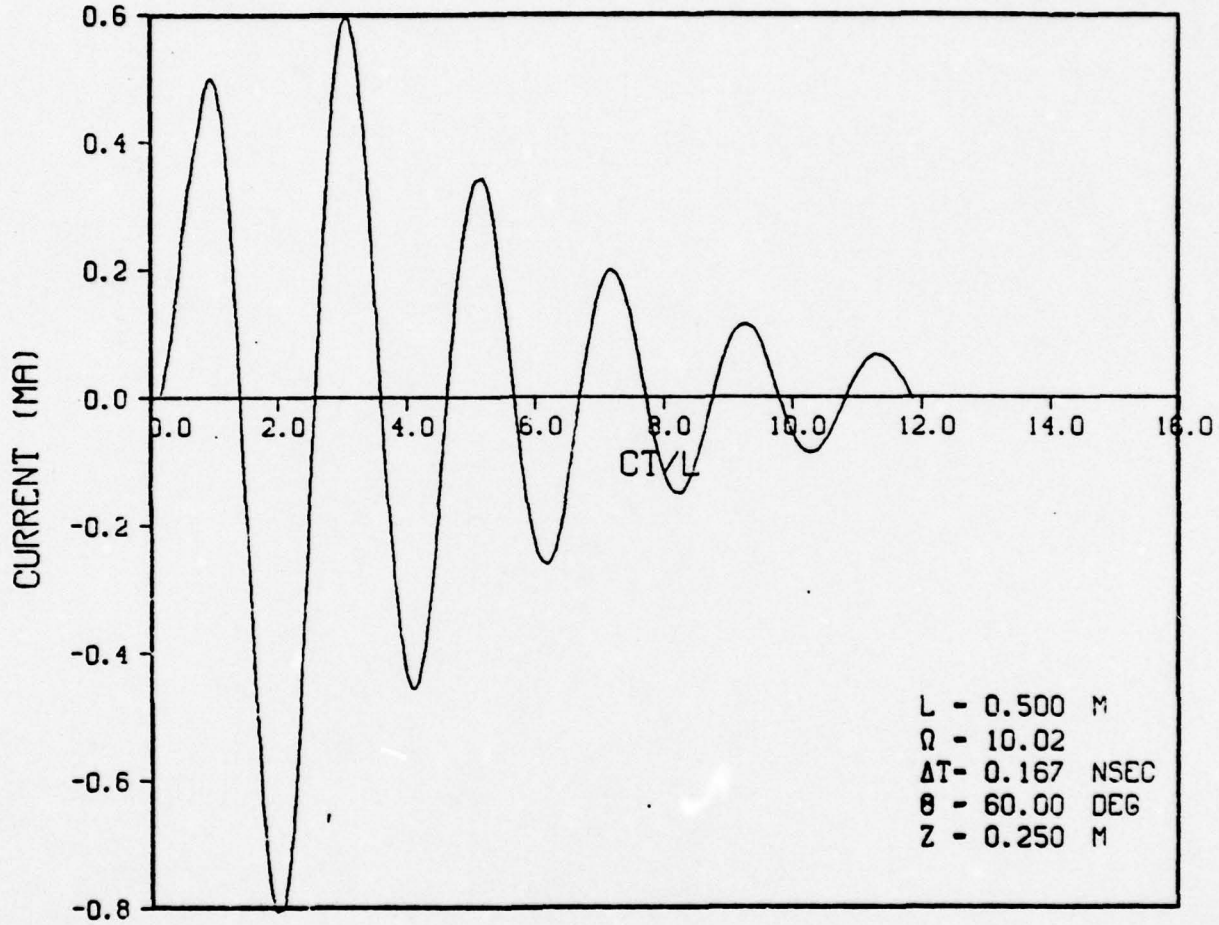

Figure 5-17. Transient Current — Gaussian Pulse

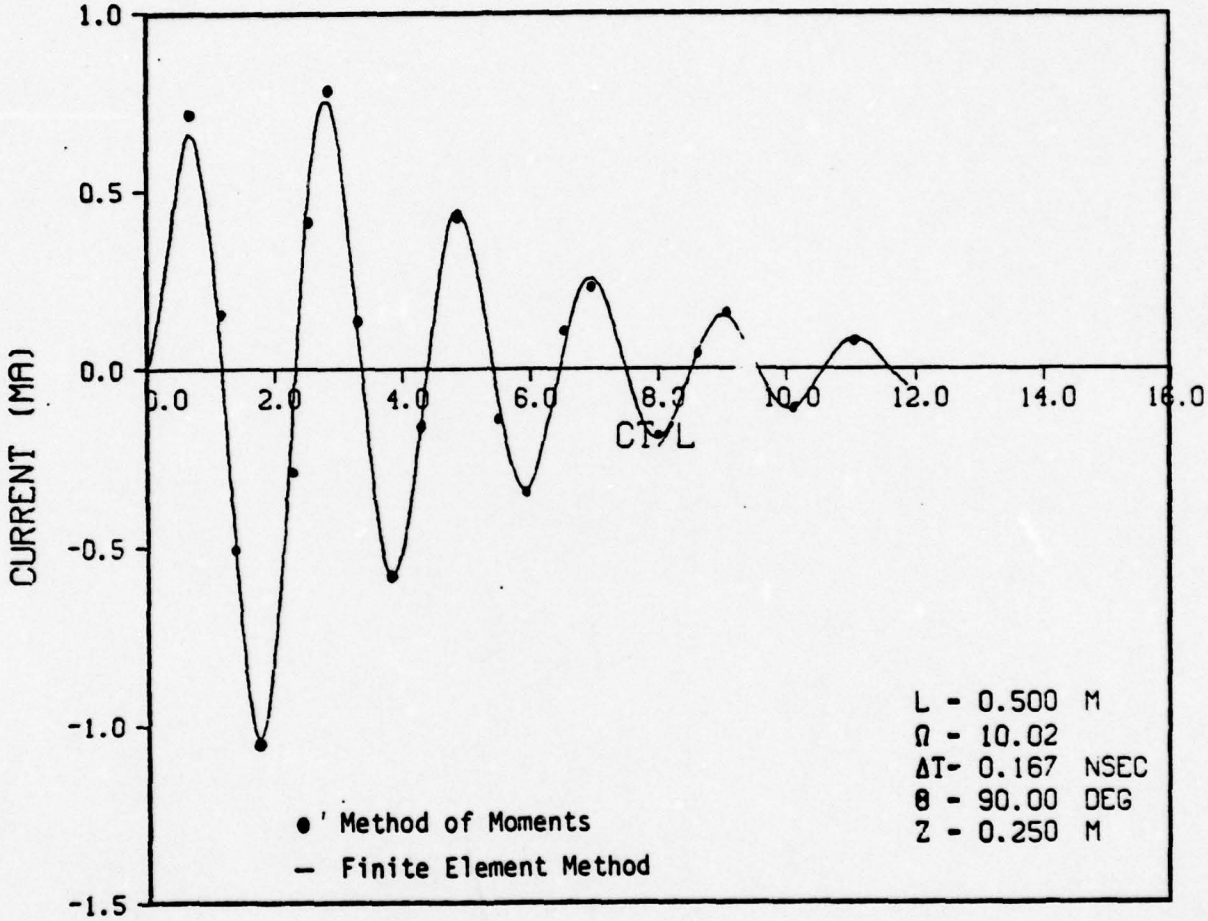

Figure 5-18. Transient Current — Gaussian Pulse

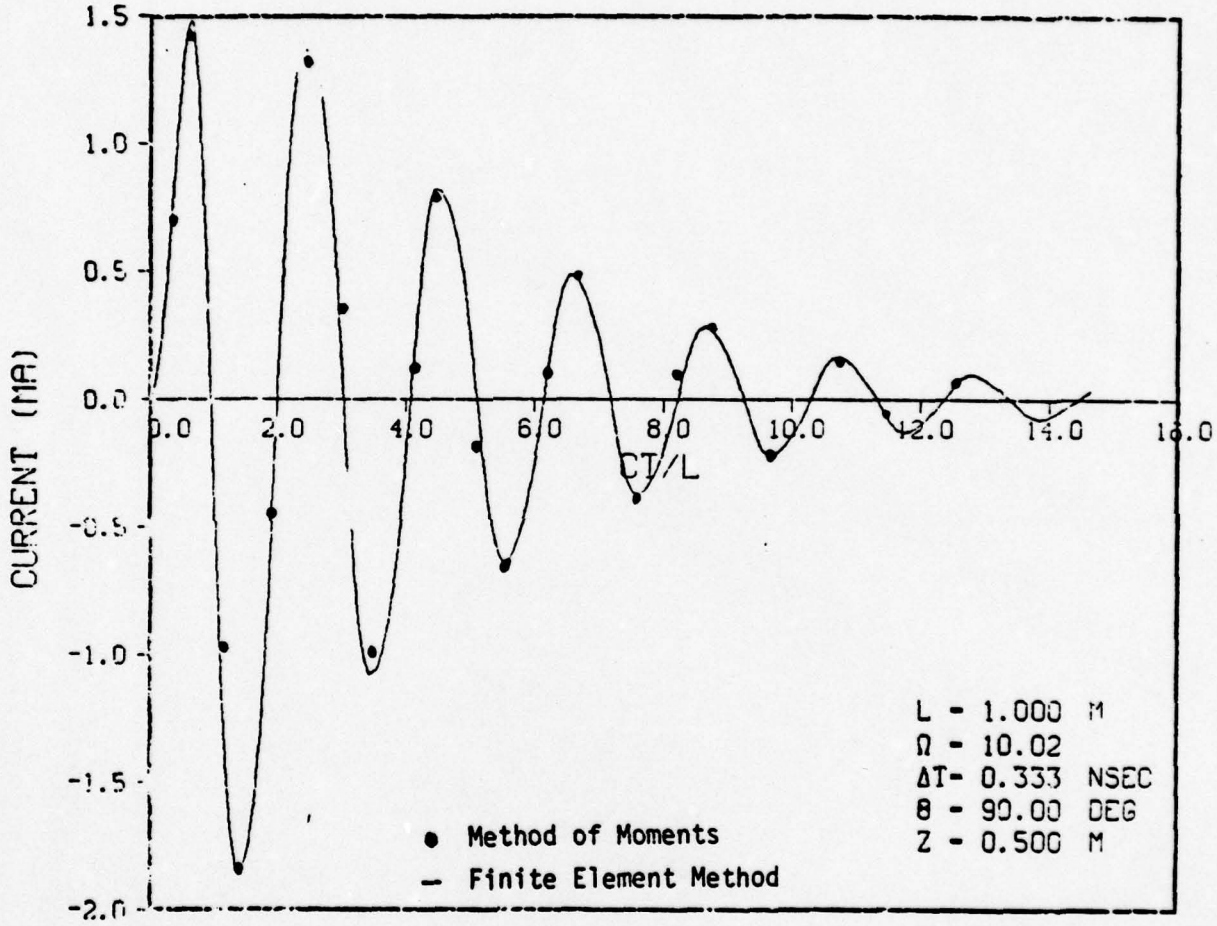

Figure 5-19. Transient Current — Gaussian Pulse

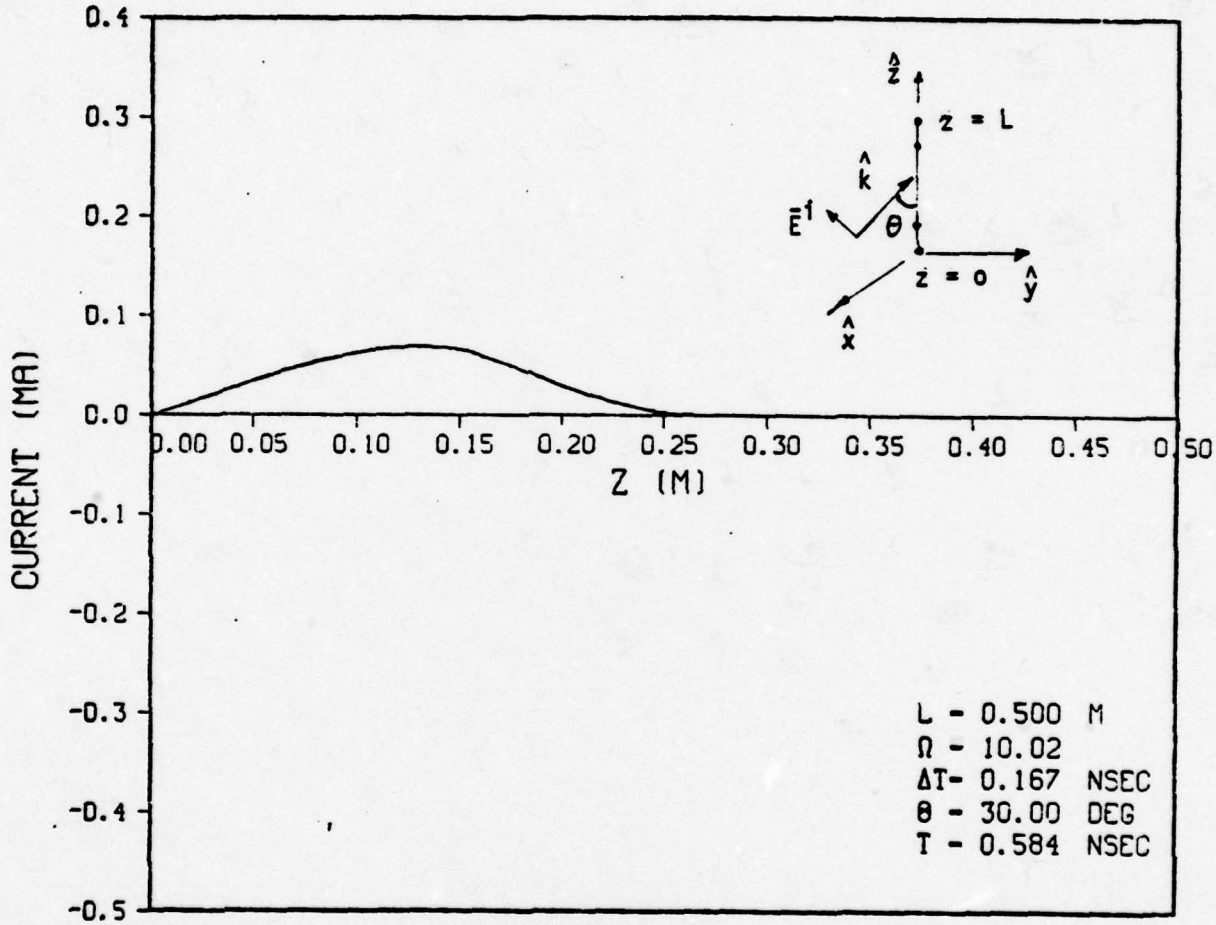

Figure 5-20. Current Distribution — Gaussian Pulse

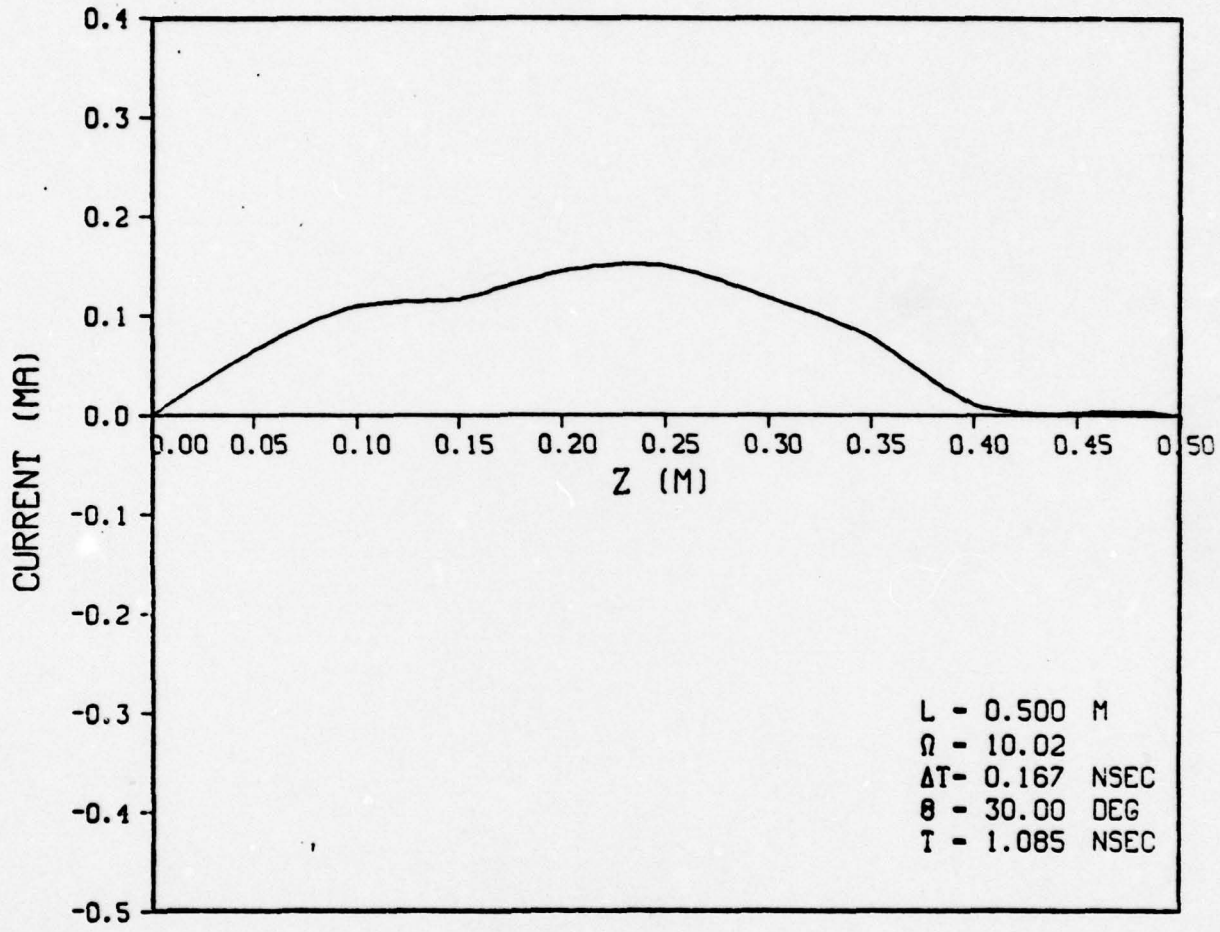

Figure 5-21. Current Distribution — Gaussian Pulse

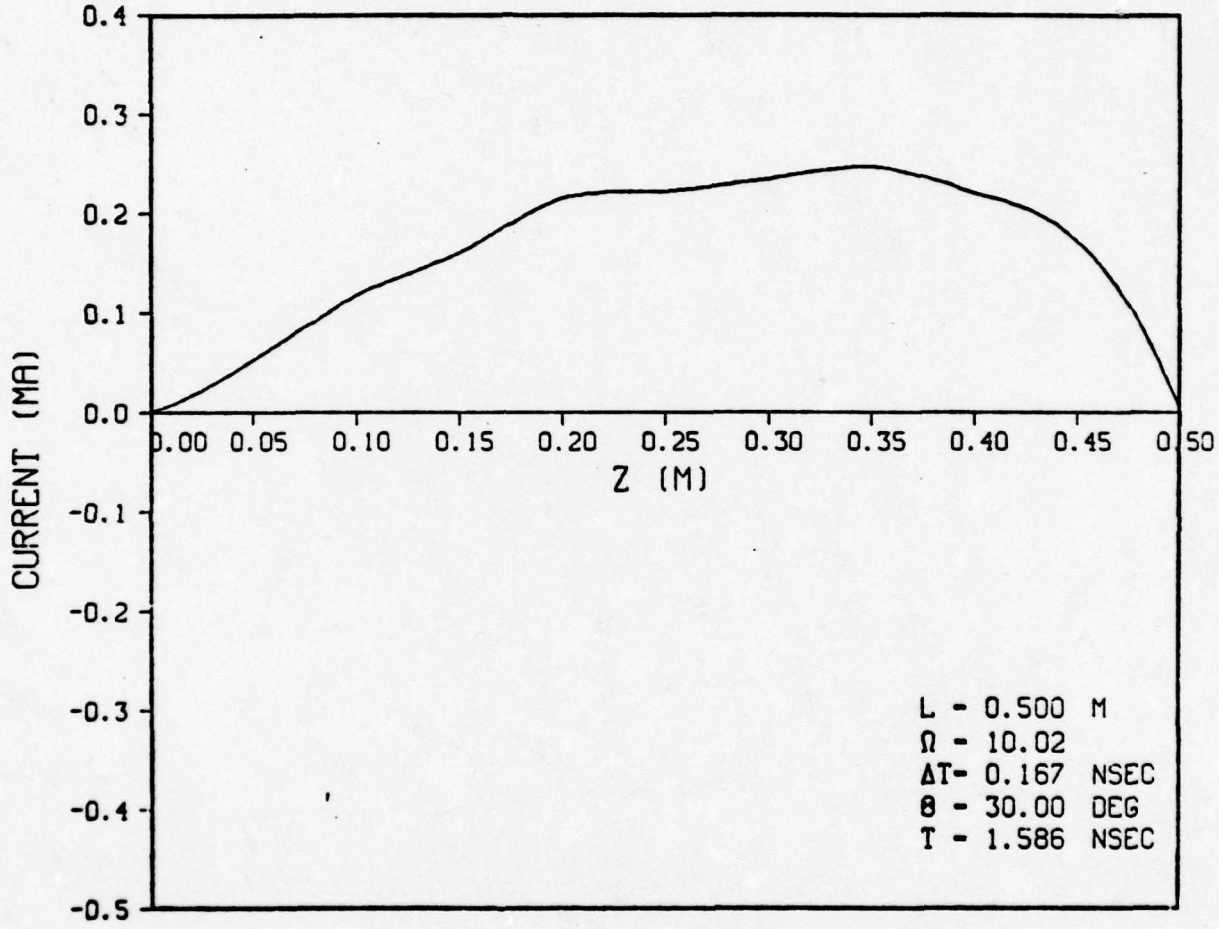

Figure 5-22. Current Distribution — Gaussian Pulse

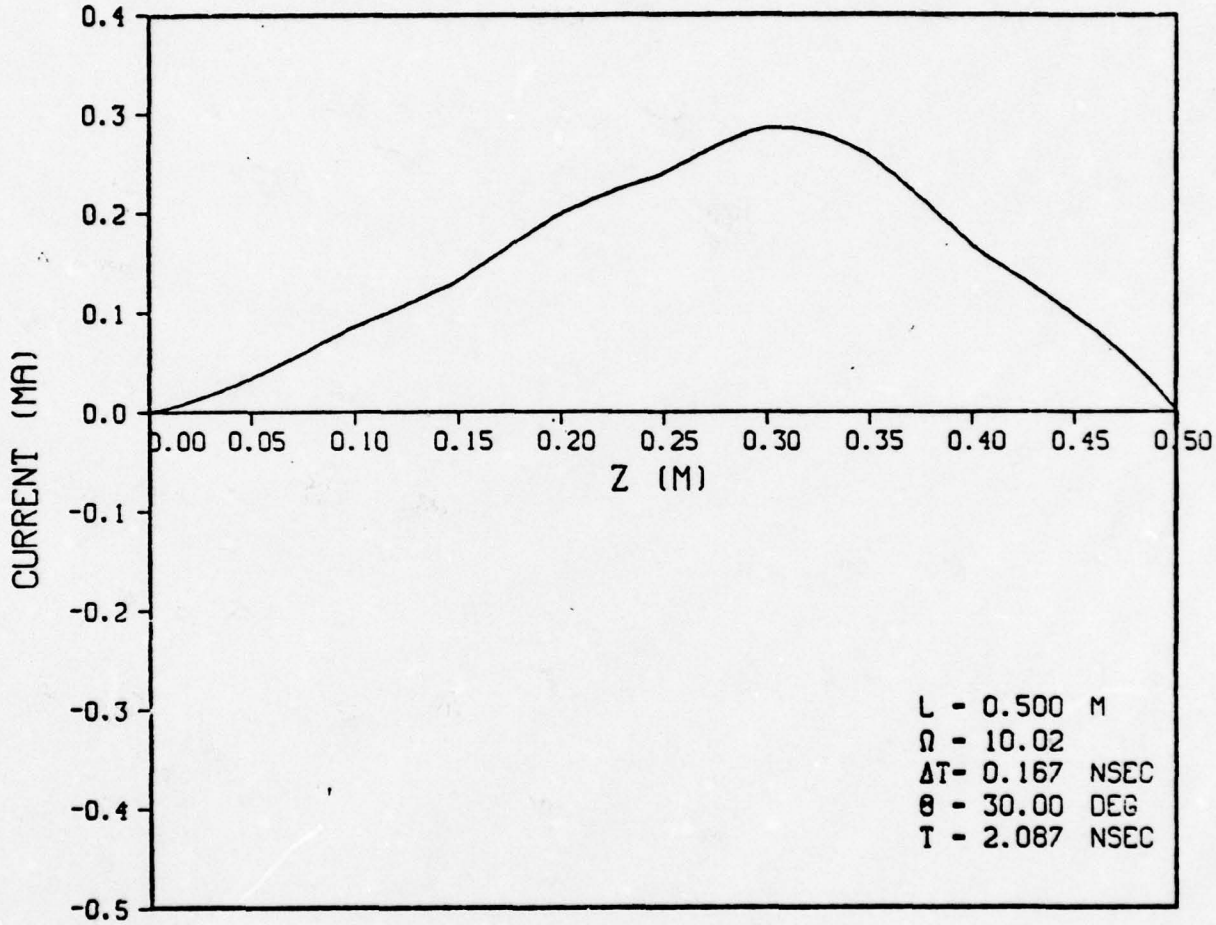

Figure 5-23. Current Distribution — Gaussian Pulse

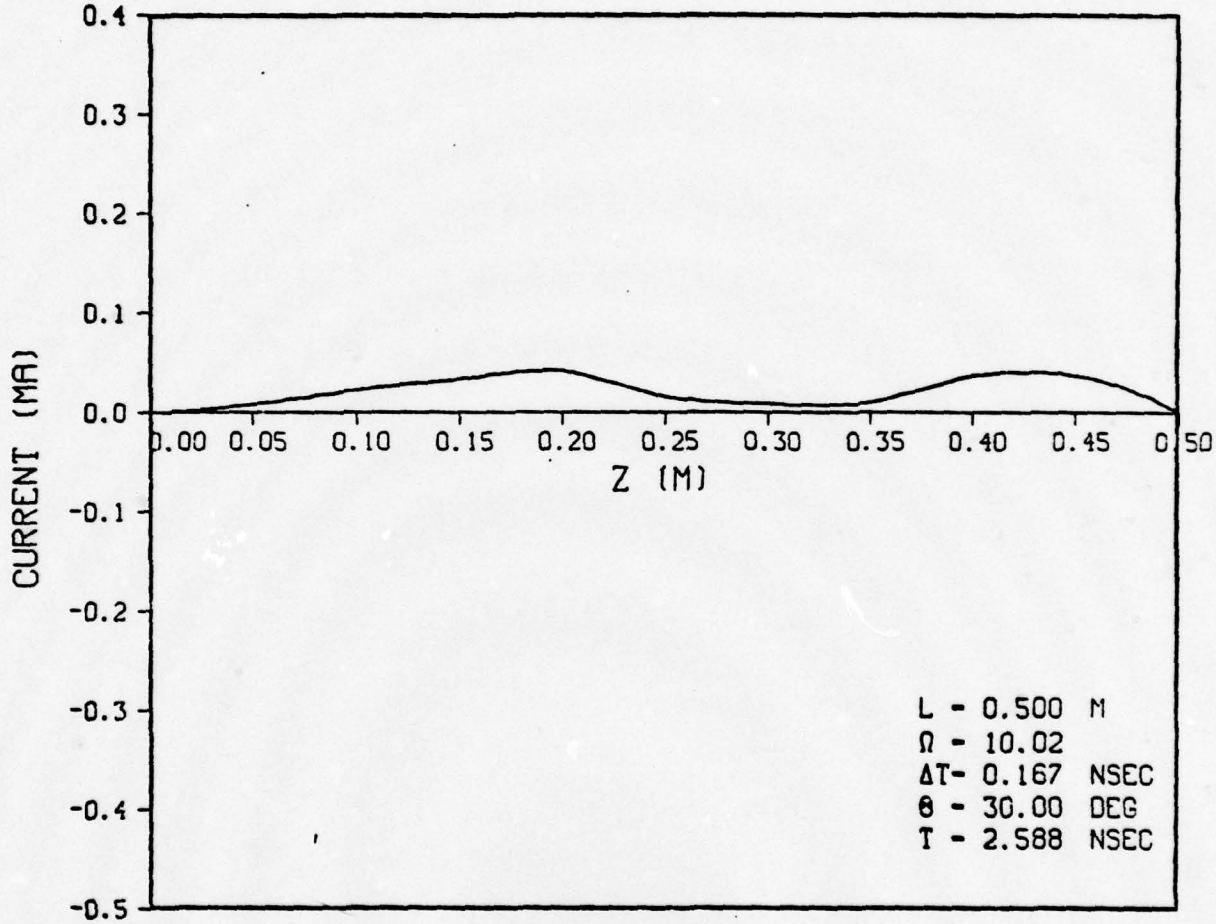

Figure 5-24. Current Distribution — Gaussian Pulse

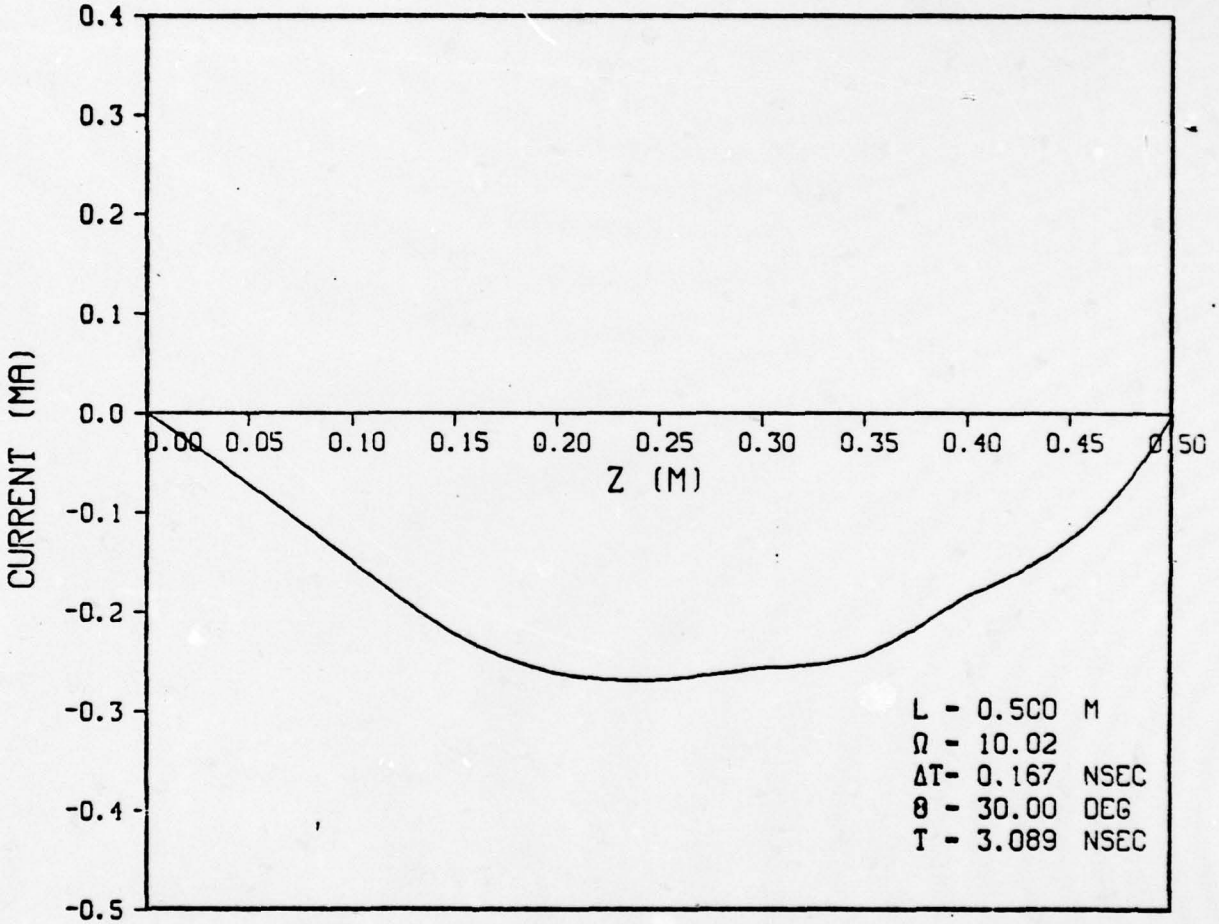

Figure 5-25. Current Distribution — Gaussian Pulse

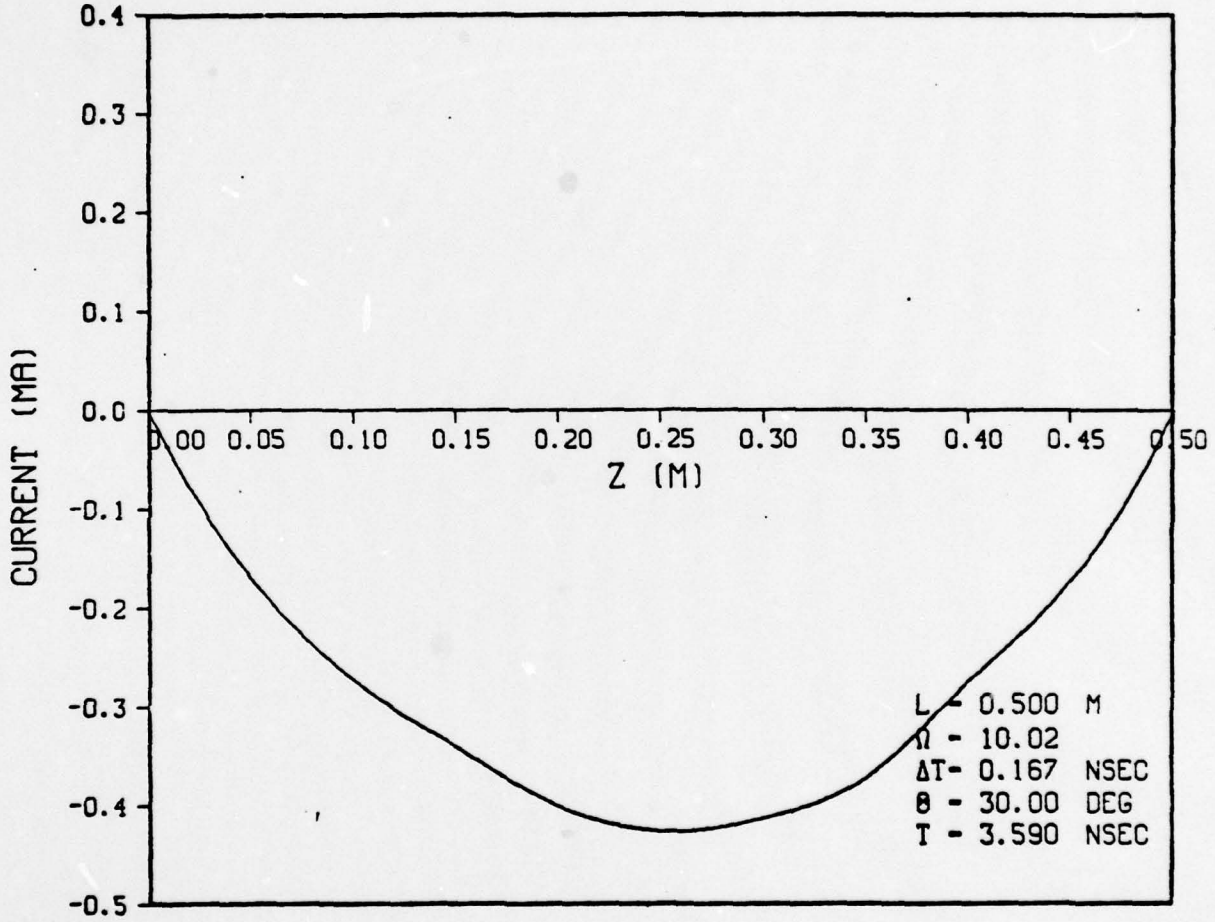

Figure 5-26. Current Distribution — Gaussian Pulse

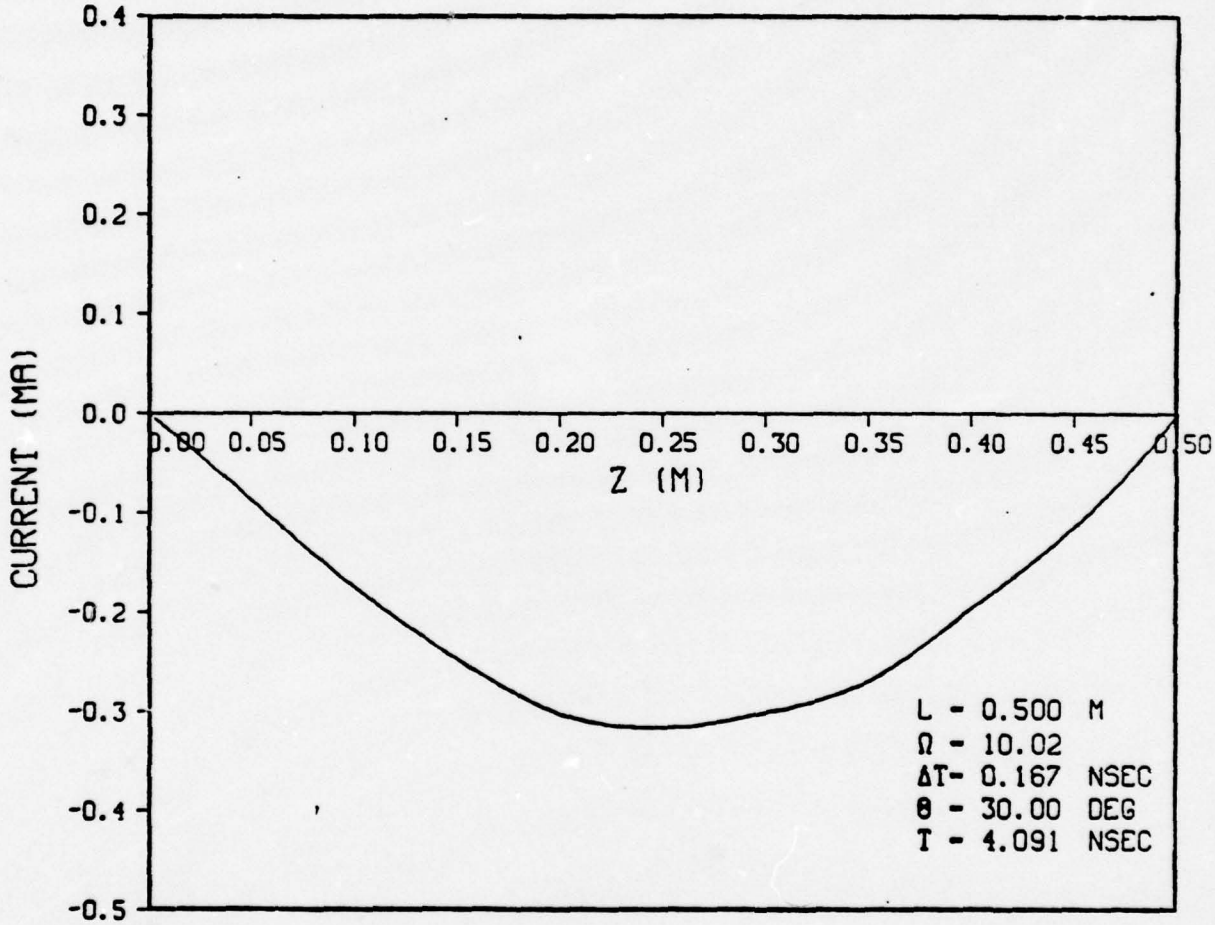

Figure 5-27. Current Distribution — Gaussian Pulse

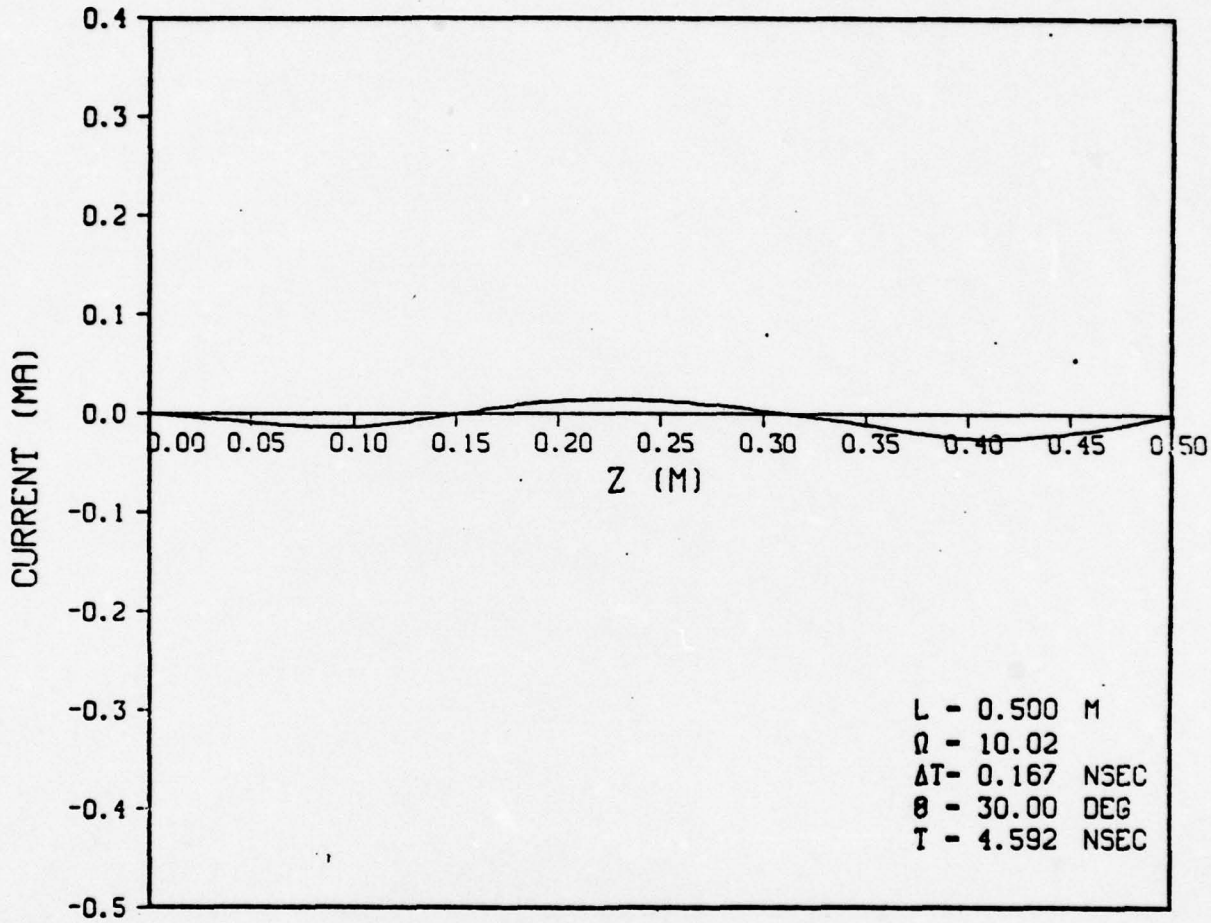

Figure 5-28. Current Distribution — Gaussian Pulse

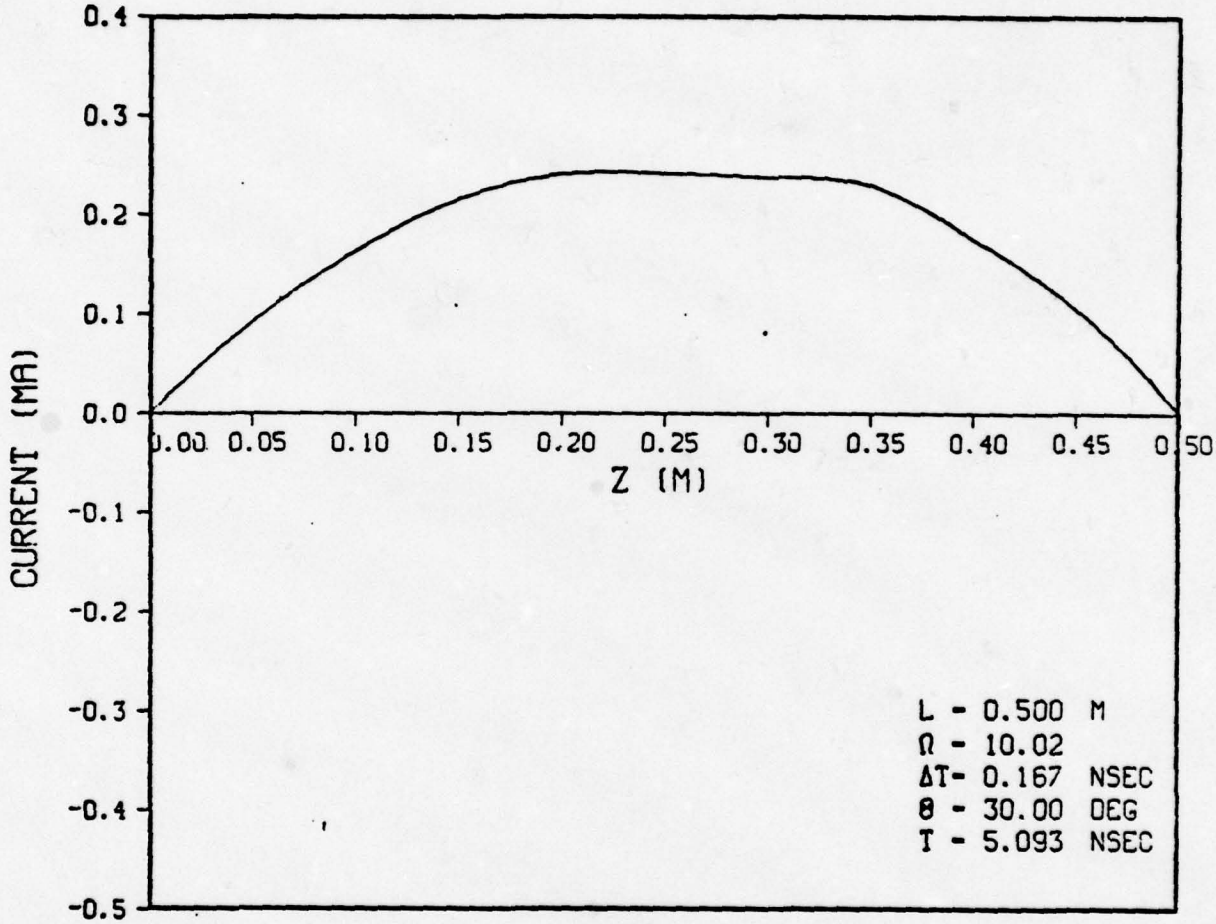

Figure 5-29. Current Distribution — Gaussian Pulse

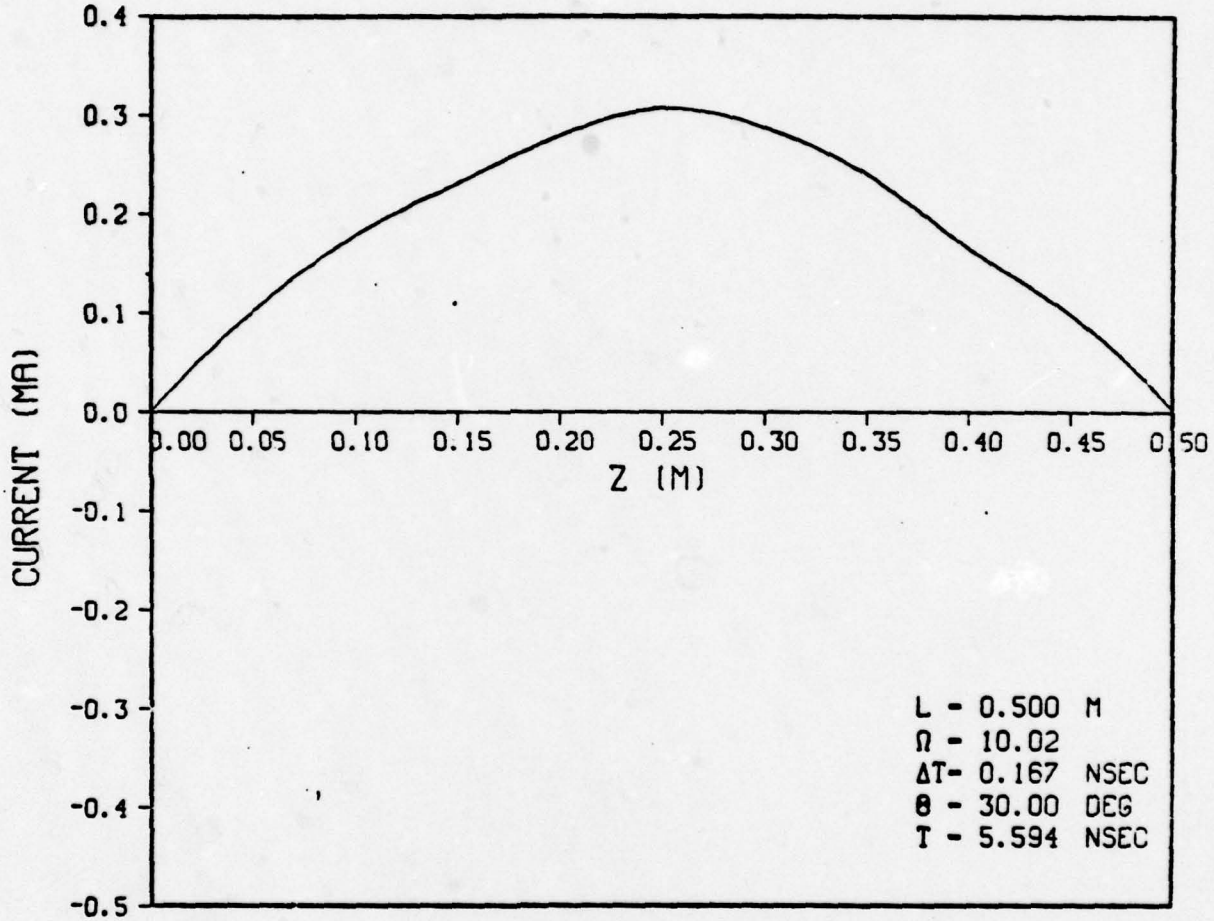

Figure 5-30. Current Distribution — Gaussian Pulse

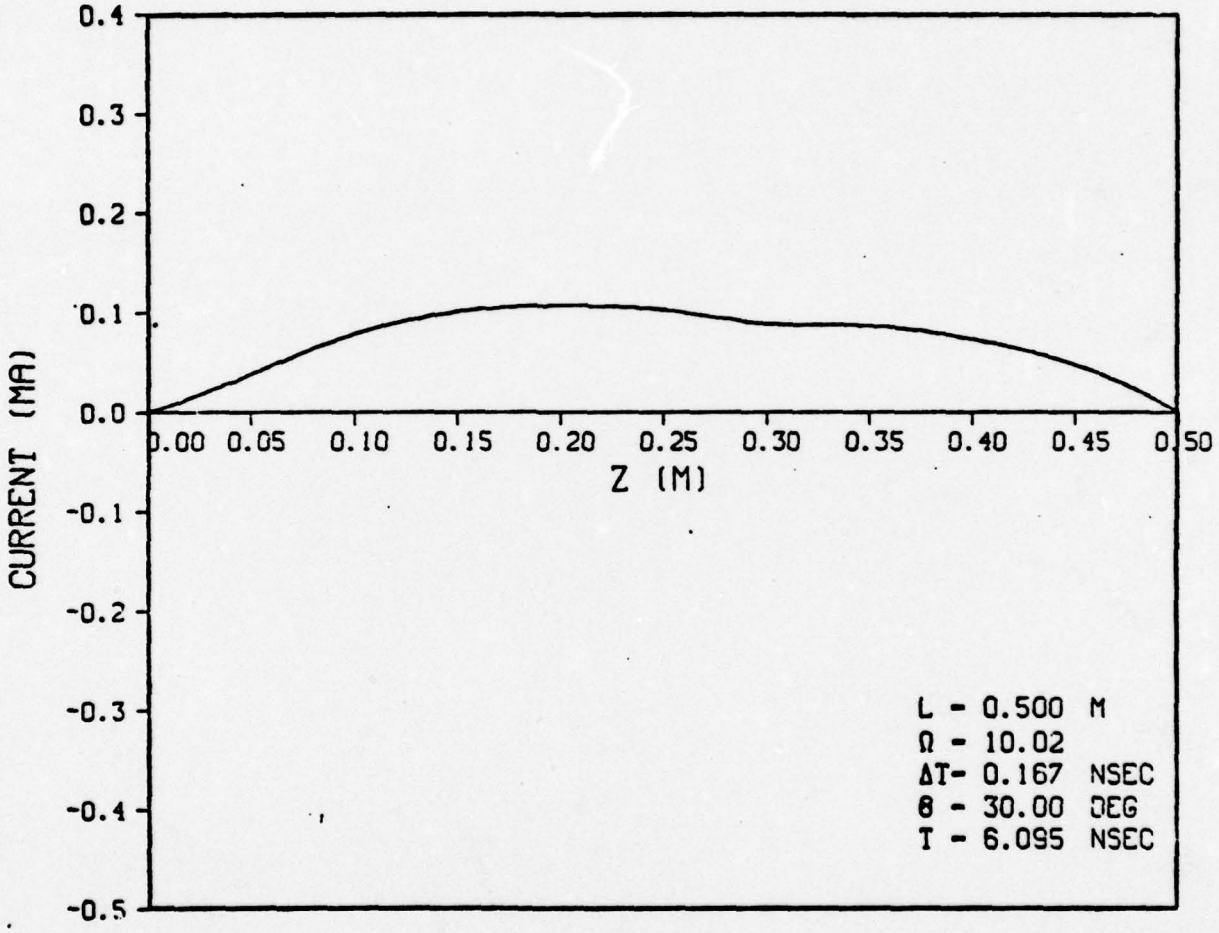

Figure 5-31. Current Distribution — Gaussian Pulse

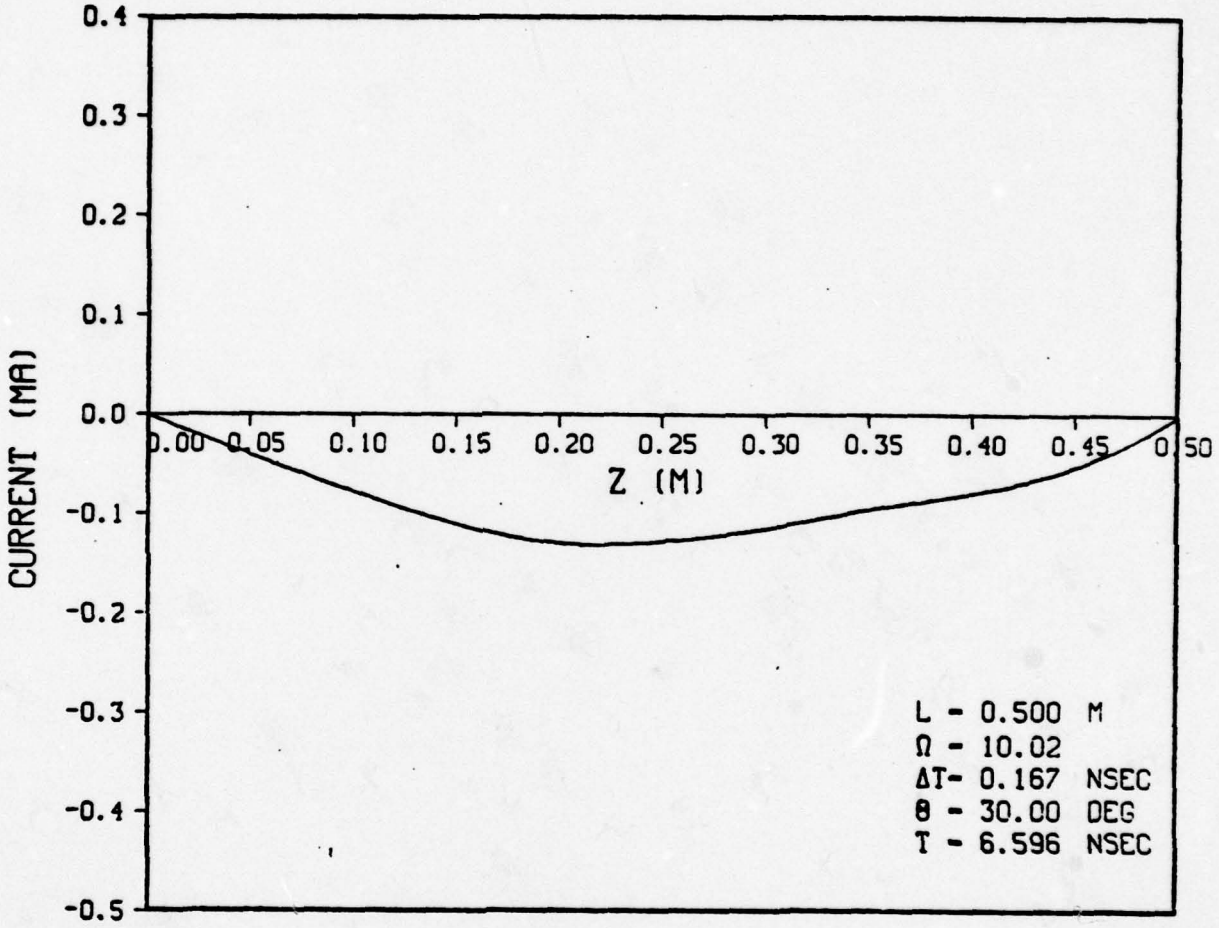

Figure 5-32. Current Distribution — Gaussian Pulse

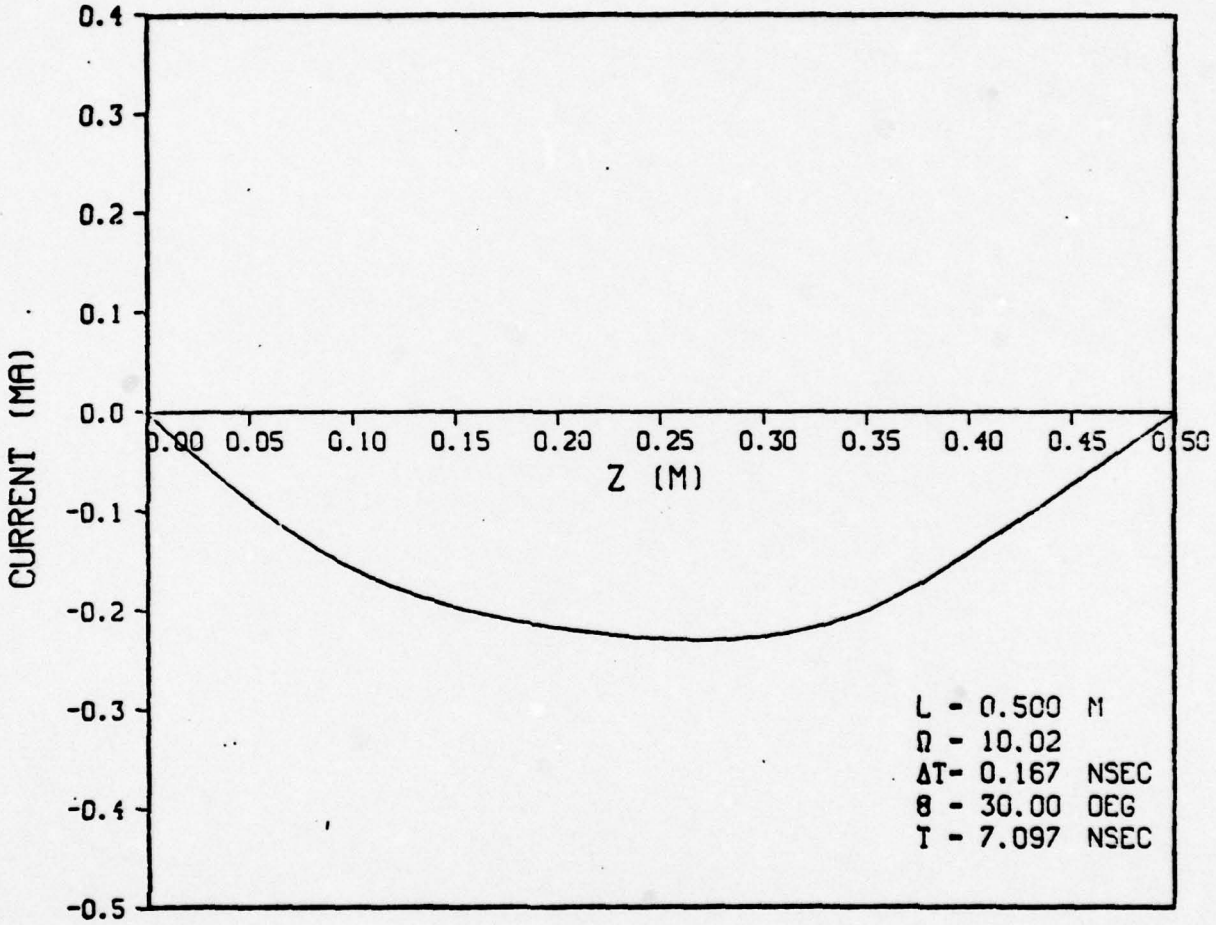

Figure 5-33. Current Distribution — Gaussian Pulse

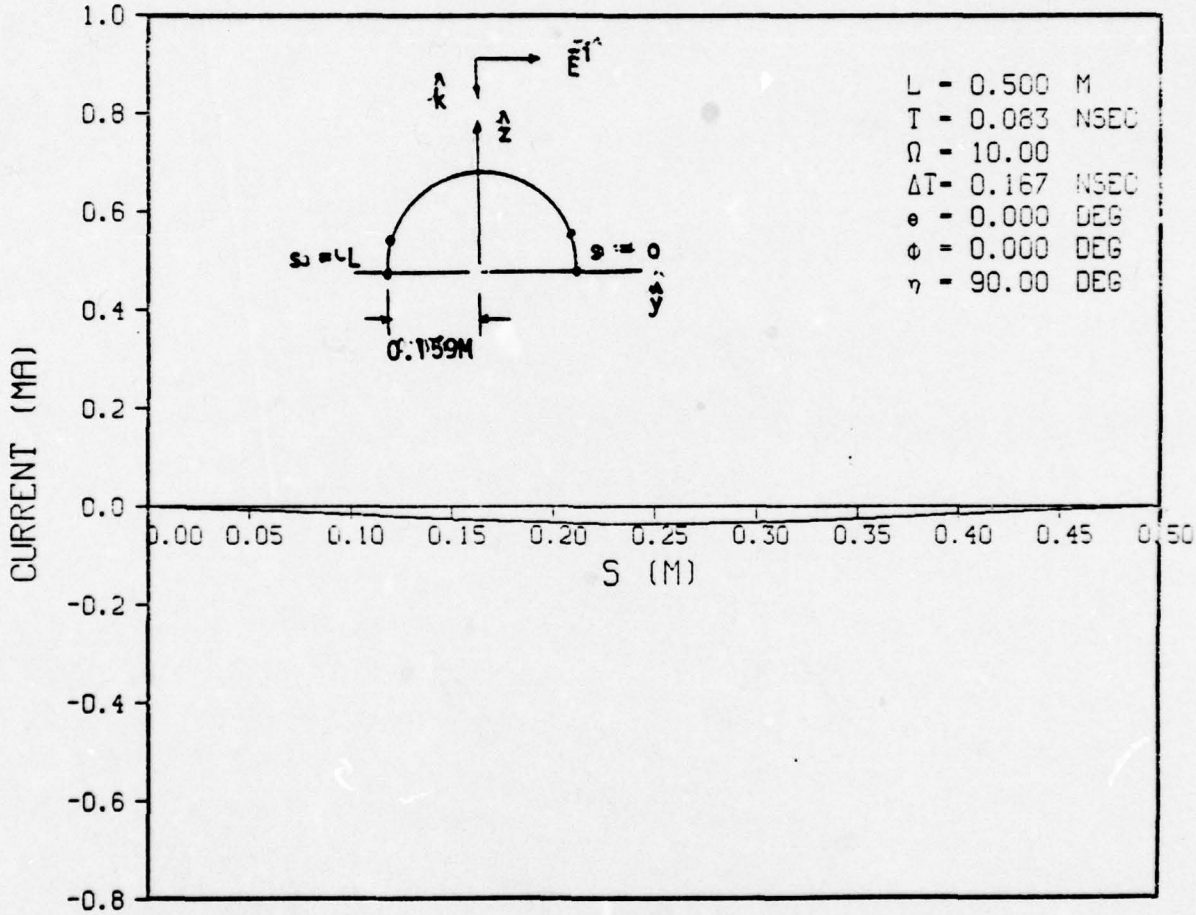

Figure 5-34. CURRENT DISTRIBUTION-GAUSSIAN PULSE

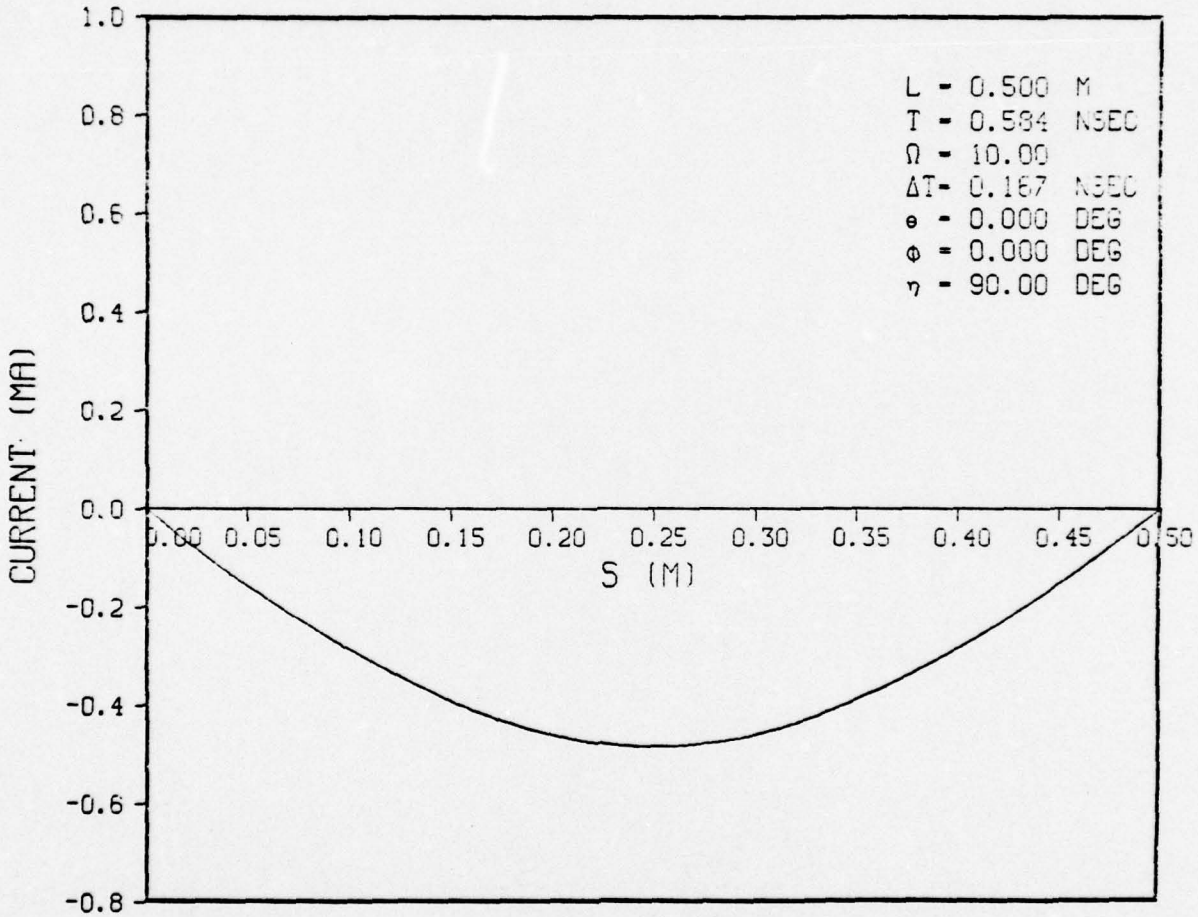

Figure 5-35. CURRENT DISTRIBUTION-GAUSSIAN PULSE

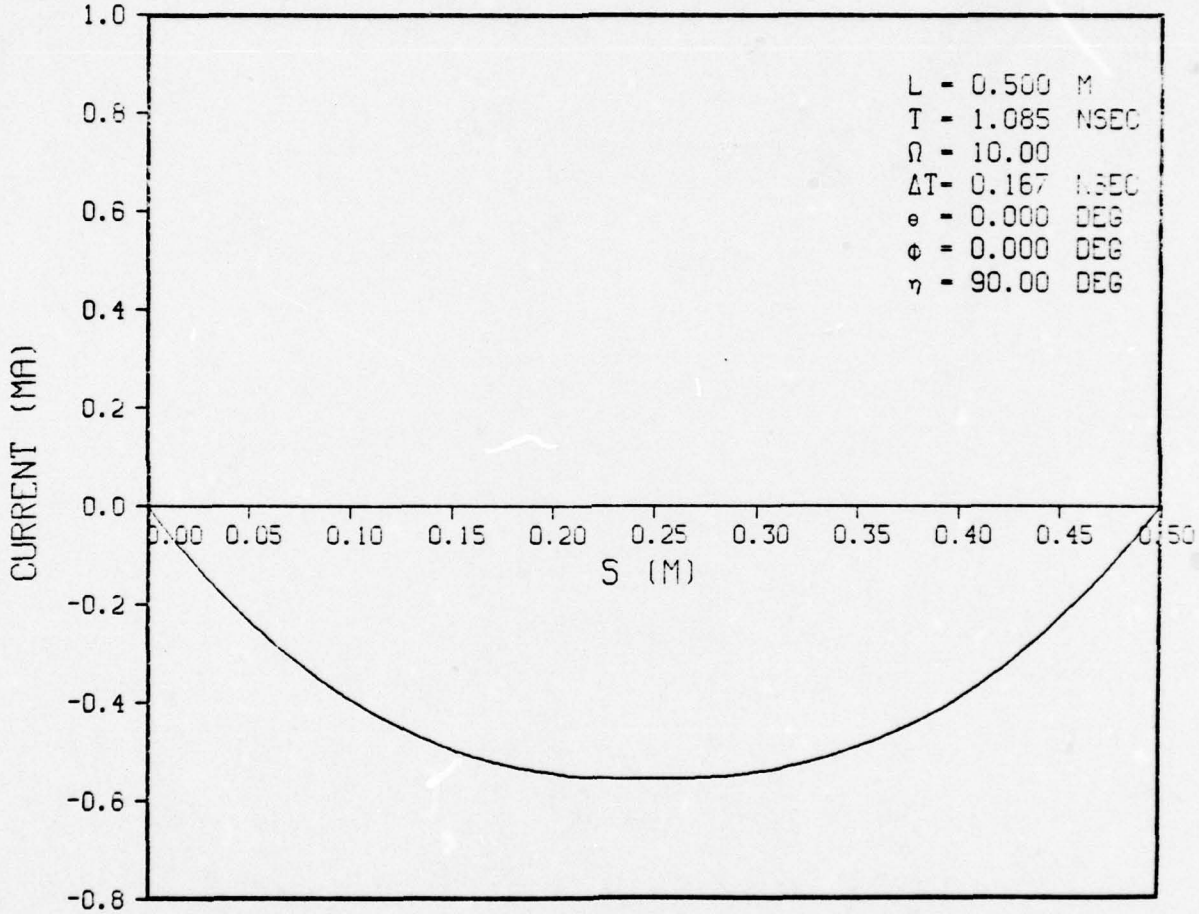

Figure 5-36. CURRENT DISTRIBUTION-GAUSSIAN PULSE

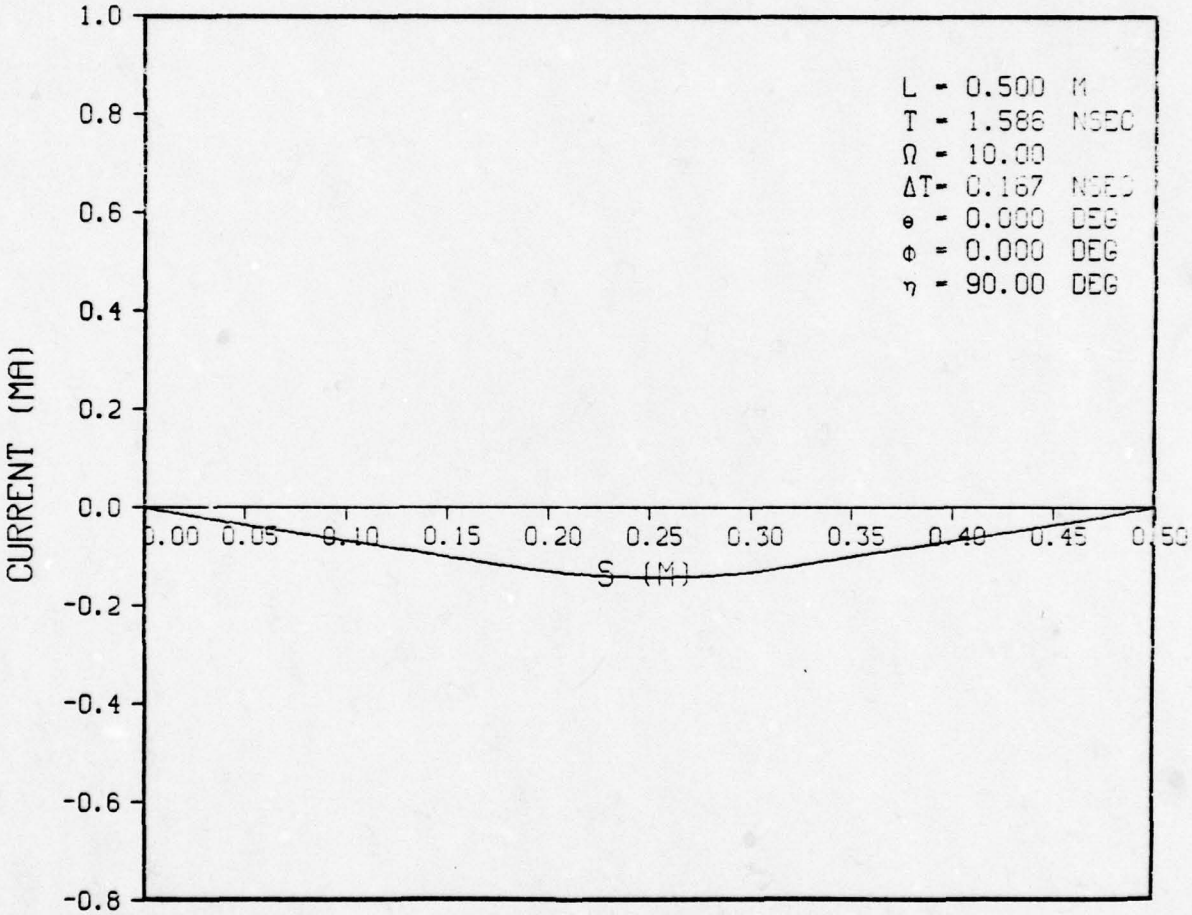

Figure 5-37. CURRENT DISTRIBUTION-GAUSSIAN PULSE

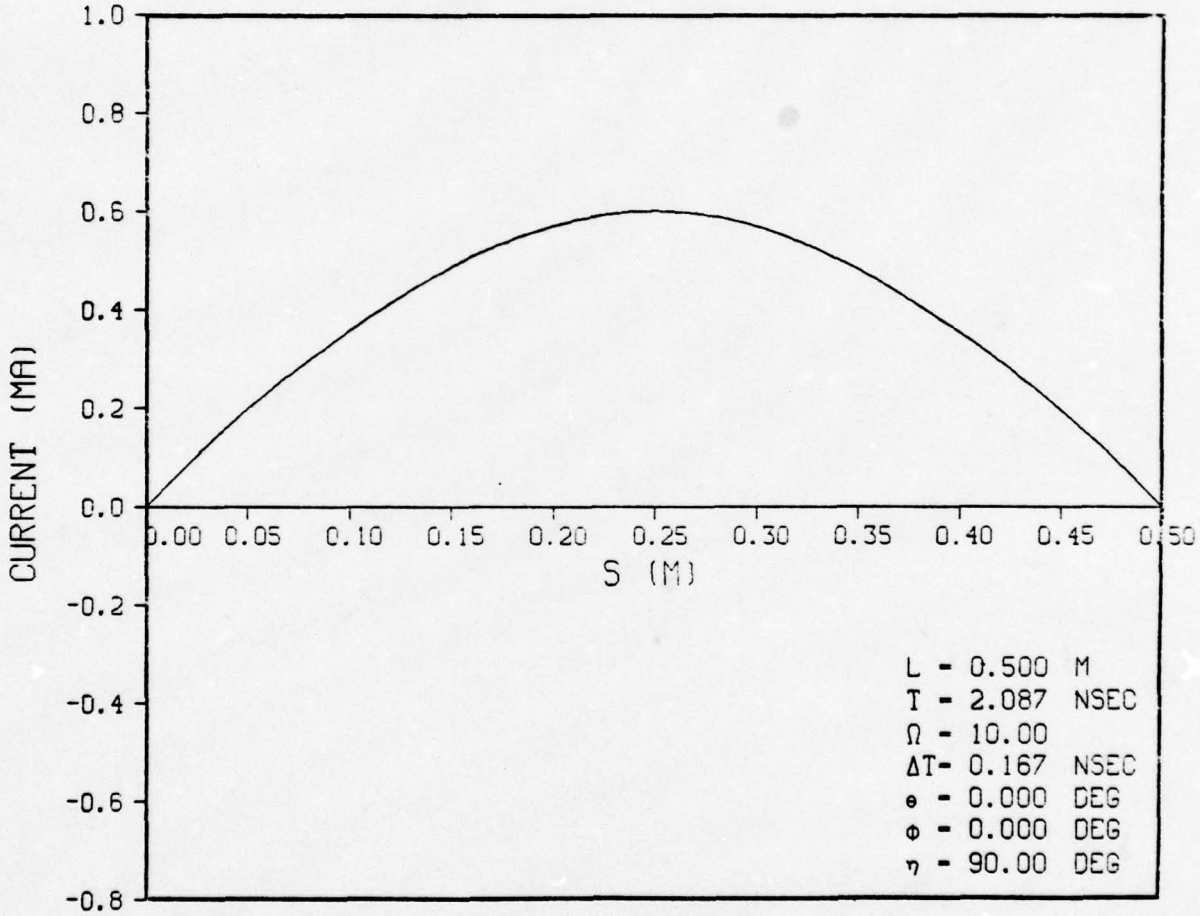

Figure 5-38. CURRENT DISTRIBUTION-GAUSSIAN PULSE

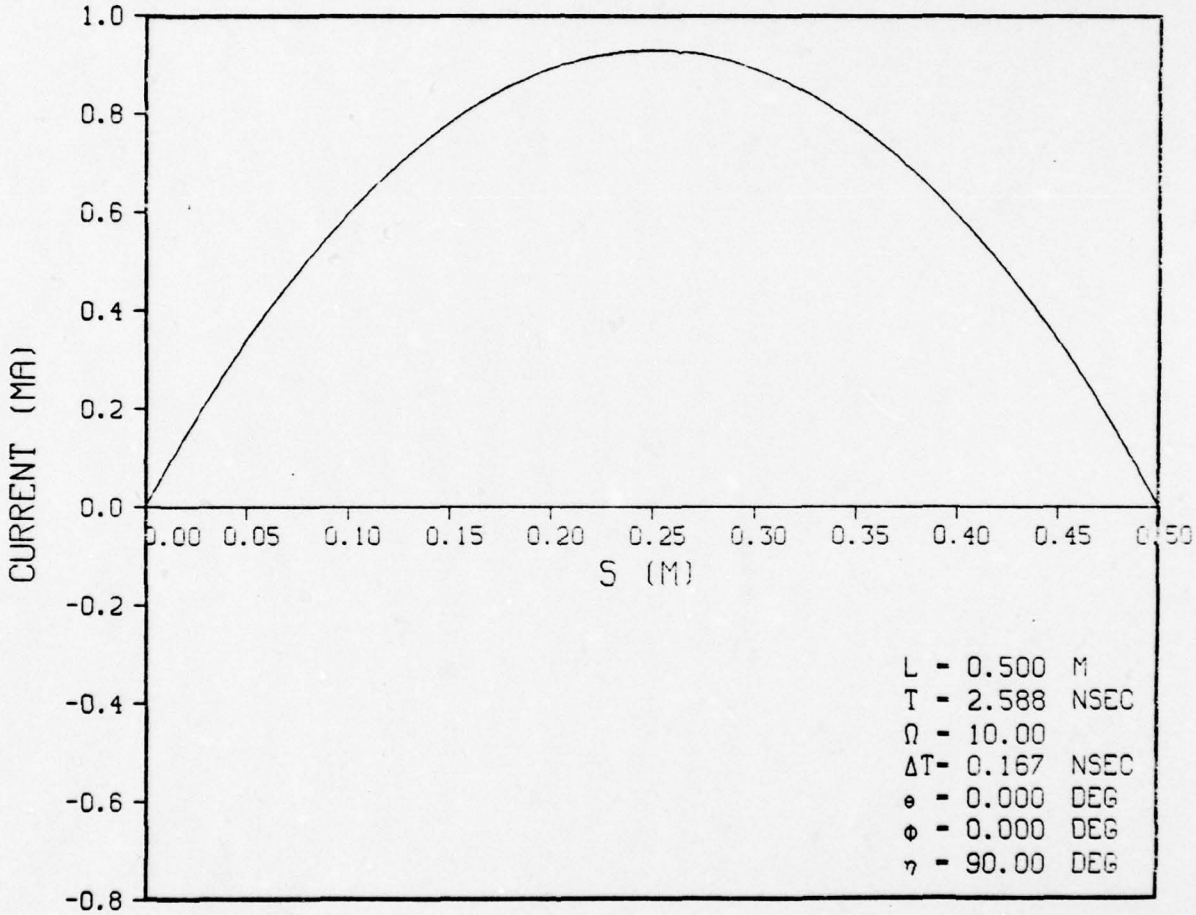

Figure 5-39. CURRENT DISTRIBUTION-GAUSSIAN PULSE

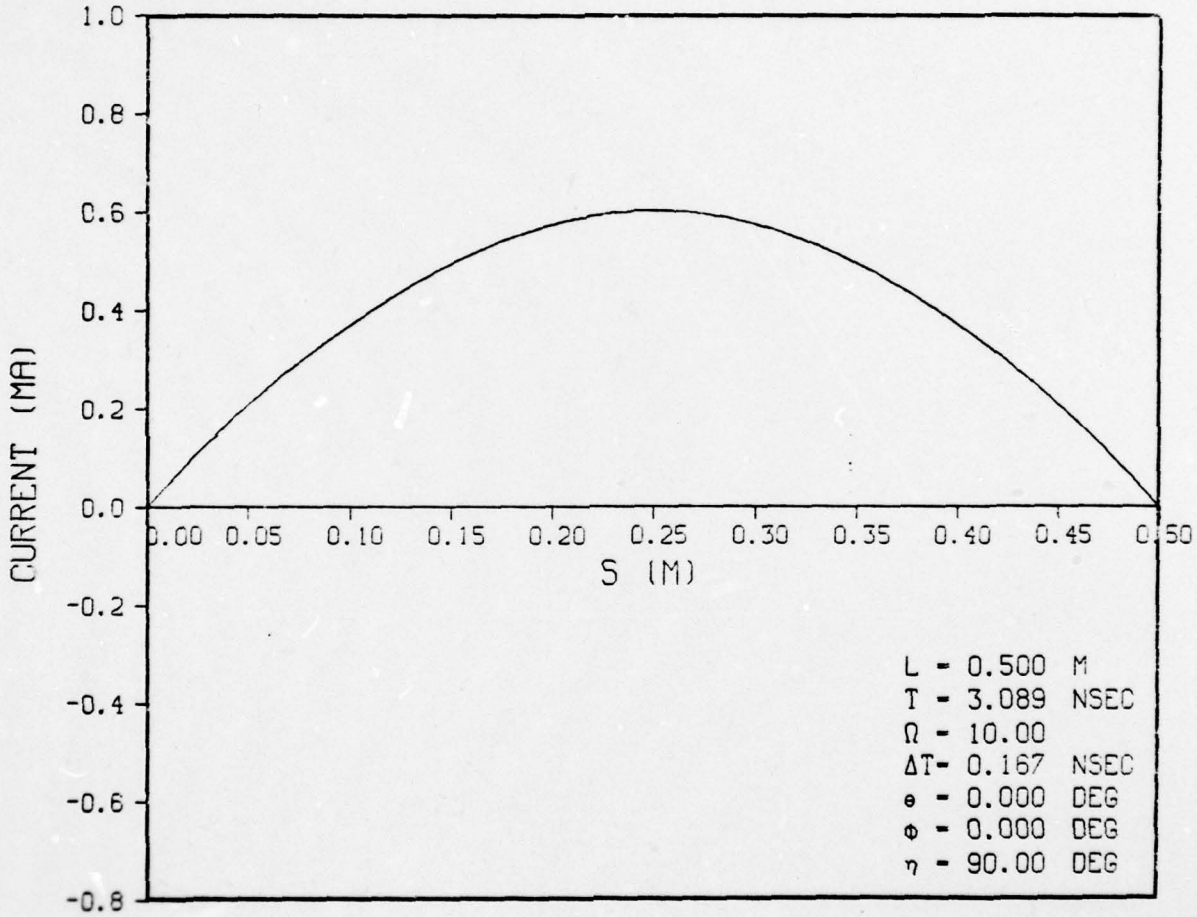

Figure 5-40. CURRENT DISTRIBUTION-GAUSSIAN PULSE

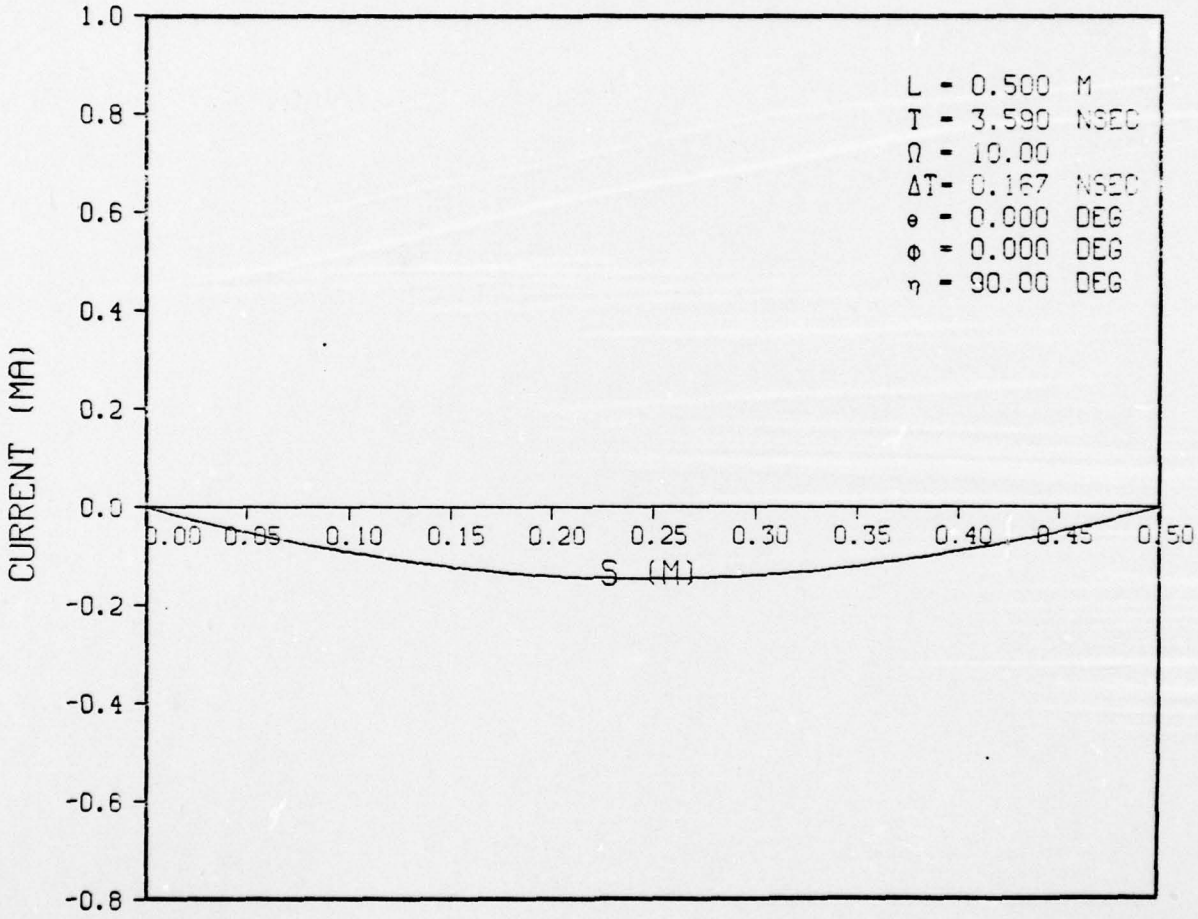

Figure 5-41. CURRENT DISTRIBUTION-GAUSSIAN PULSE

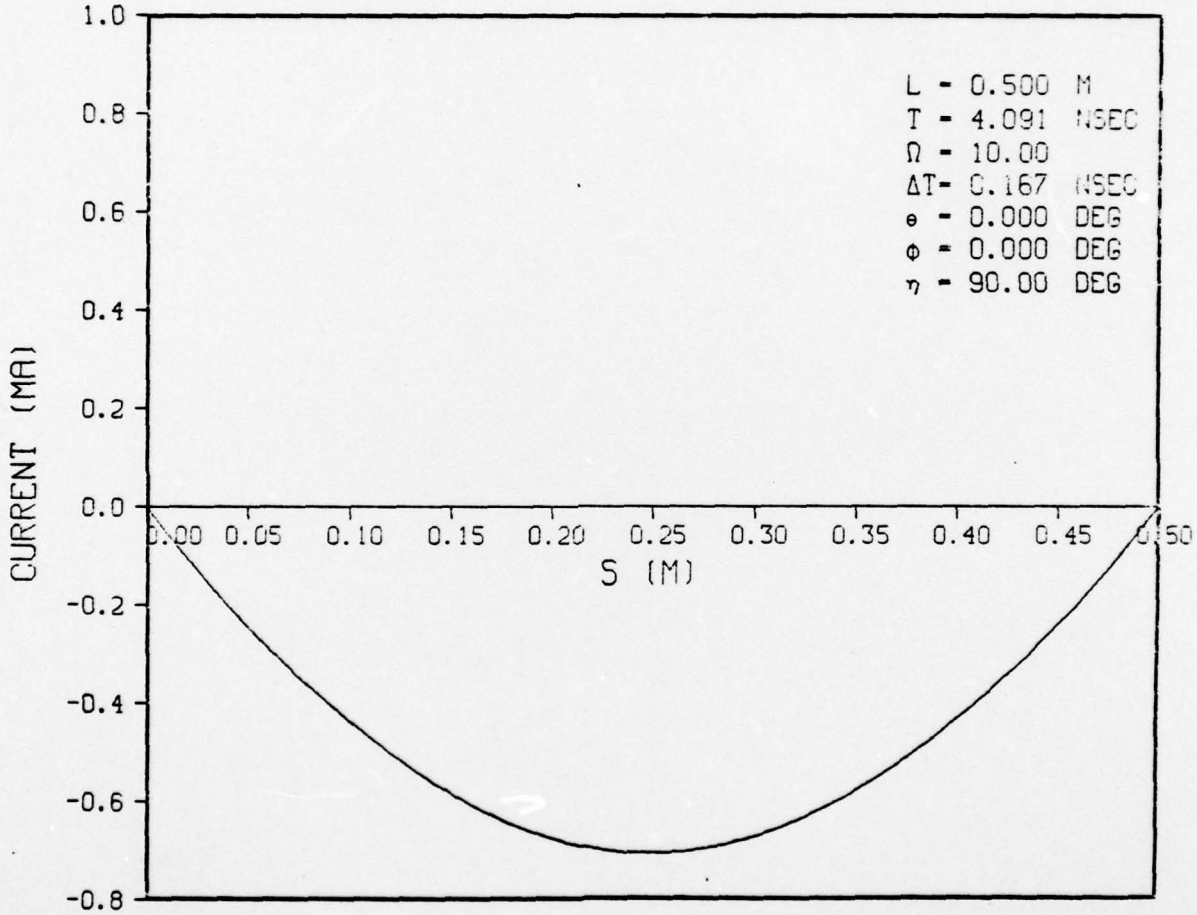

Figure 5-42. CURRENT DISTRIBUTION-GAUSSIAN PULSE

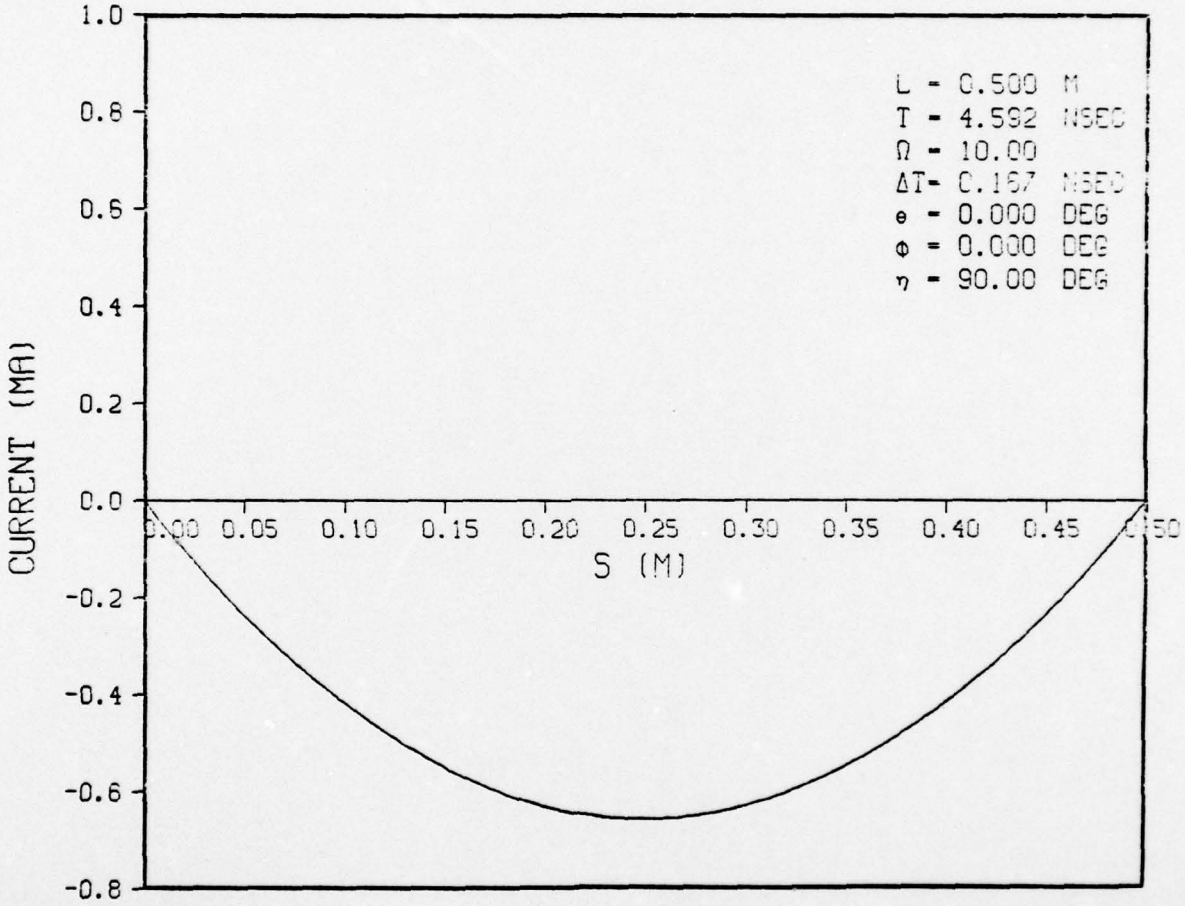

Figure 5-43. CURRENT DISTRIBUTION-GAUSSIAN PULSE

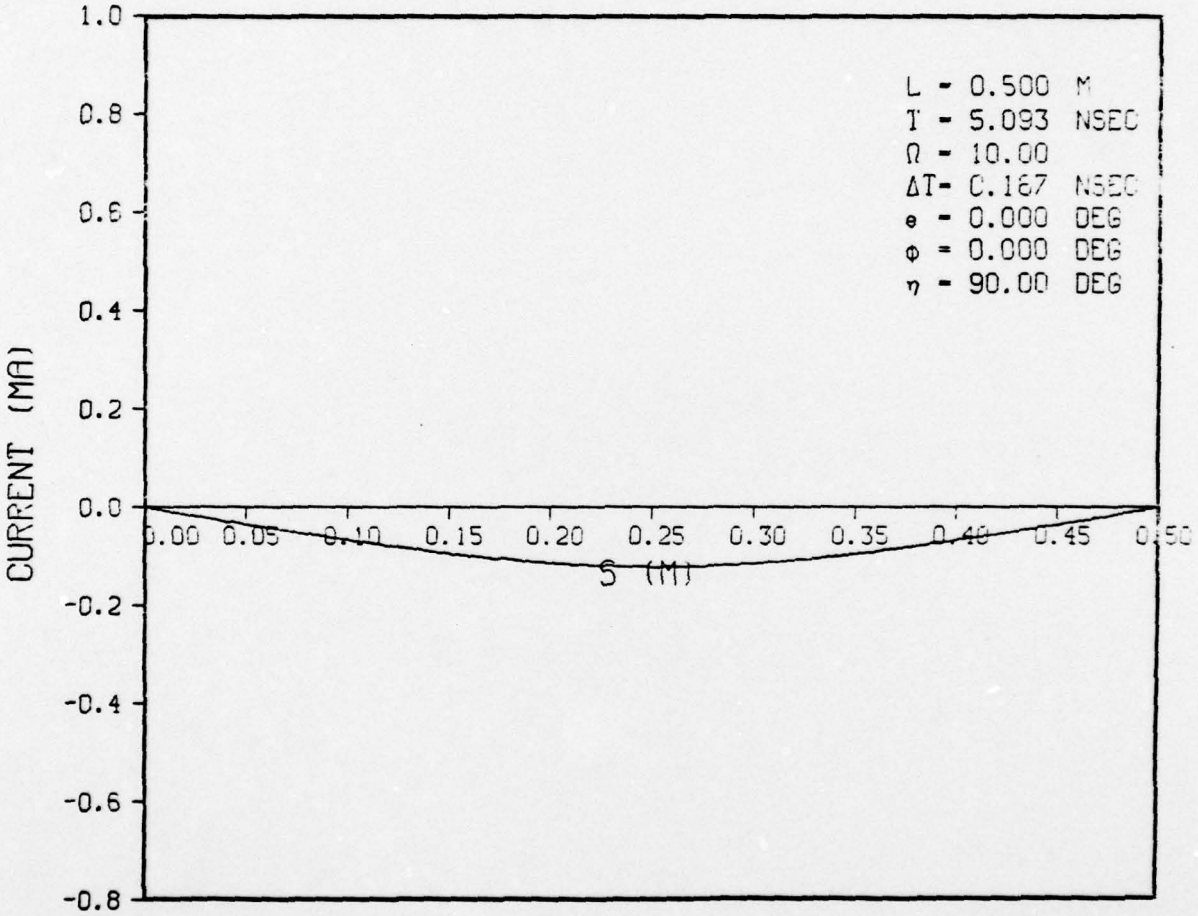

Figure 5-44. CURRENT DISTRIBUTION-GAUSSIAN PULSE

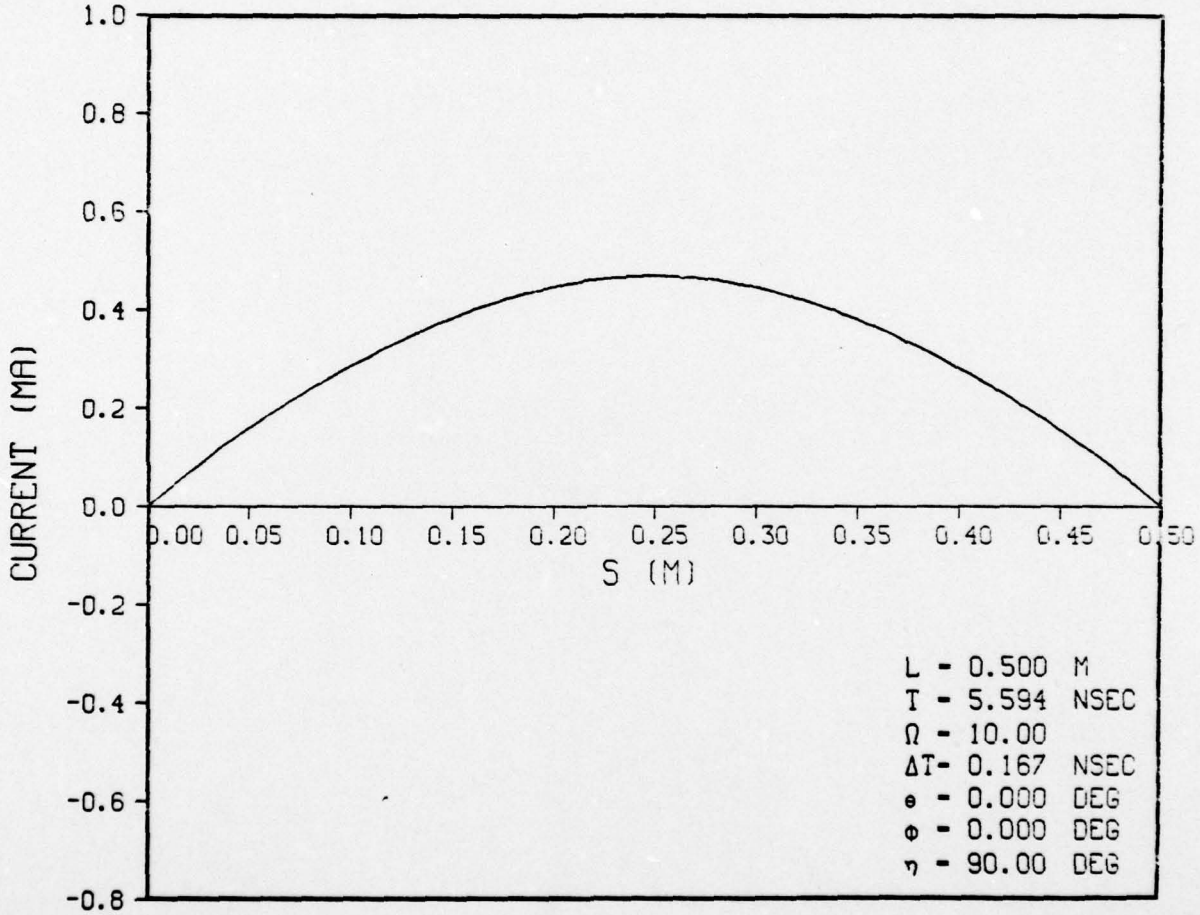

Figure 5-45. CURRENT DISTRIBUTION-GAUSSIAN PULSE

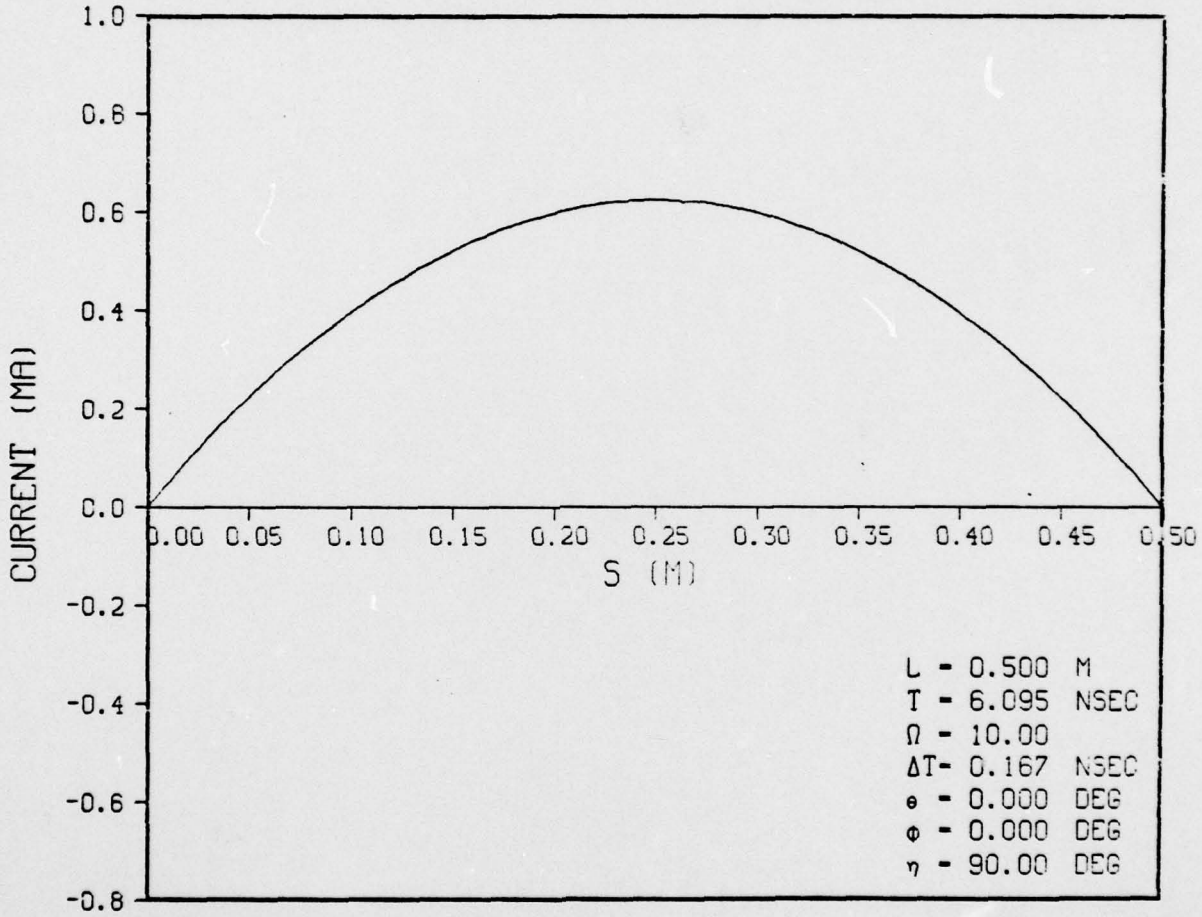

Figure 5-46. CURRENT DISTRIBUTION-GAUSSIAN PULSE

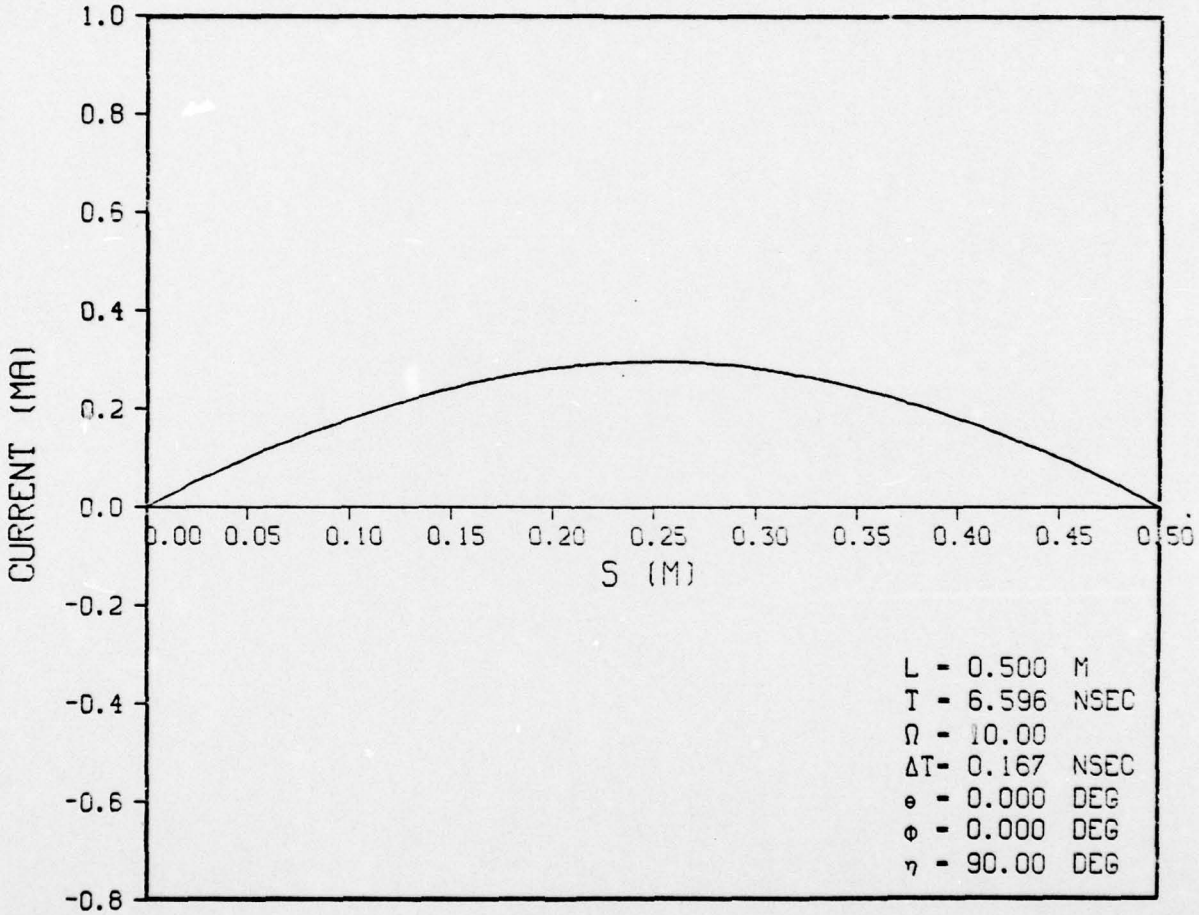

Figure 5-47. CURRENT DISTRIBUTION-GAUSSIAN PULSE

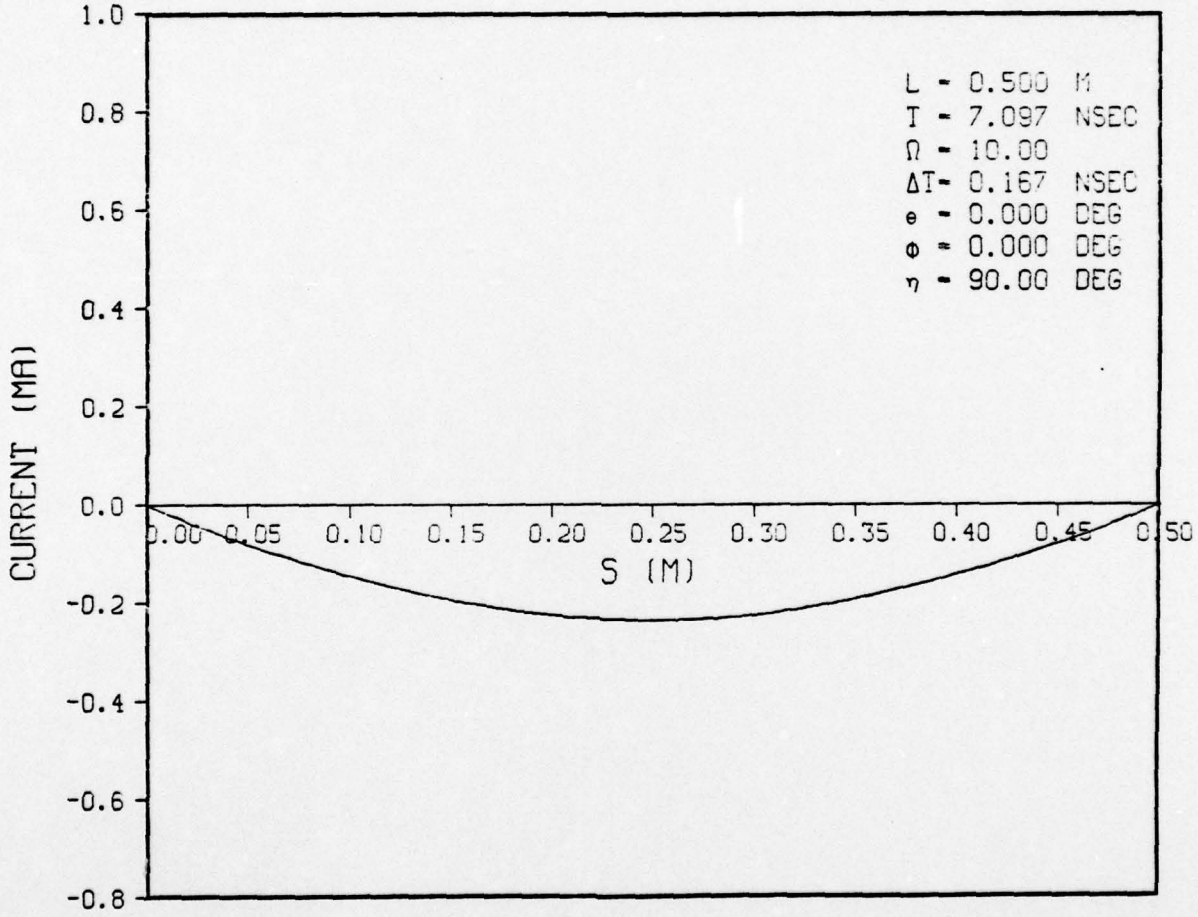

Figure 5-48. CURRENT DISTRIBUTION-GAUSSIAN PULSE

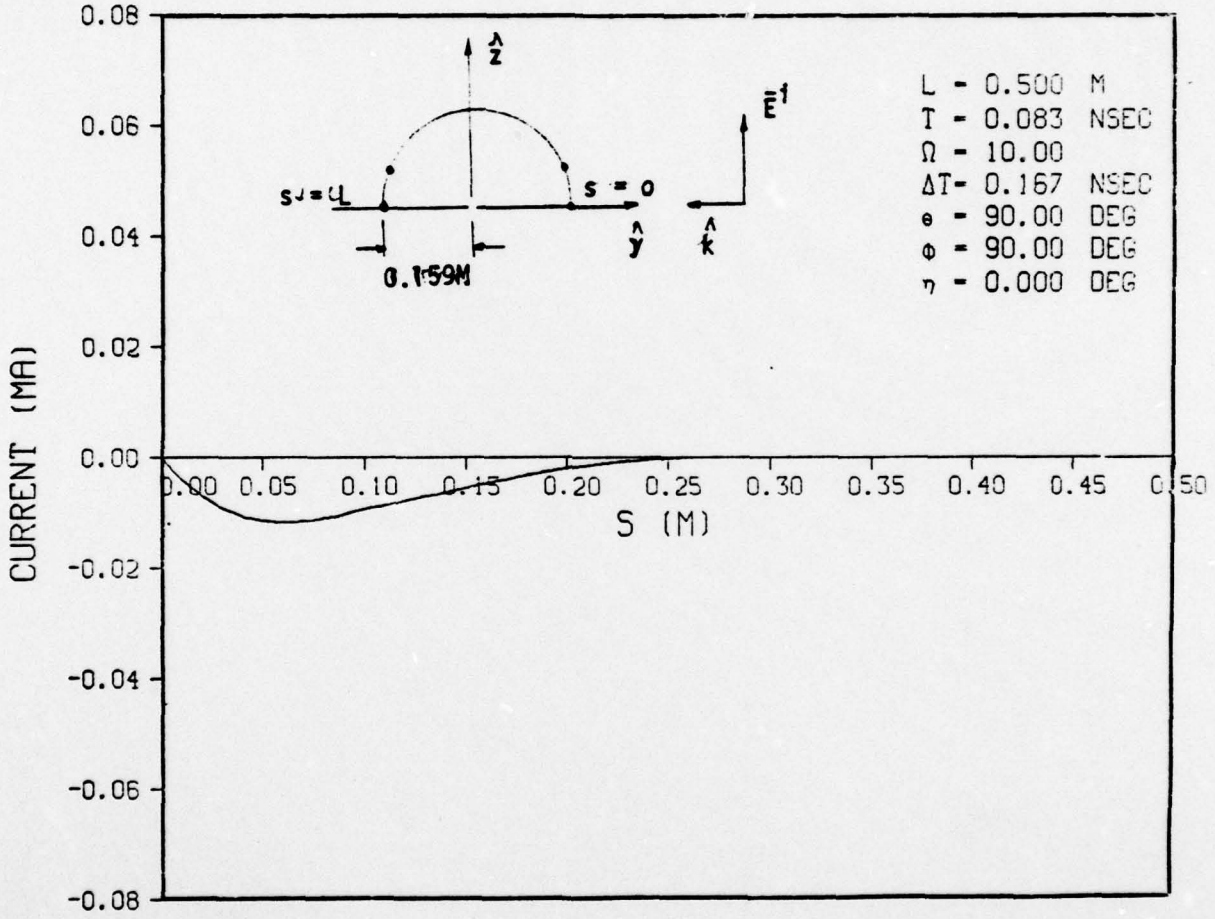

Figure 5-49. CURRENT DISTRIBUTION-DOUBLE EXPONENTIAL PULSE

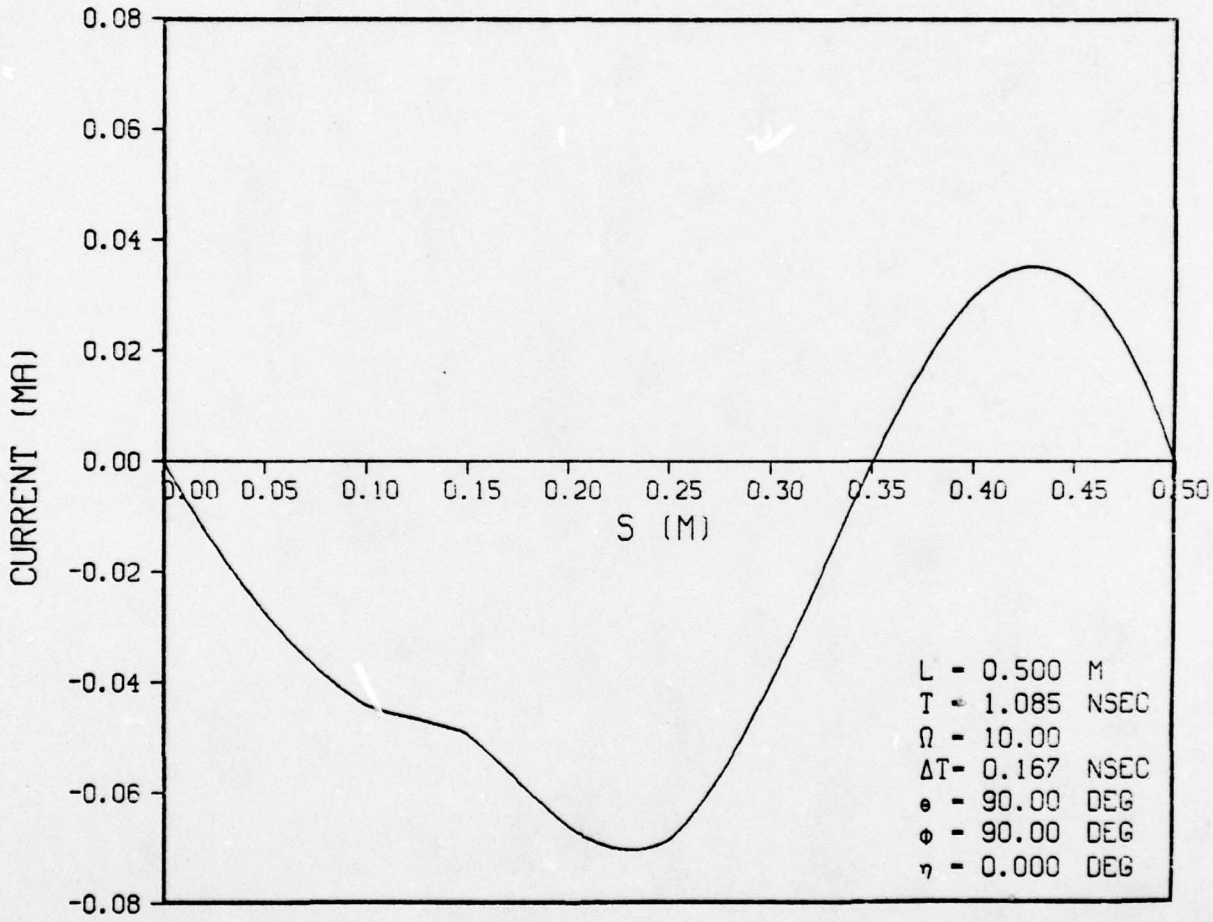

Figure 5-50. CURRENT DISTRIBUTION-DOUBLE EXPONENTIAL PULSE

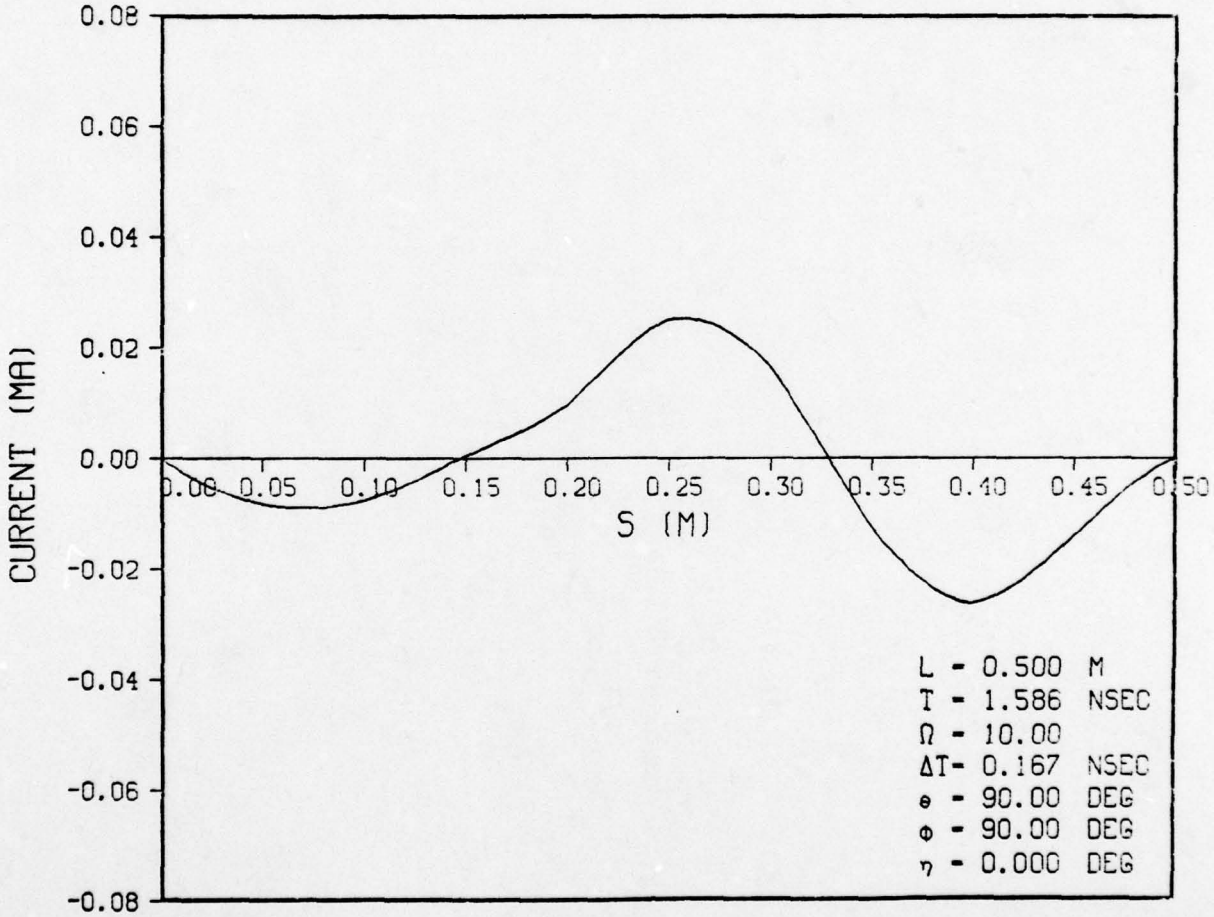

Figure 5-51. CURRENT DISTRIBUTION-DOUBLE EXPONENTIAL PULSE

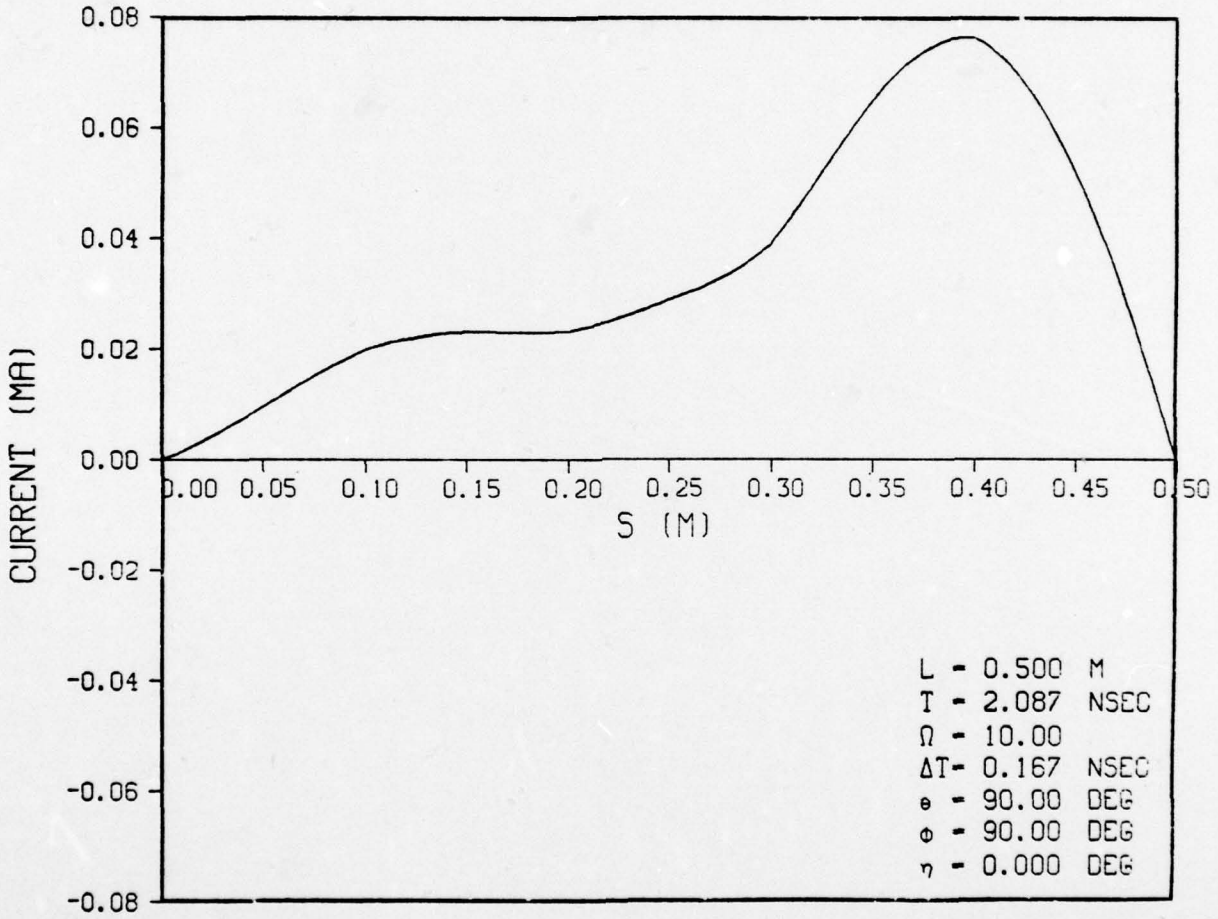

Figure 5-52. CURRENT DISTRIBUTION-DOUBLE EXPONENTIAL PULSE

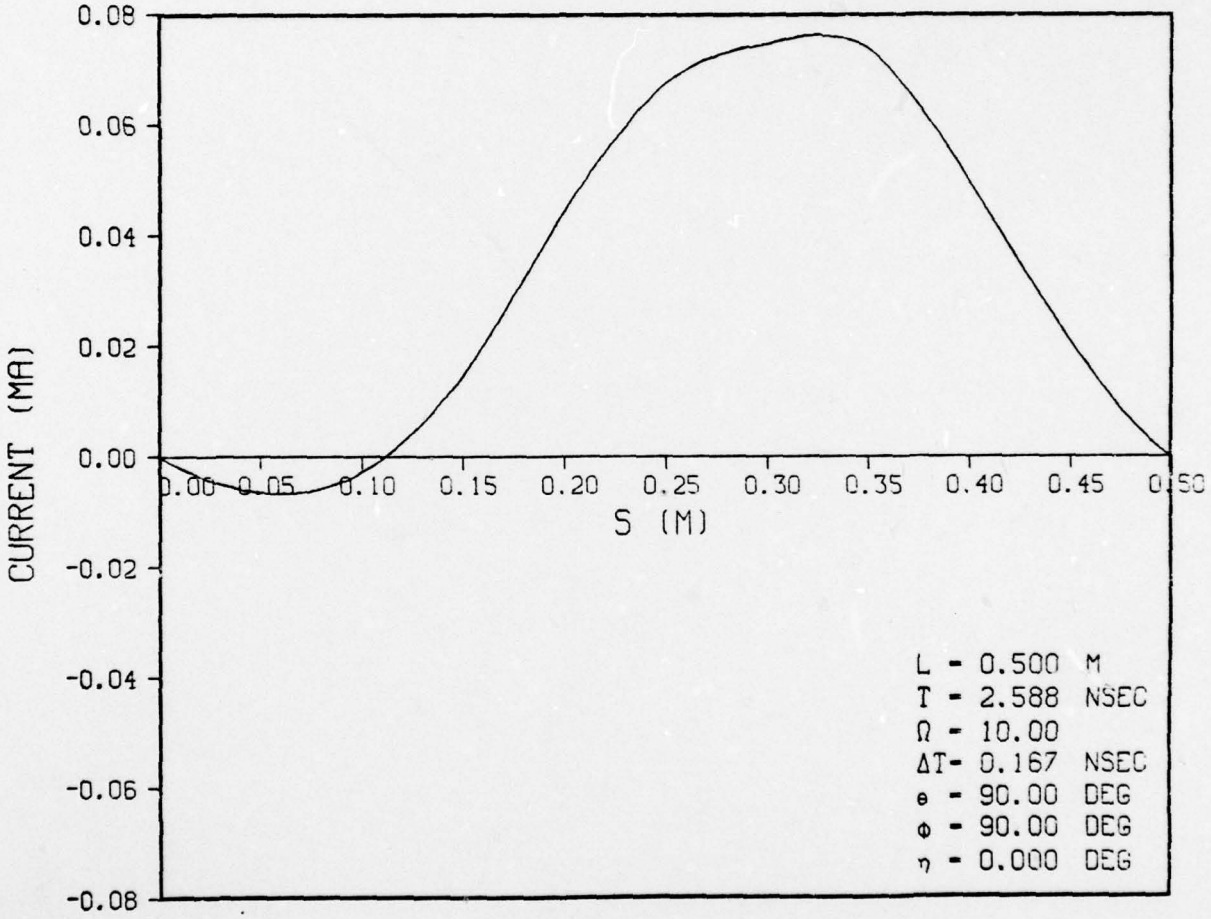

Figure 5-53. CURRENT DISTRIBUTION-DOUBLE EXPONENTIAL PULSE

AD-A078 682 TRW DEFENSE AND SPACE SYSTEMS GROUP REDONDO BEACH CA F/G 20/3
FINITE ELEMENT APPLICATION TO TRANSIENT SCATTERING PROBLEMS.(U)
OCT 79 A SANKAR , T C TONG F49620-78-C-0049
UNCLASSIFIED TRW-79-002-AFOSR AFOSR-TR-79-1302 NL

2 OF 2
AD
A078682

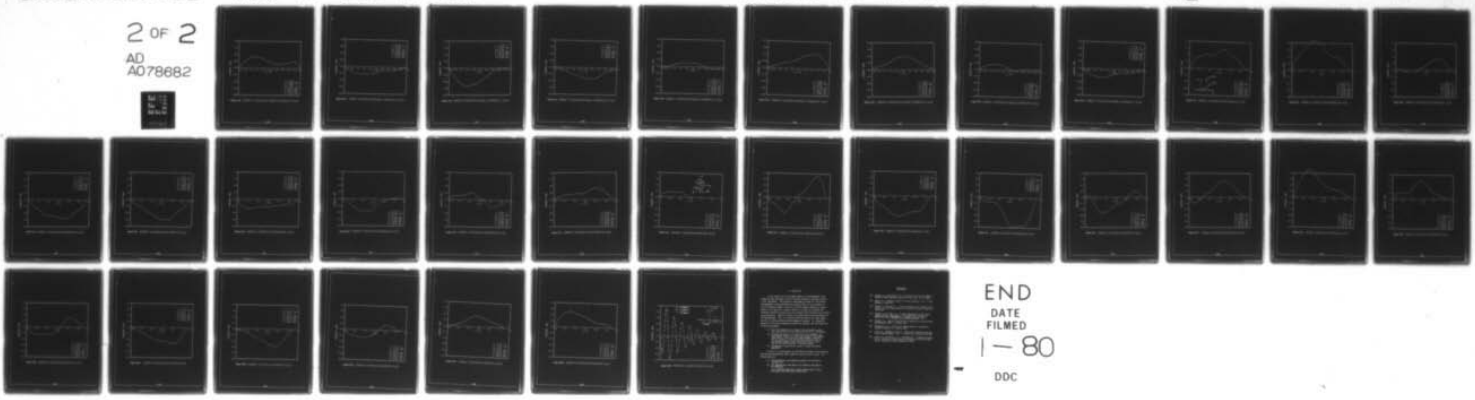

END
DATE
FILMED
1-80
DDC

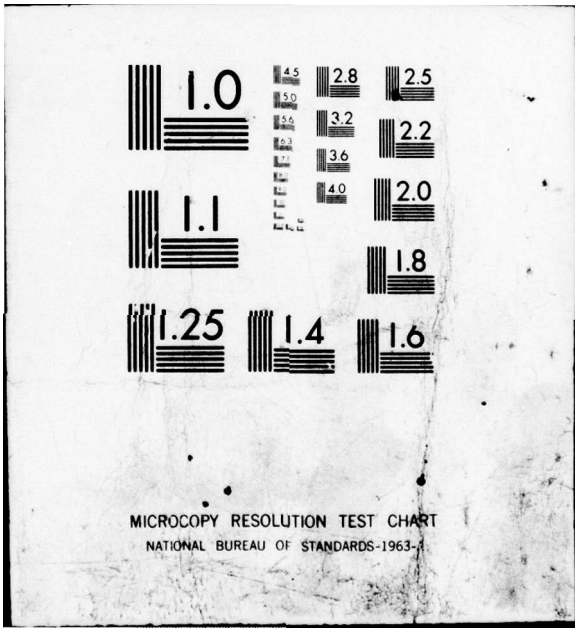
1.0
1.1
1.25
1.4
1.6
1.8
2.0
2.2
2.5
2.8
3.2
3.6
4.0
4.5
5.0
5.6
MICROCOPY RESOLUTION TEST CHART
NATIONAL BUREAU OF STANDARDS-1963-A

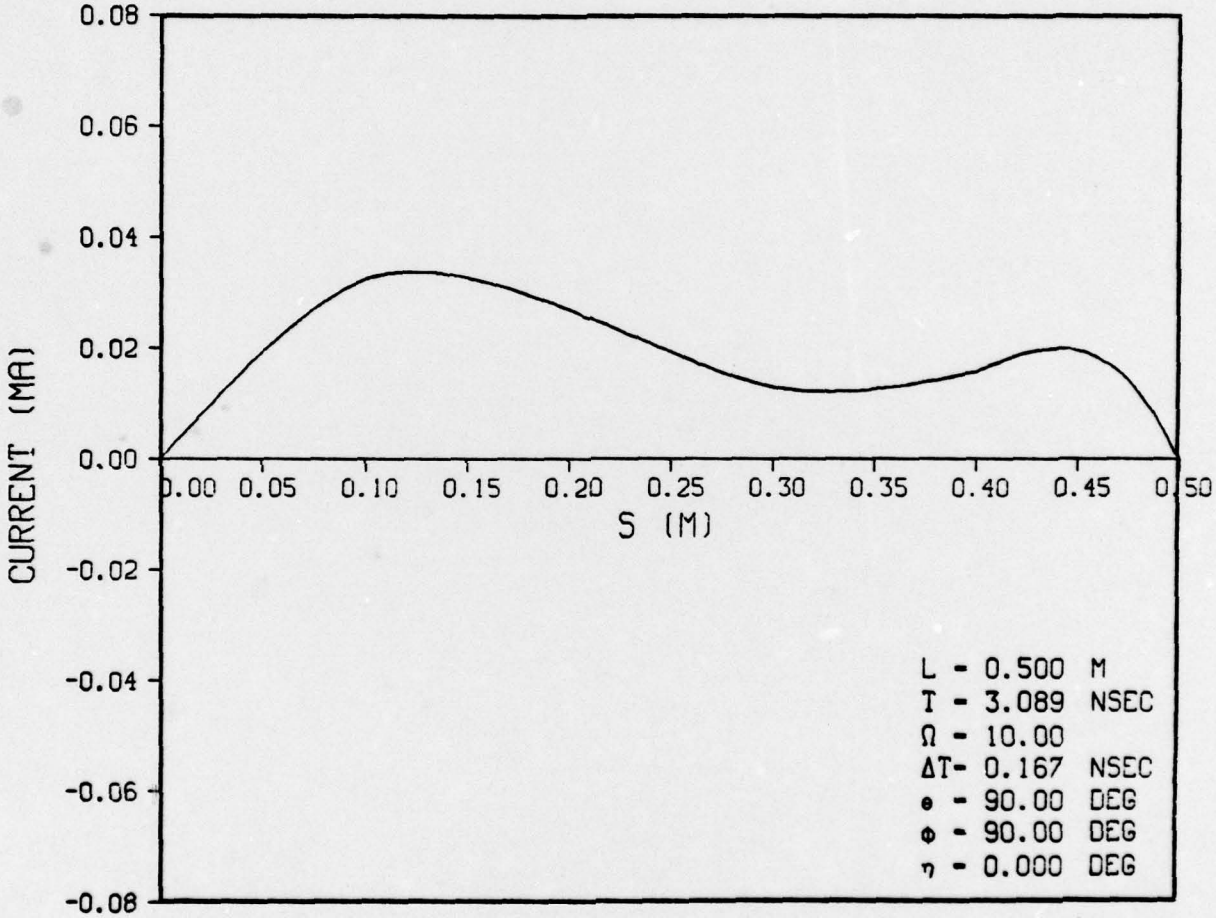

Figure 5-54. CURRENT DISTRIBUTION-DOUBLE EXPONENTIAL PULSE

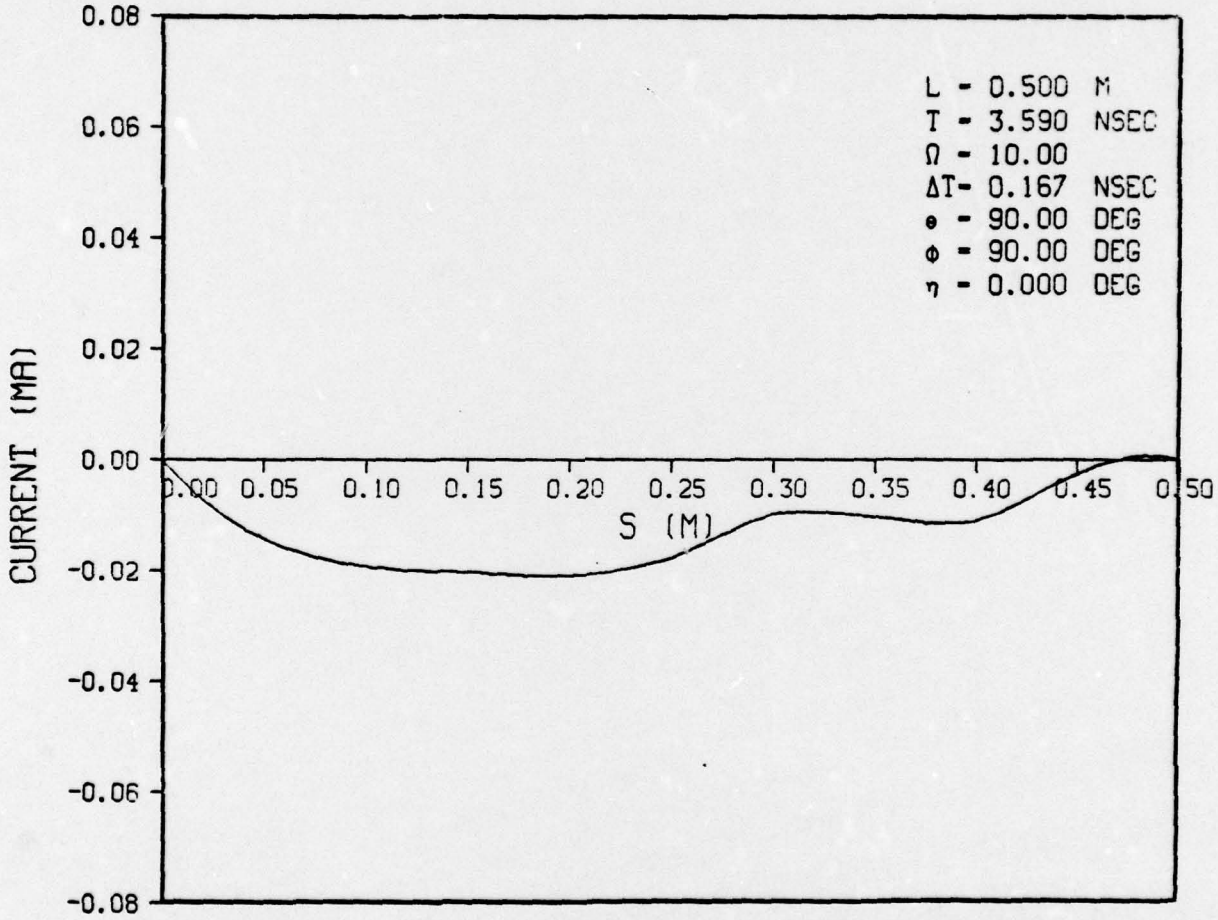

Figure 5-55. CURRENT DISTRIBUTION-DOUBLE EXPONENTIAL PULSE

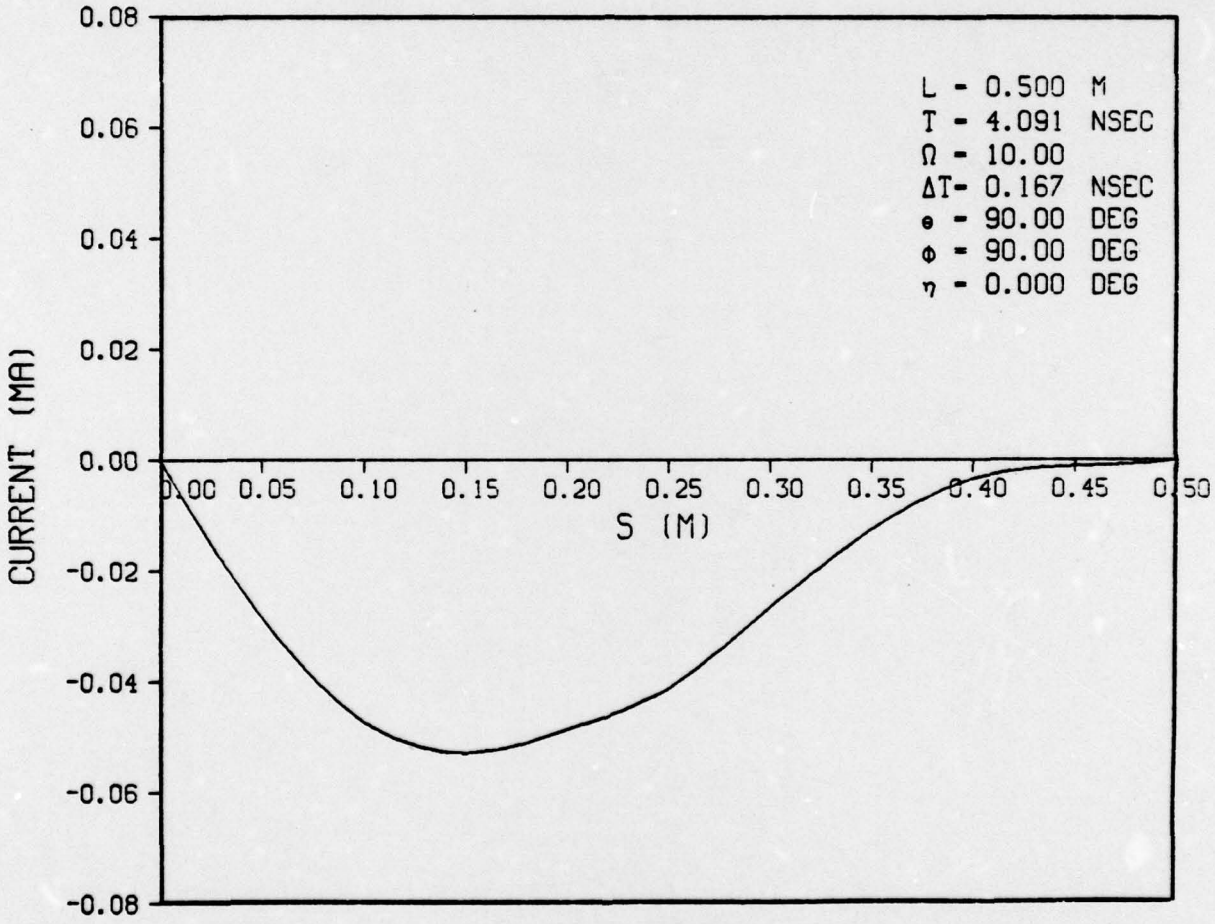

Figure 5-56. CURRENT DISTRIBUTION-DOUBLE EXPONENTIAL PULSE

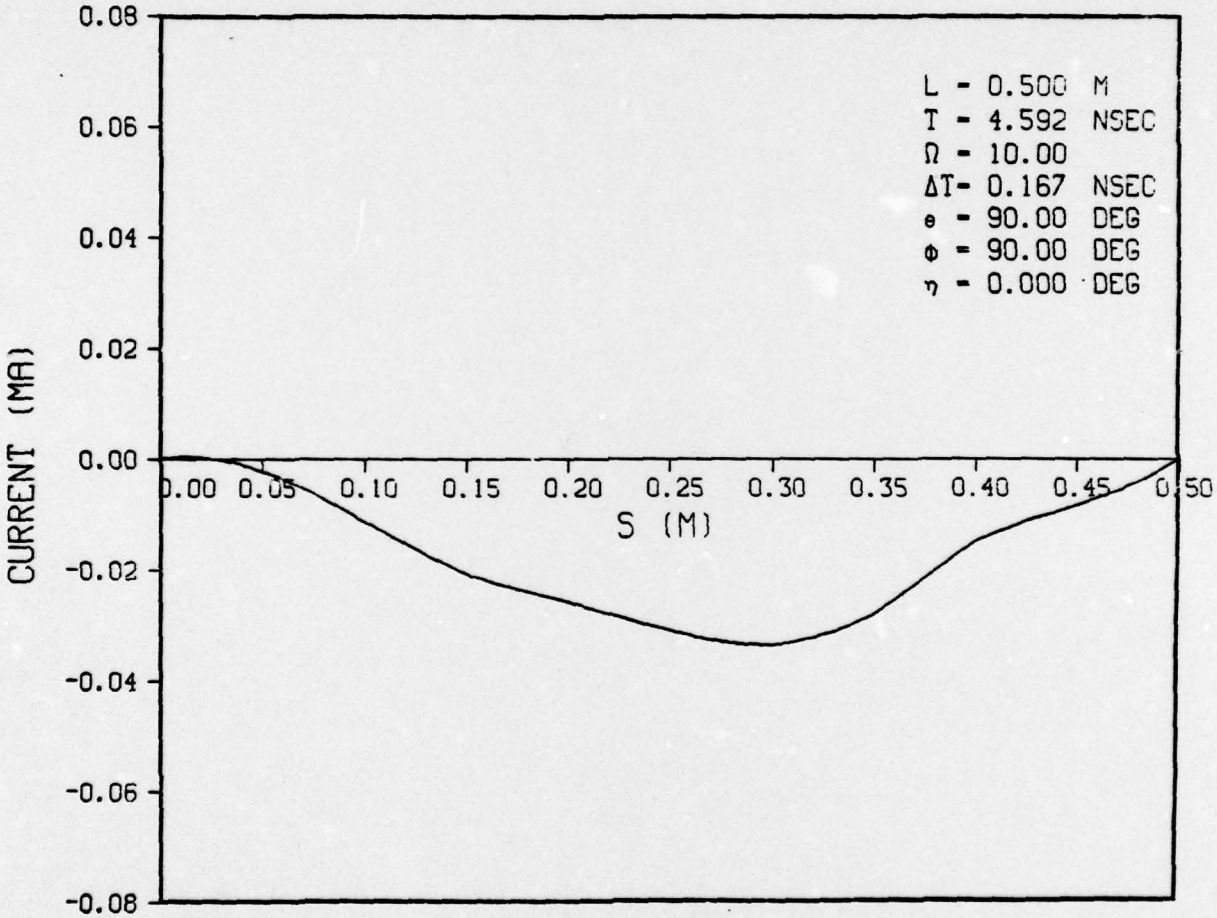

Figure 5-57. CURRENT DISTRIBUTION-DOUBLE EXPONENTIAL PULSE

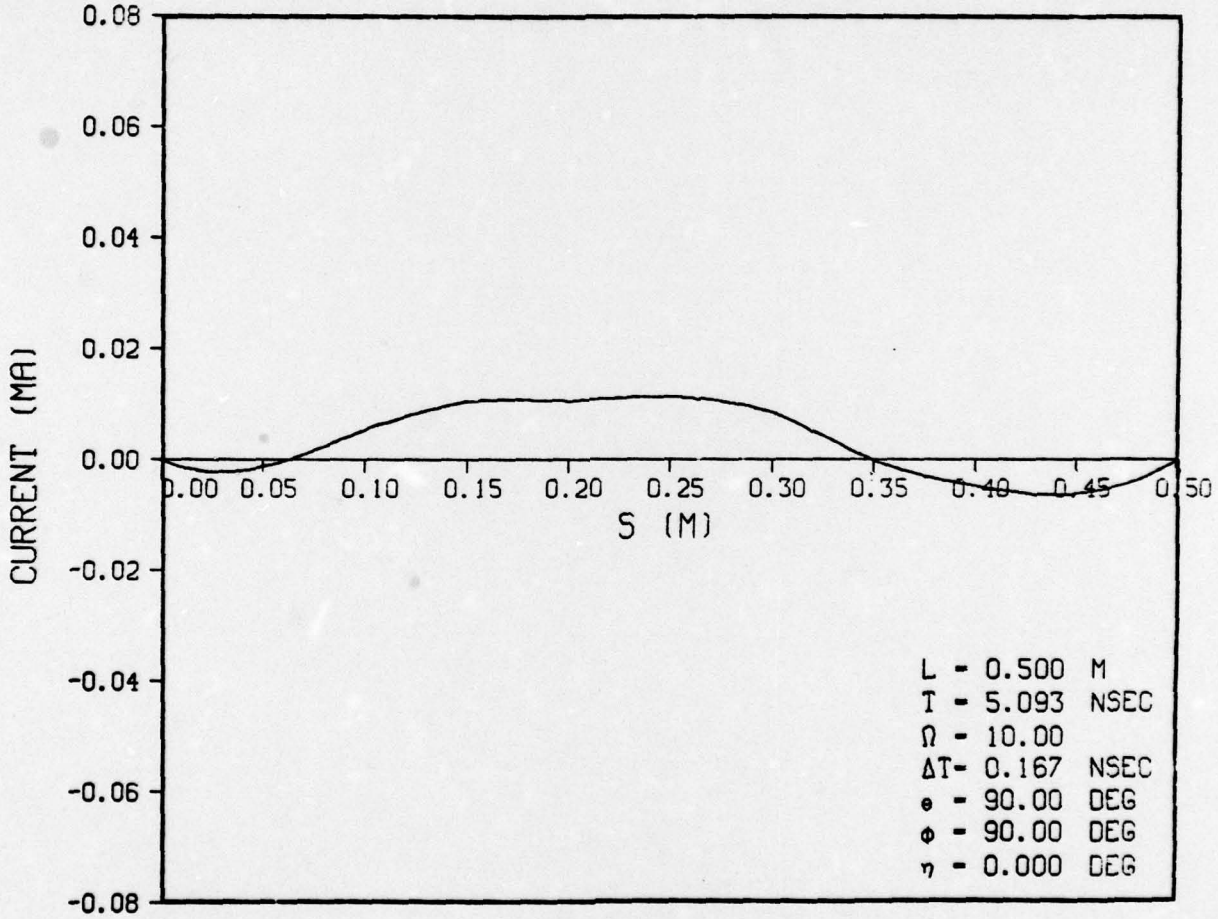

Figure 5-58. CURRENT DISTRIBUTION-DOUBLE EXPONENTIAL PULSE

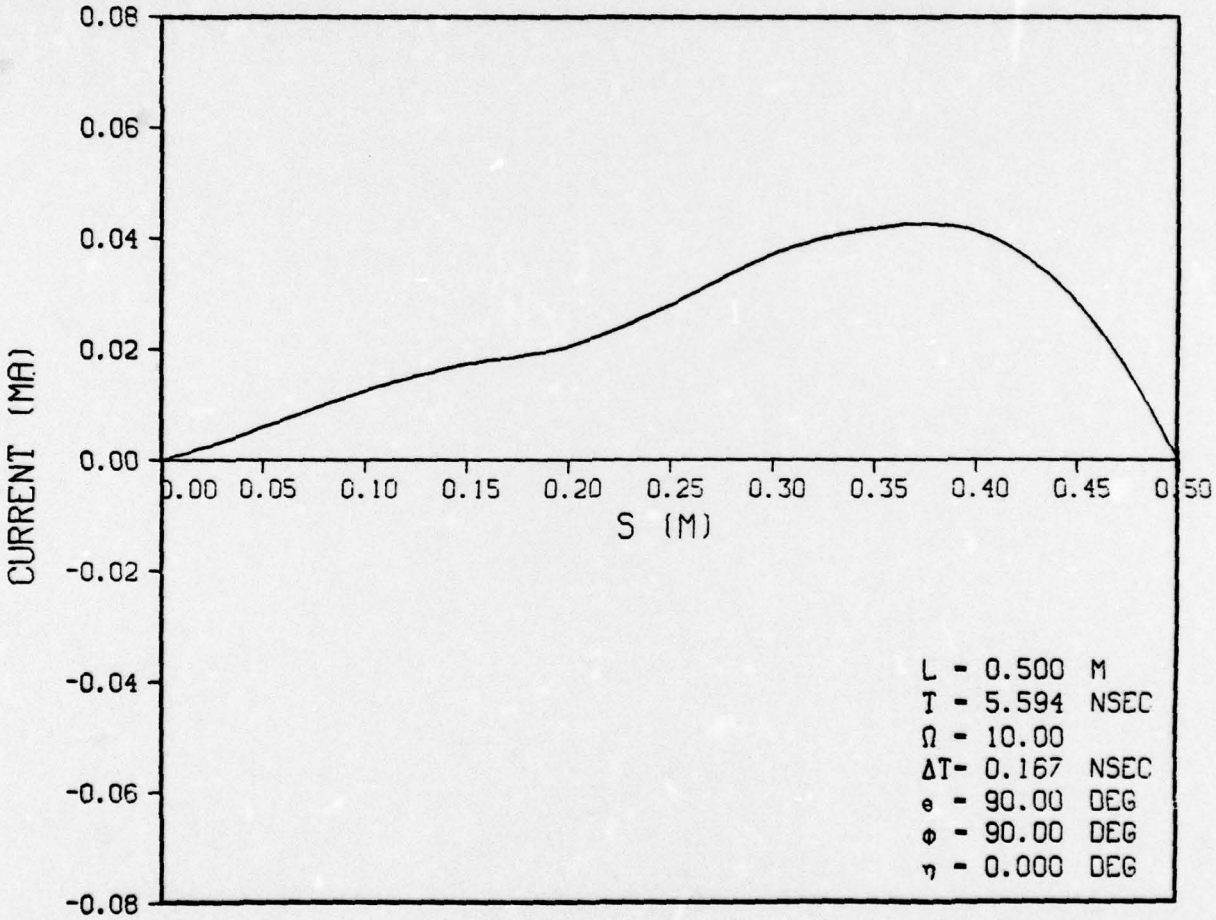

Figure 5-59. CURRENT DISTRIBUTION-DOUBLE EXPONENTIAL PULSE

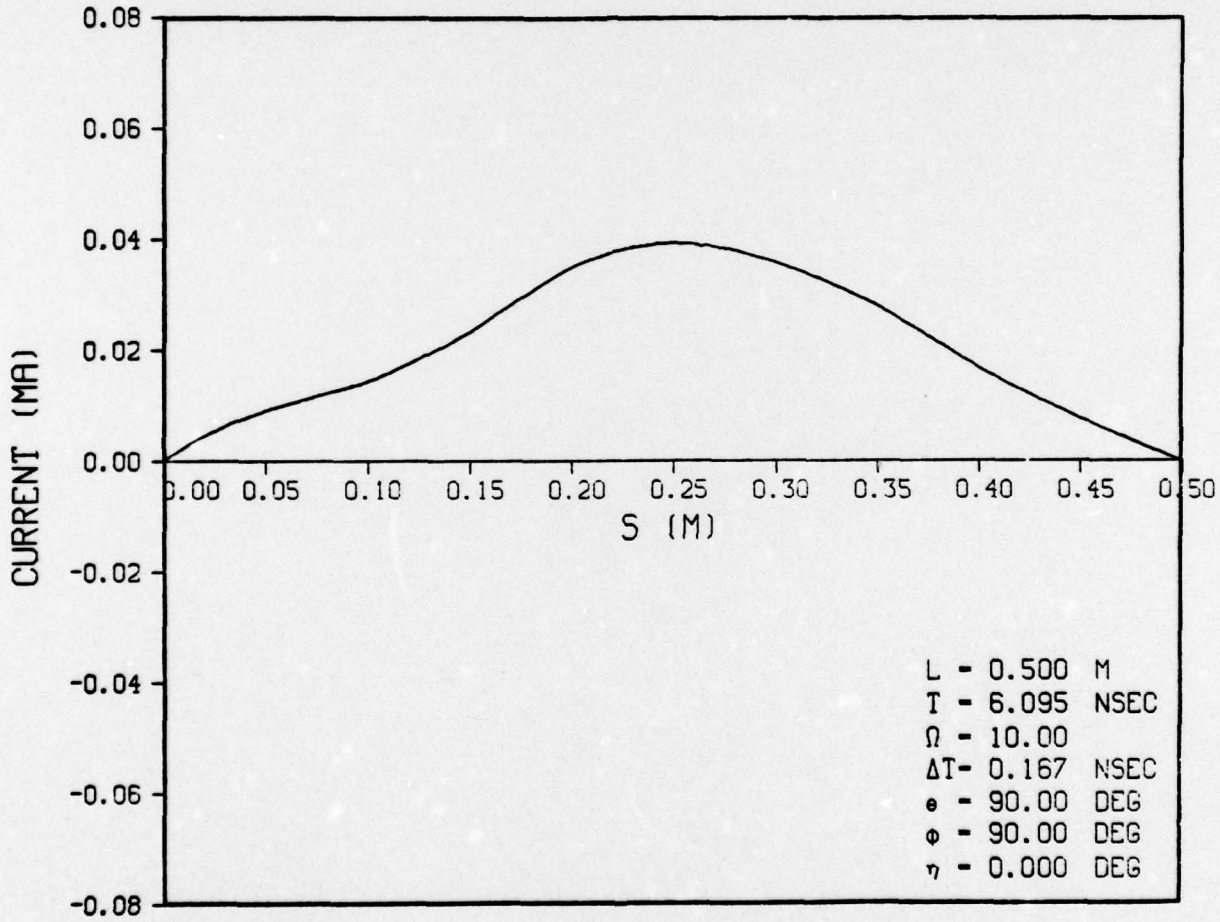

Figure 5-60. CURRENT DISTRIBUTION-DOUBLE EXPONENTIAL PULSE

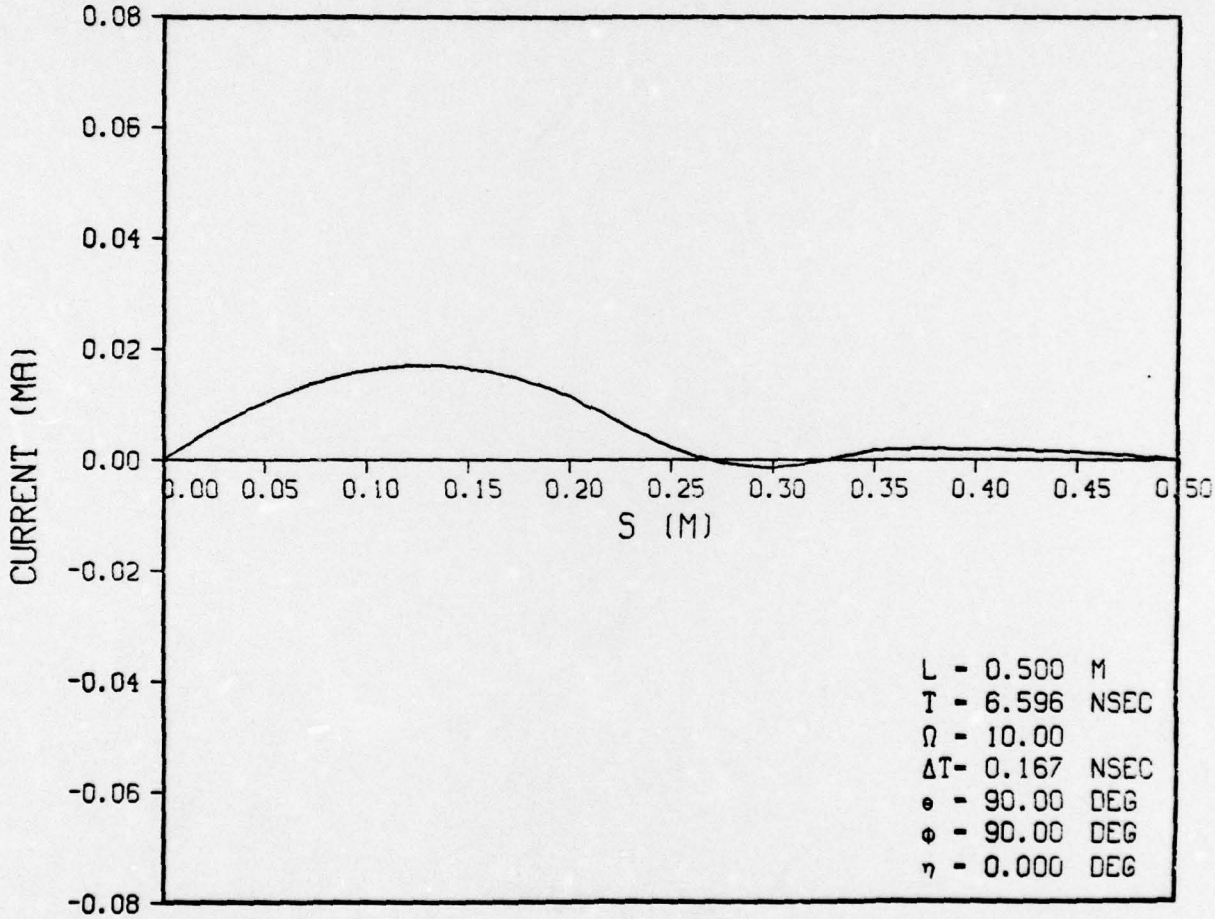

Figure 5-61. CURRENT DISTRIBUTION-DOUBLE EXPONENTIAL PULSE

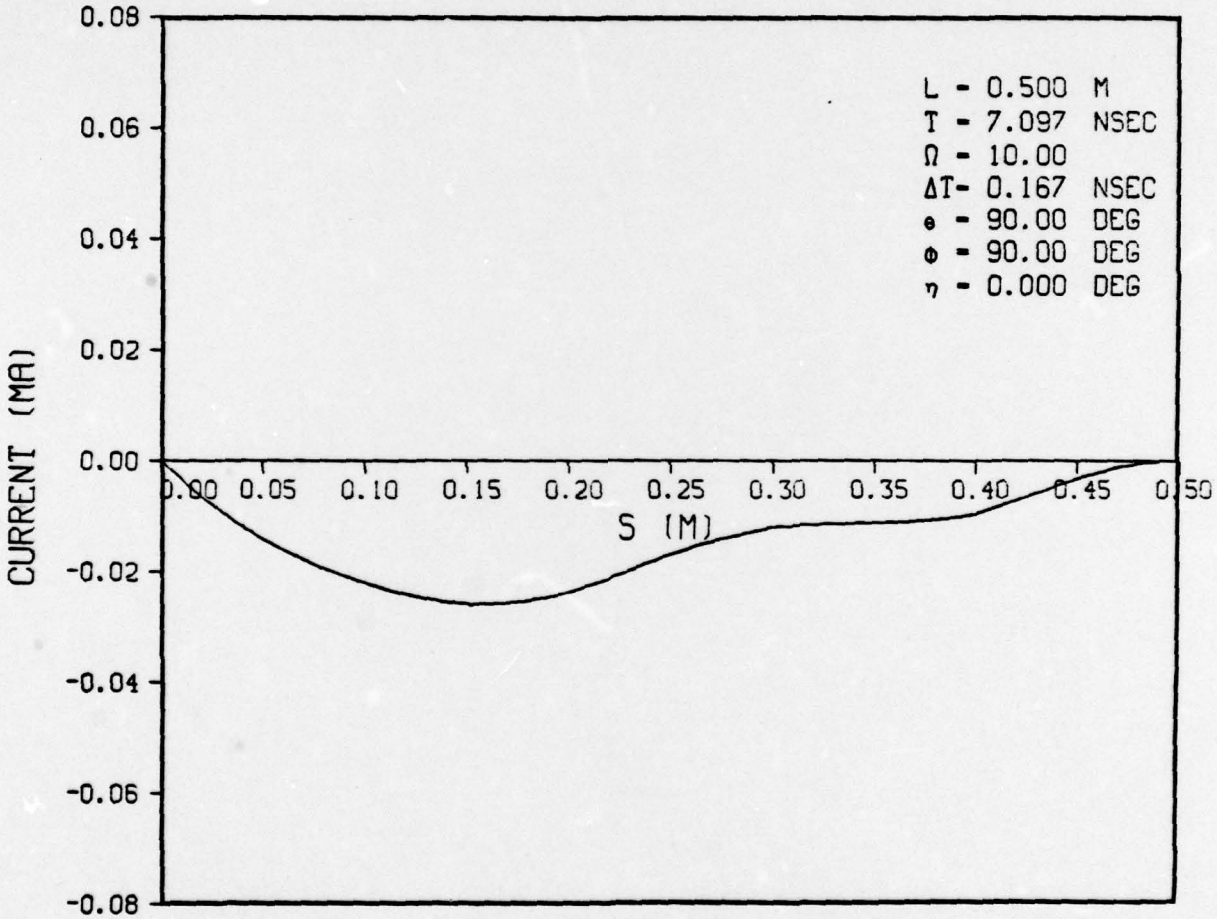

Figure 5-62. CURRENT DISTRIBUTION-DOUBLE EXPONENTIAL PULSE

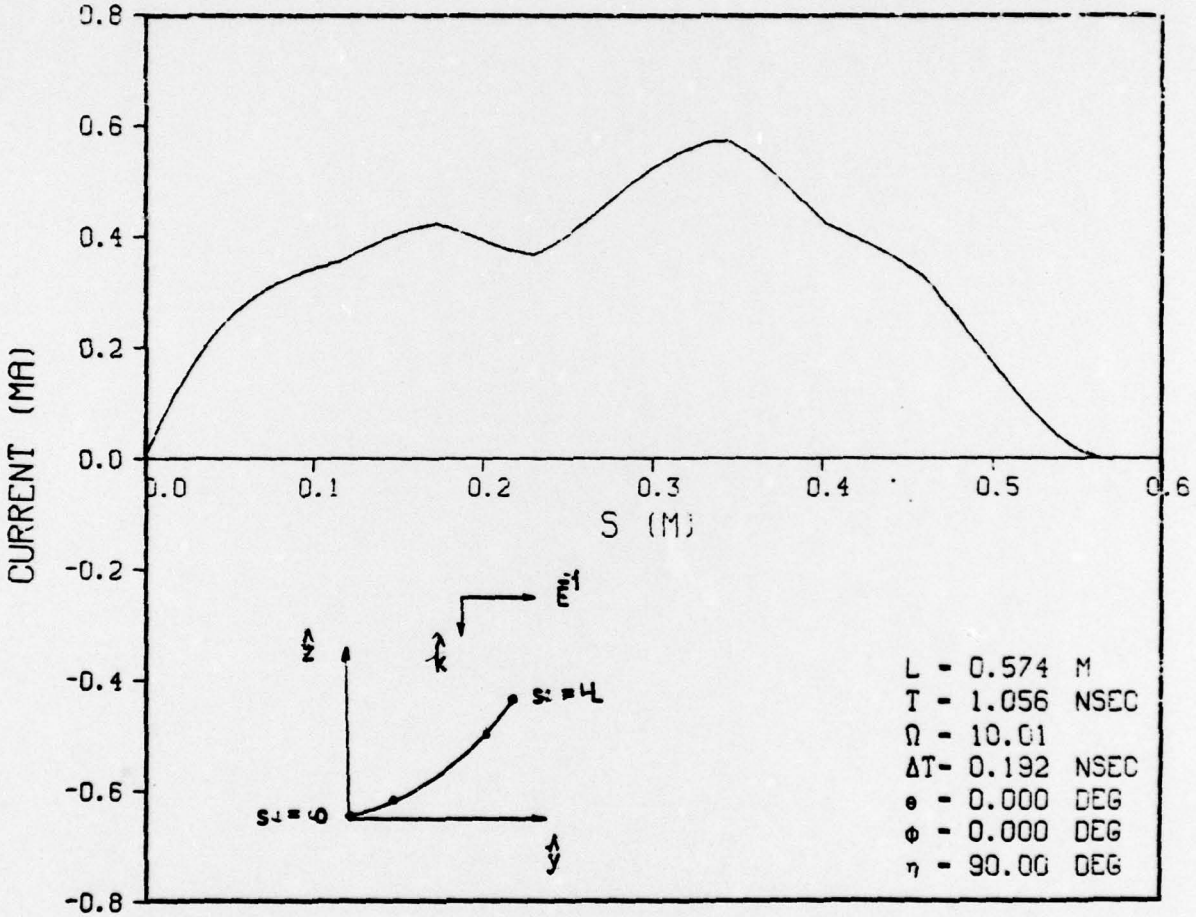

Figure 5-63. CURRENT DISTRIBUTION-RECTANGULAR PULSE

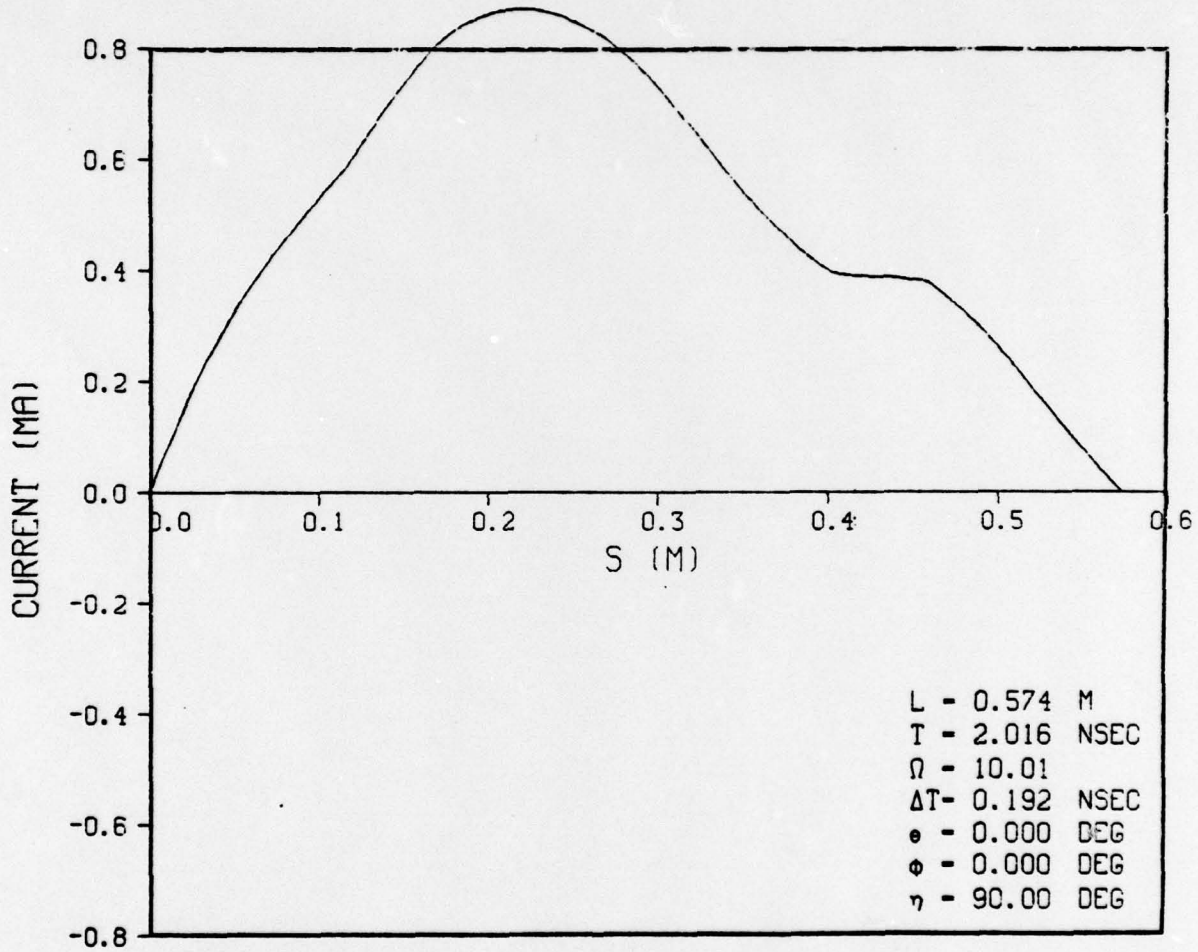

Figure 5-64. CURRENT DISTRIBUTION-RECTANGULAR PULSE

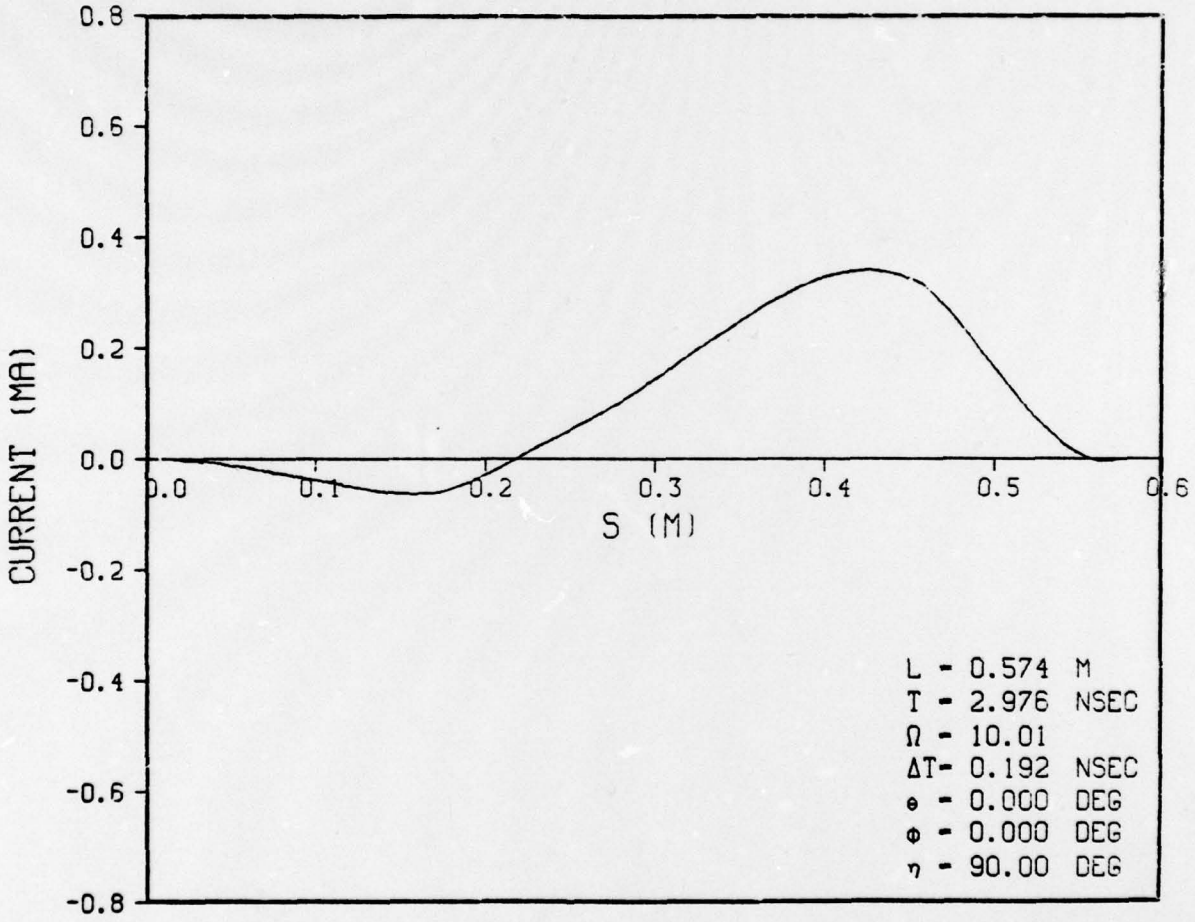

Figure 5-65. CURRENT DISTRIBUTION-RECTANGULAR PULSE

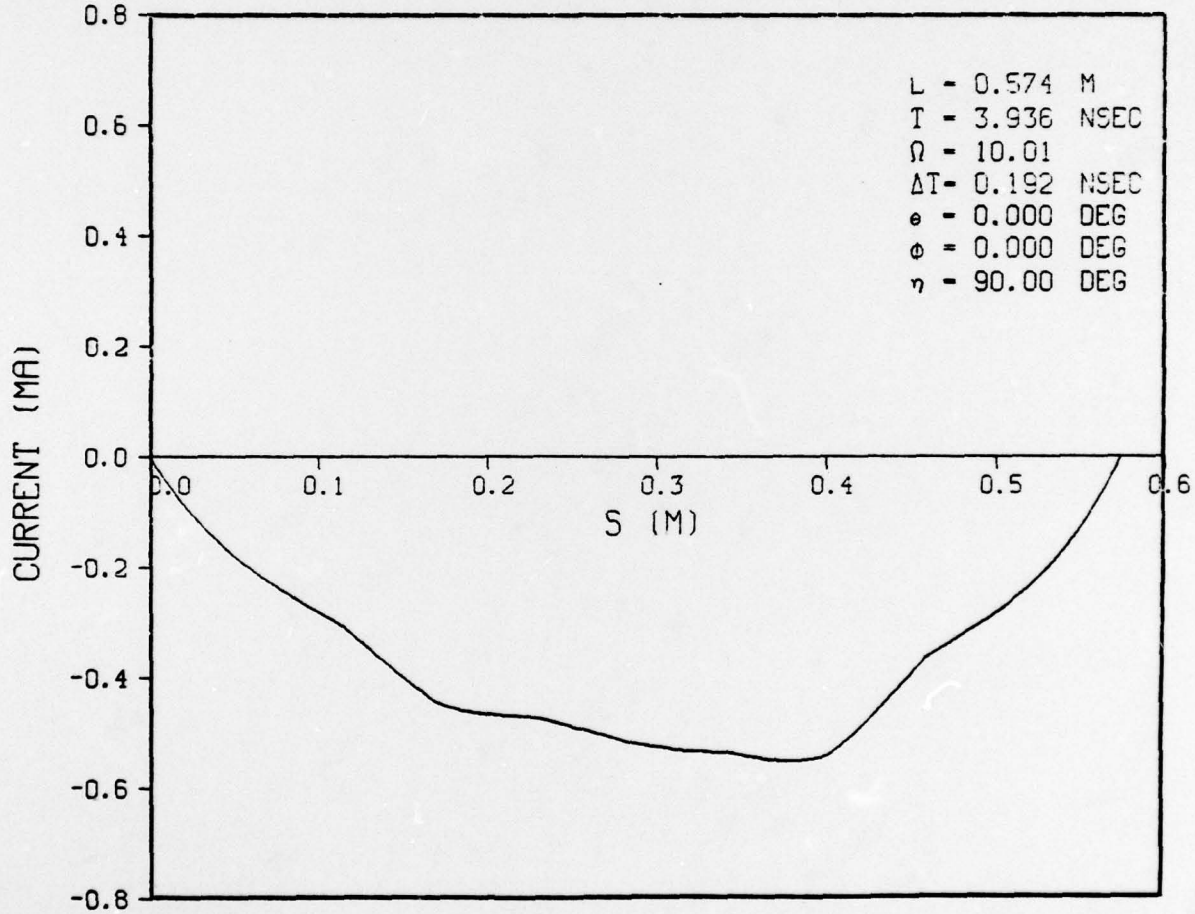

Figure 5-66. CURRENT DISTRIBUTION-RECTANGULAR PULSE

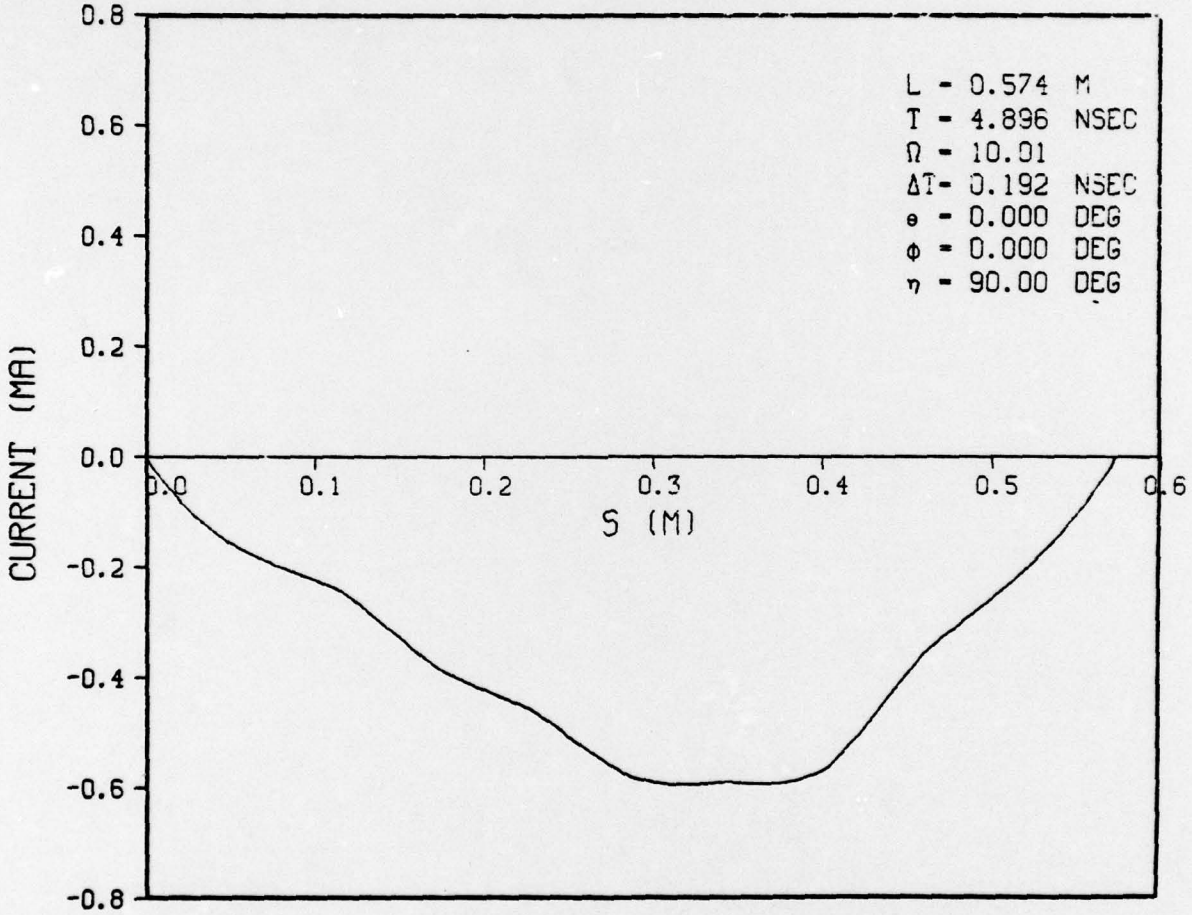

Figure 5-67. CURRENT DISTRIBUTION-RECTANGULAR PULSE

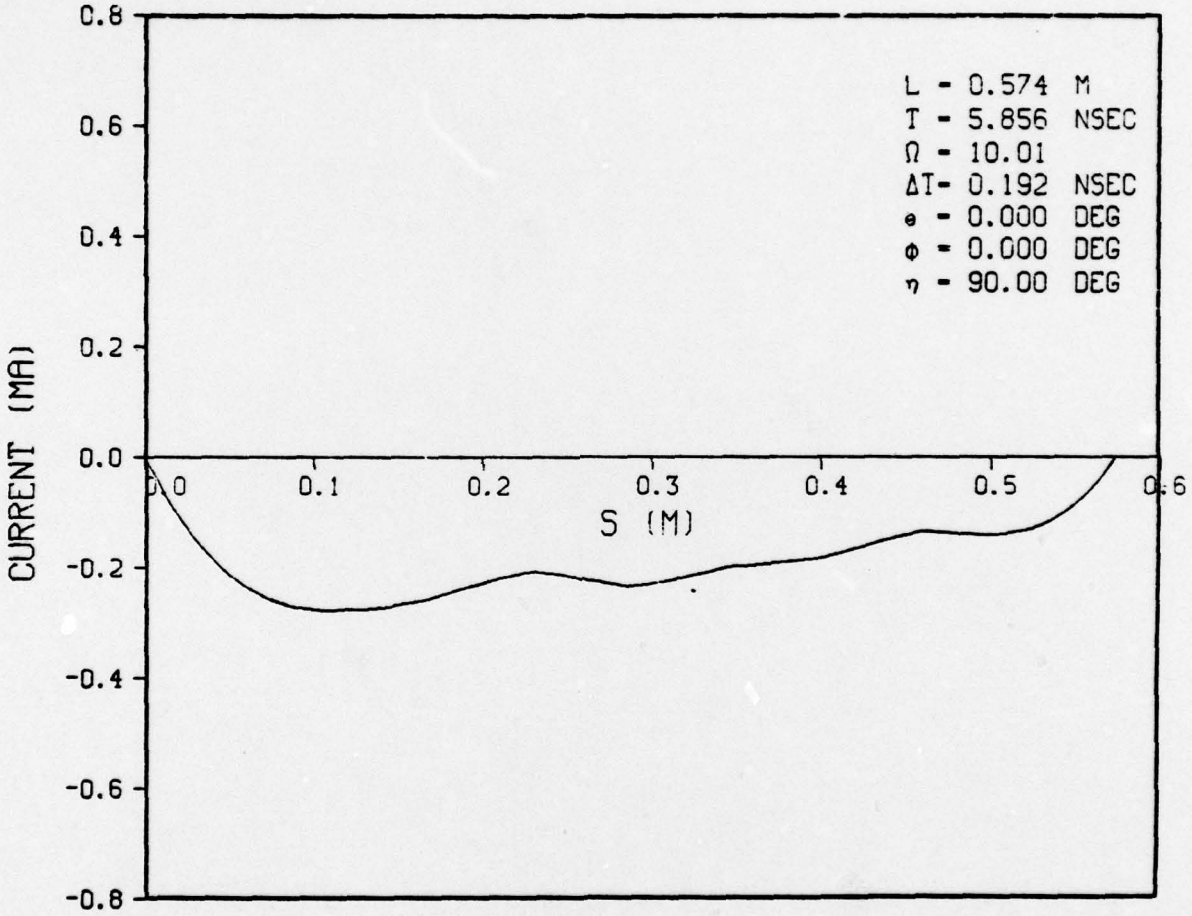

Figure 5-68. CURRENT DISTRIBUTION-RECTANGULAR PULSE

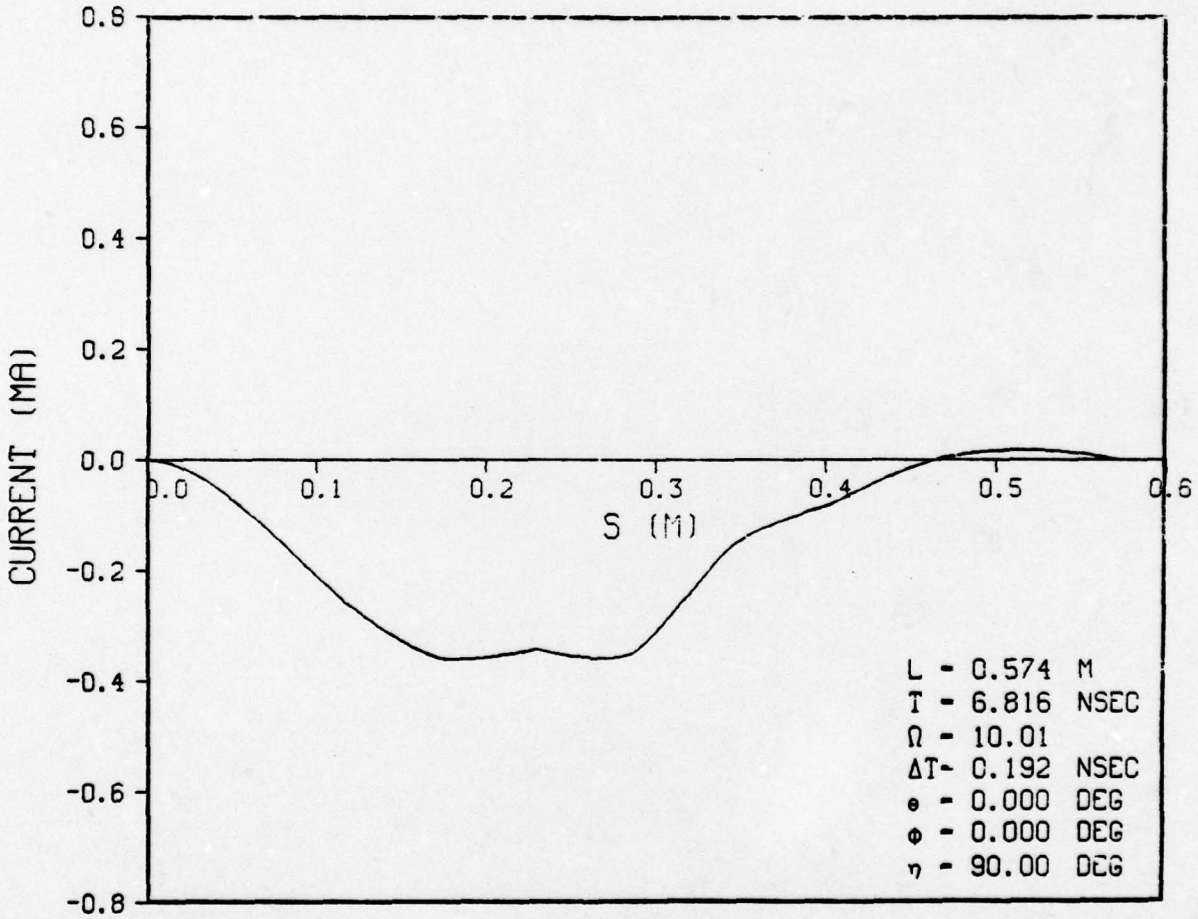

Figure 5-69. CURRENT DISTRIBUTION-RECTANGULAR PULSE

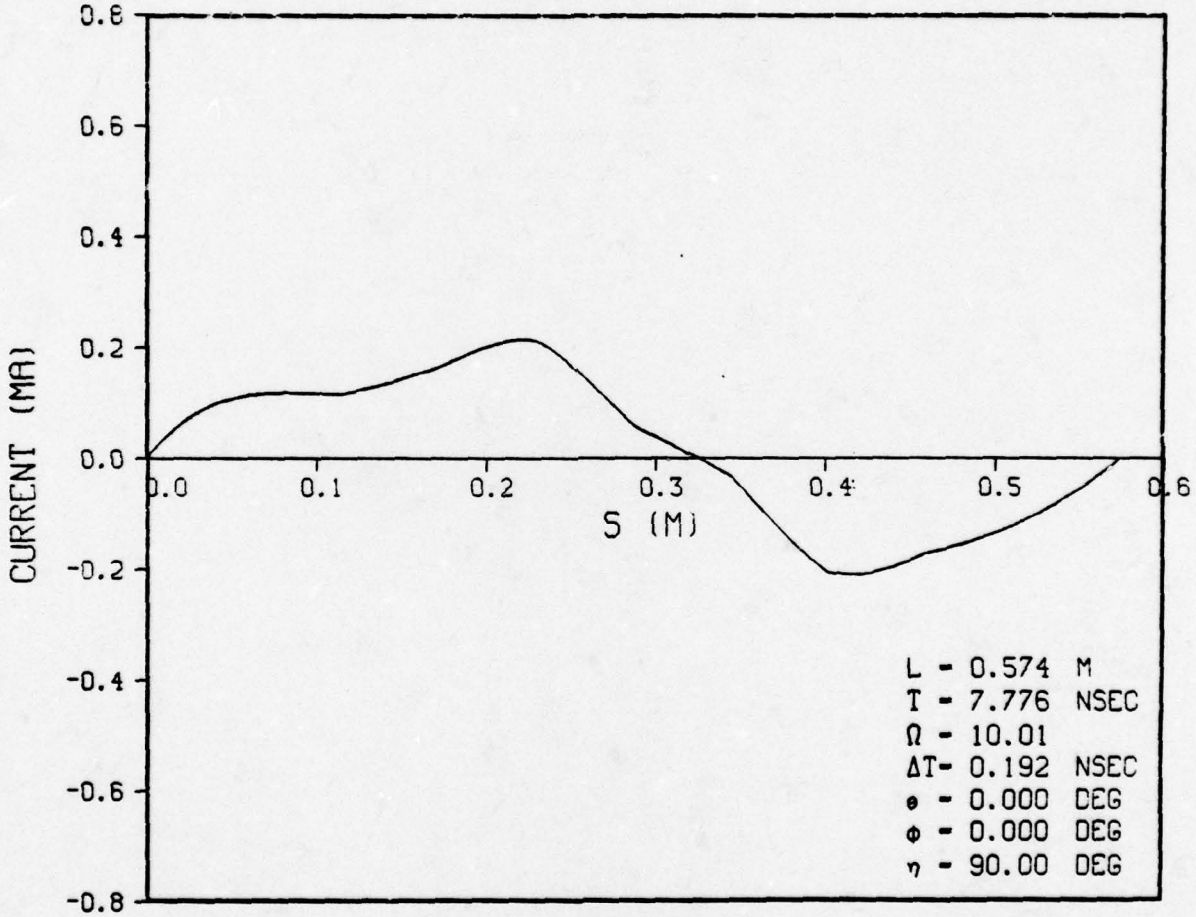

Figure 5-70. CURRENT DISTRIBUTION-RECTANGULAR PULSE

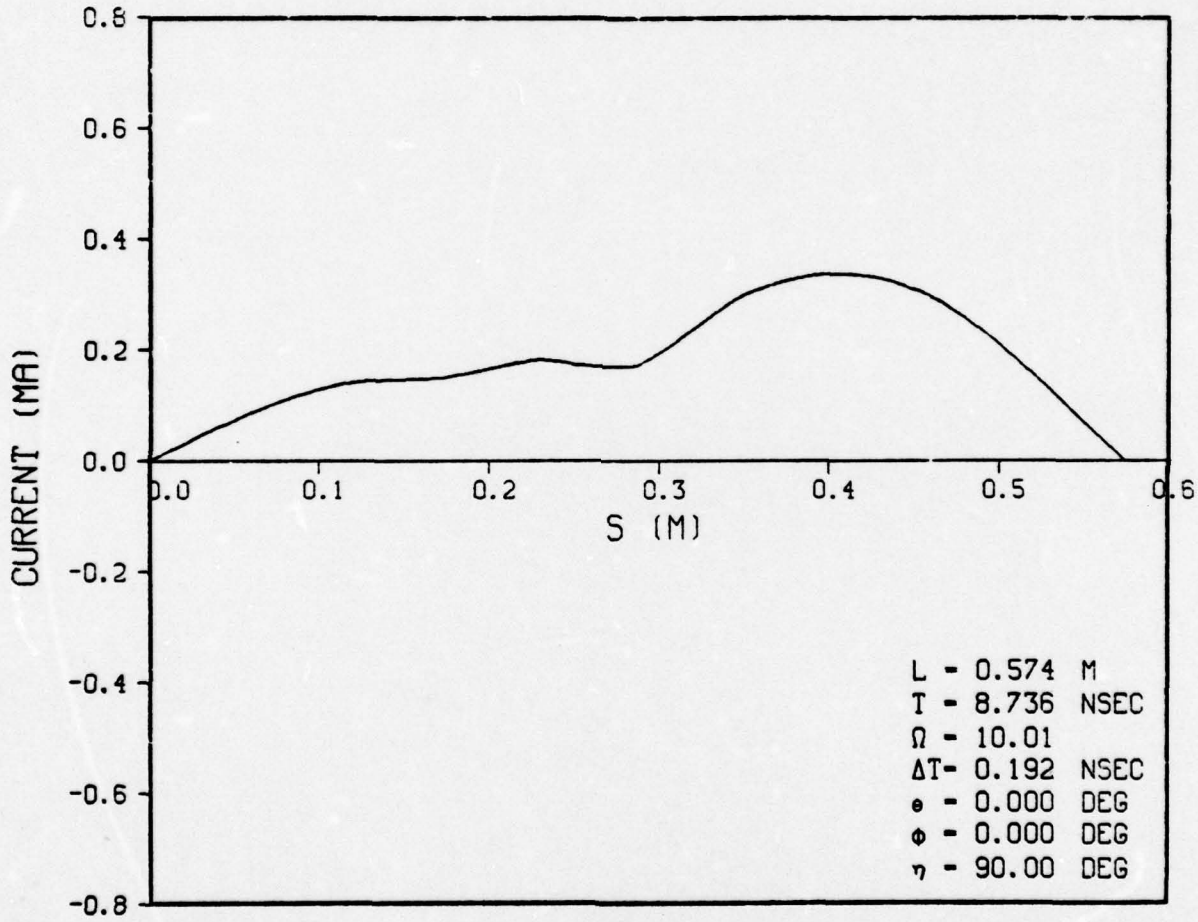

Figure 5-71. CURRENT DISTRIBUTION-RECTANGULAR PULSE

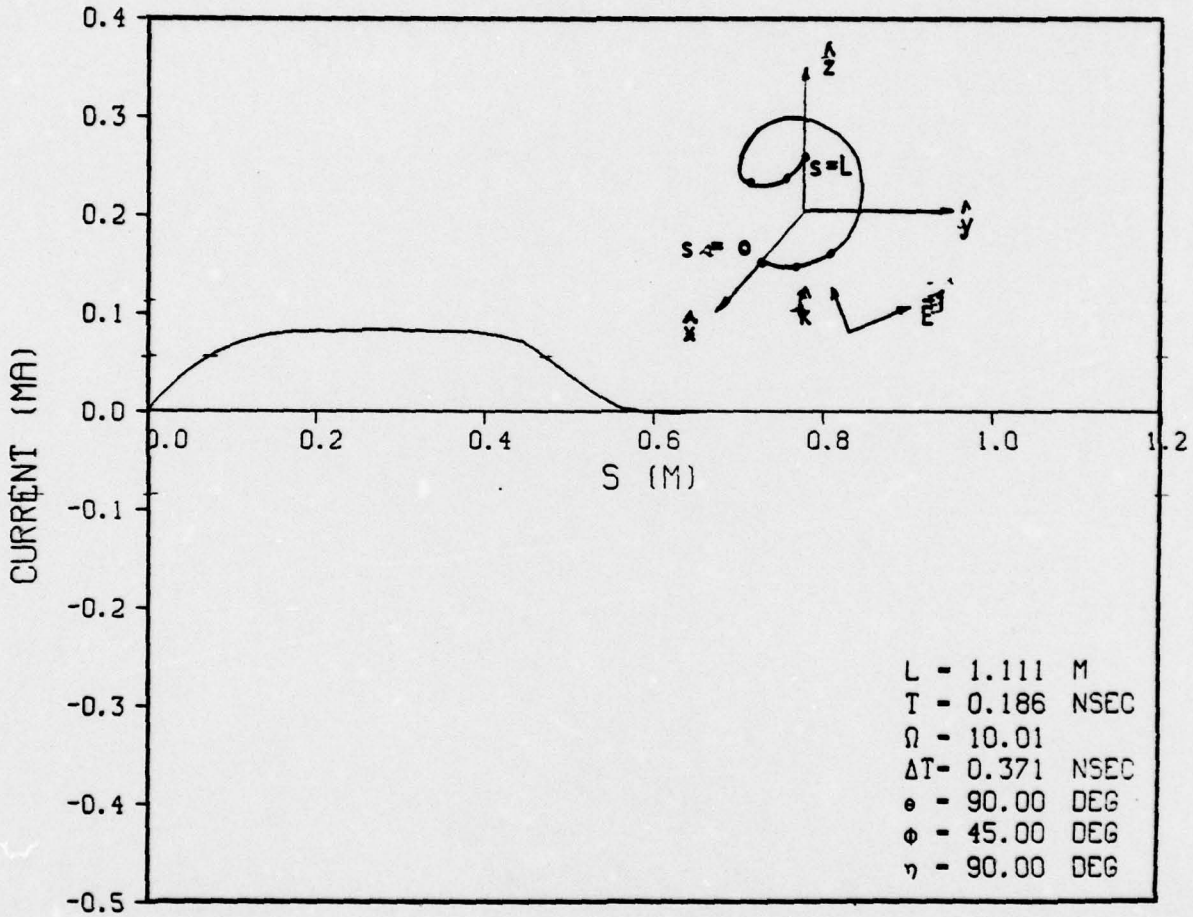

Figure 5-72. CURRENT DISTRIBUTION-GAUSSIAN PULSE

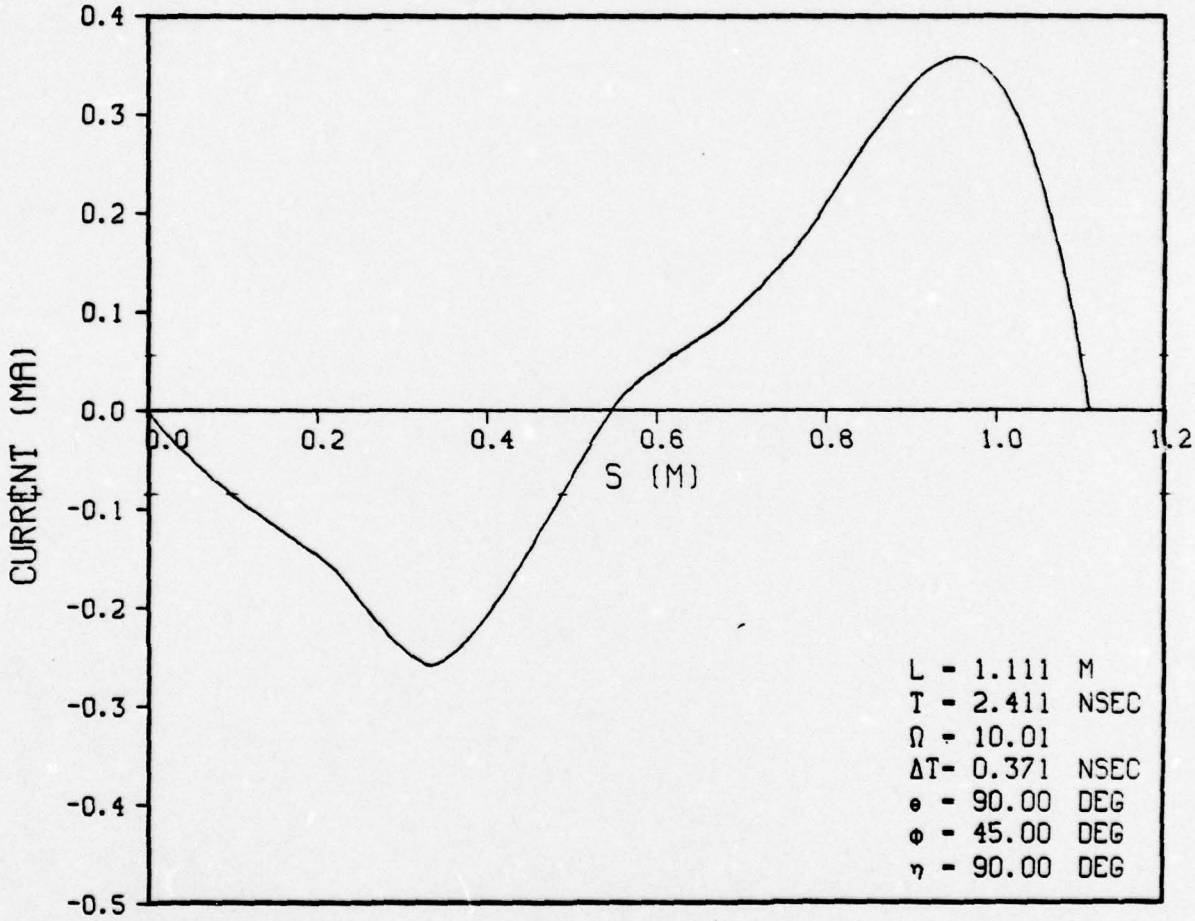

Figure 5-73. CURRENT DISTRIBUTION-GAUSSIAN PULSE

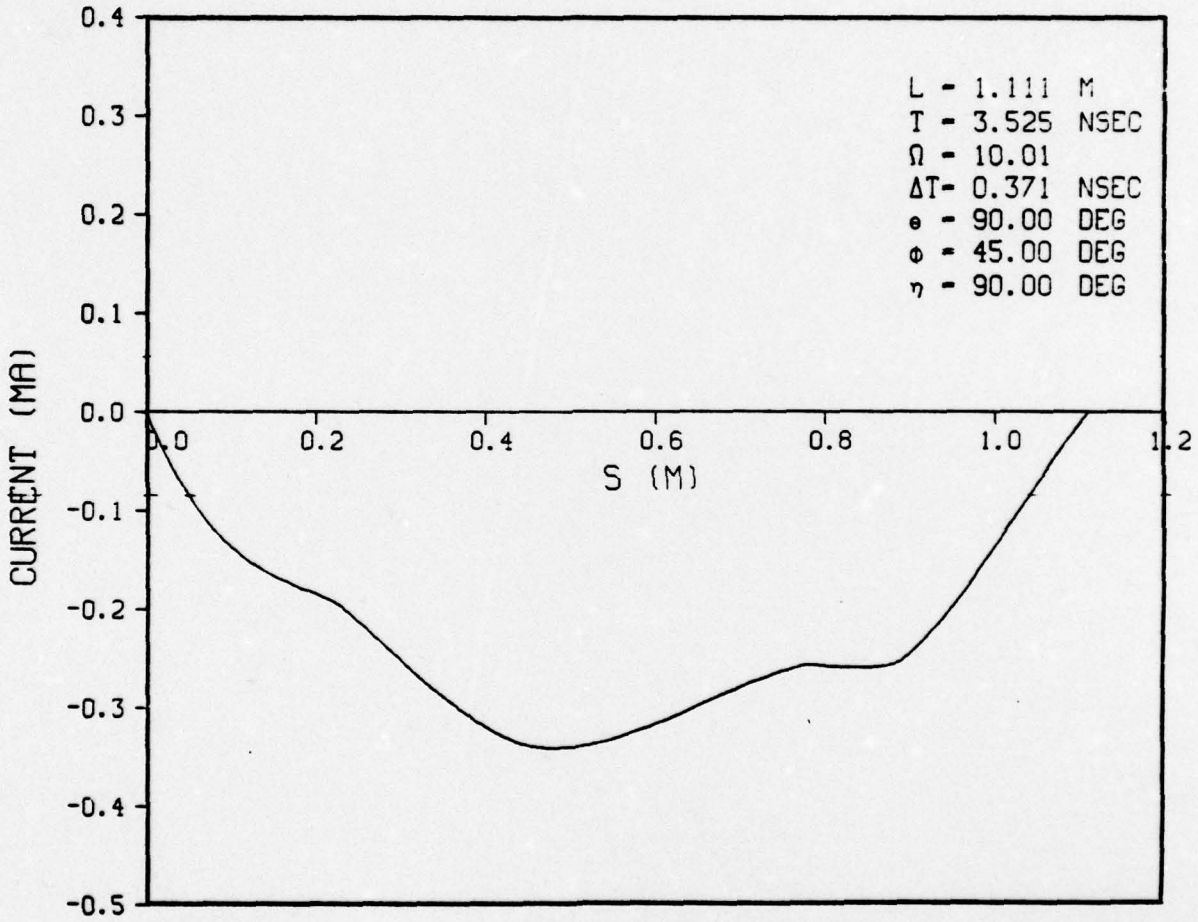

Figure 5-74. CURRENT DISTRIBUTION-GAUSSIAN PULSE

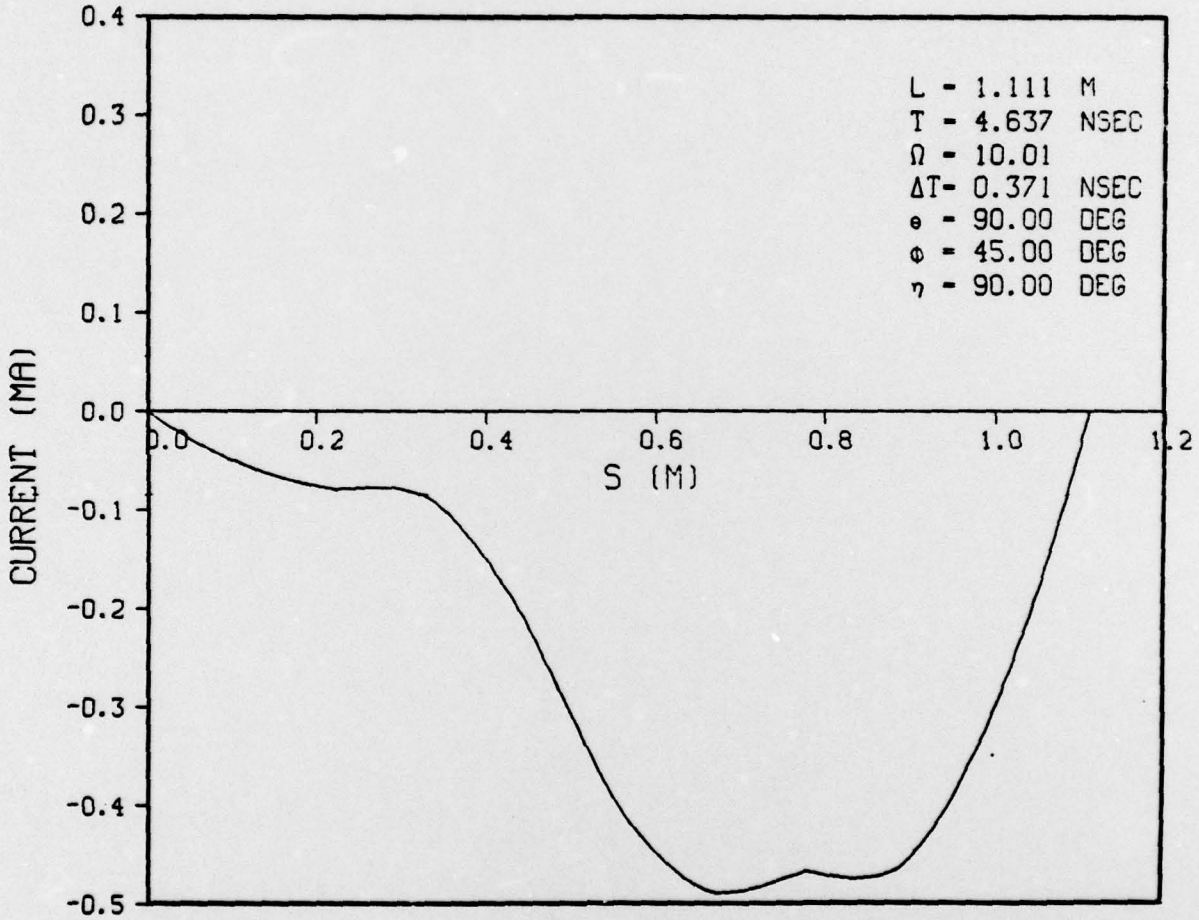

Figure 5-75. CURRENT DISTRIBUTION-GAUSSIAN PULSE

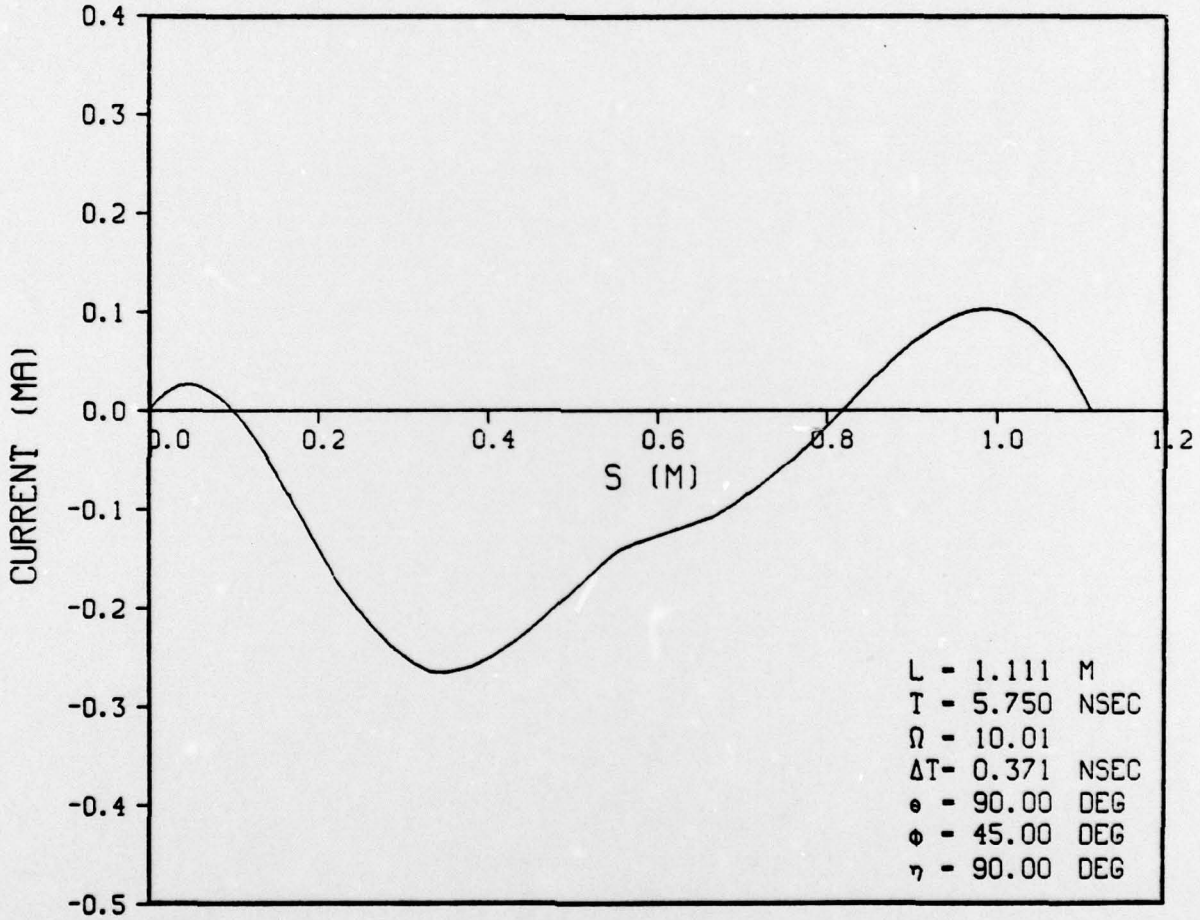

Figure 5-76. CURRENT DISTRIBUTION-GAUSSIAN PULSE

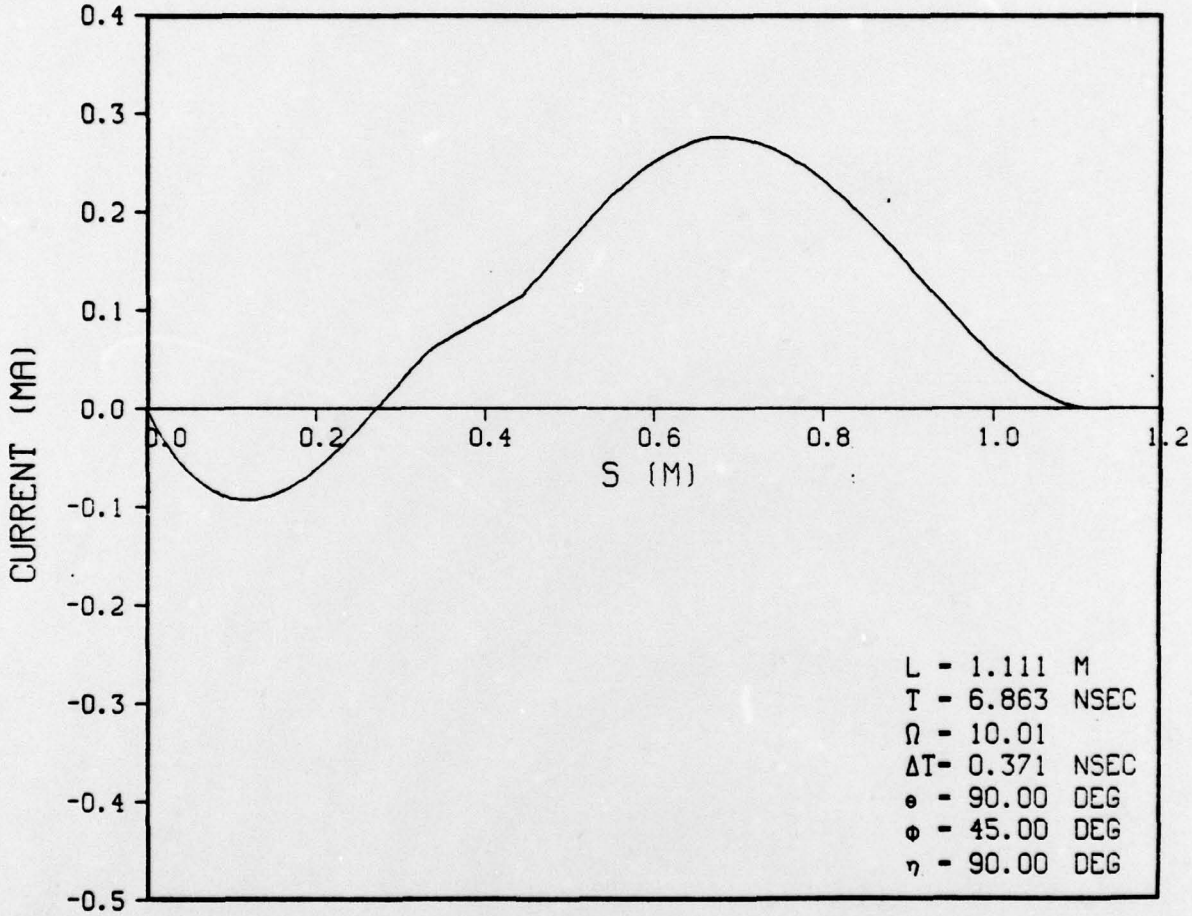

Figure 5-77. CURRENT DISTRIBUTION-GAUSSIAN PULSE

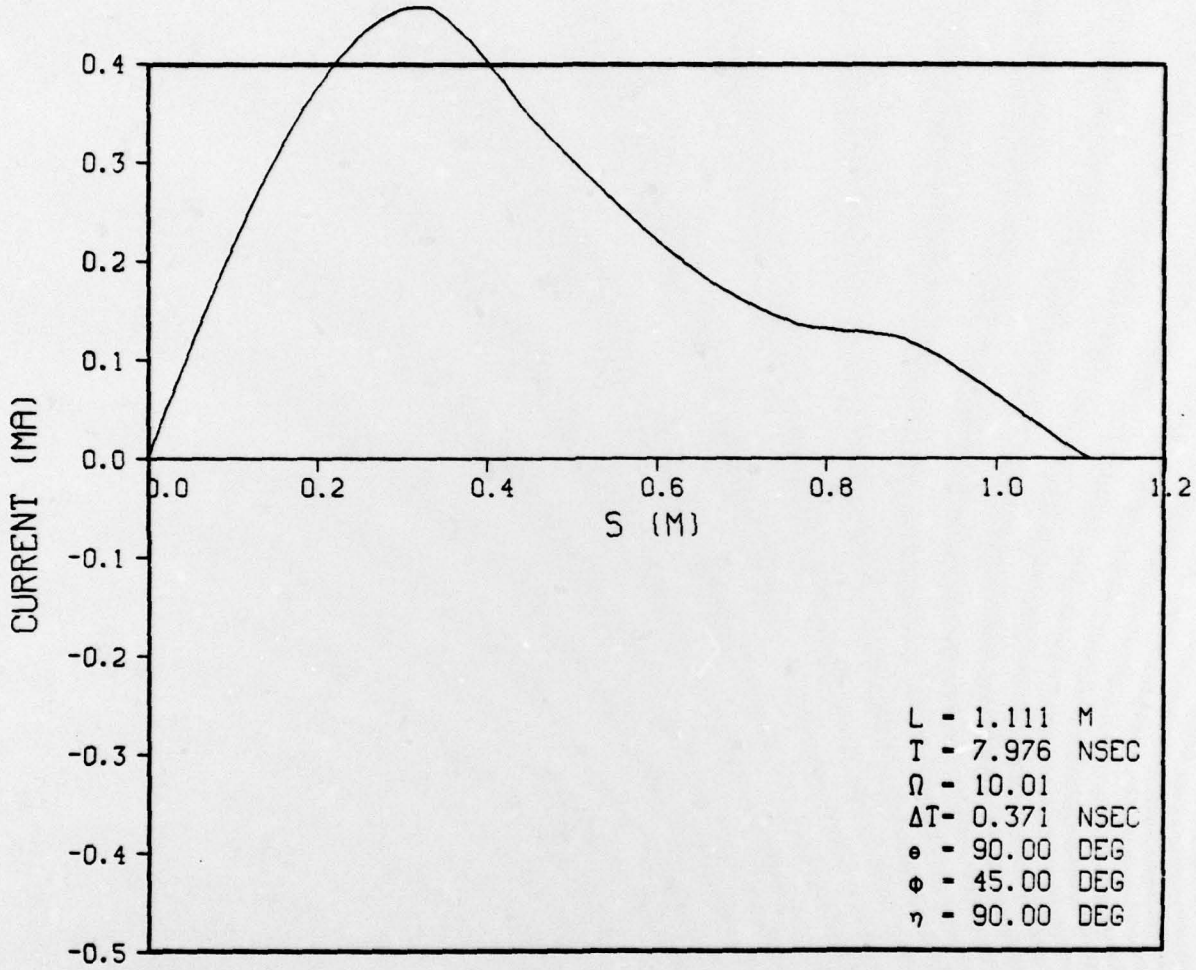

Figure 5-78. CURRENT DISTRIBUTION-GAUSSIAN PULSE

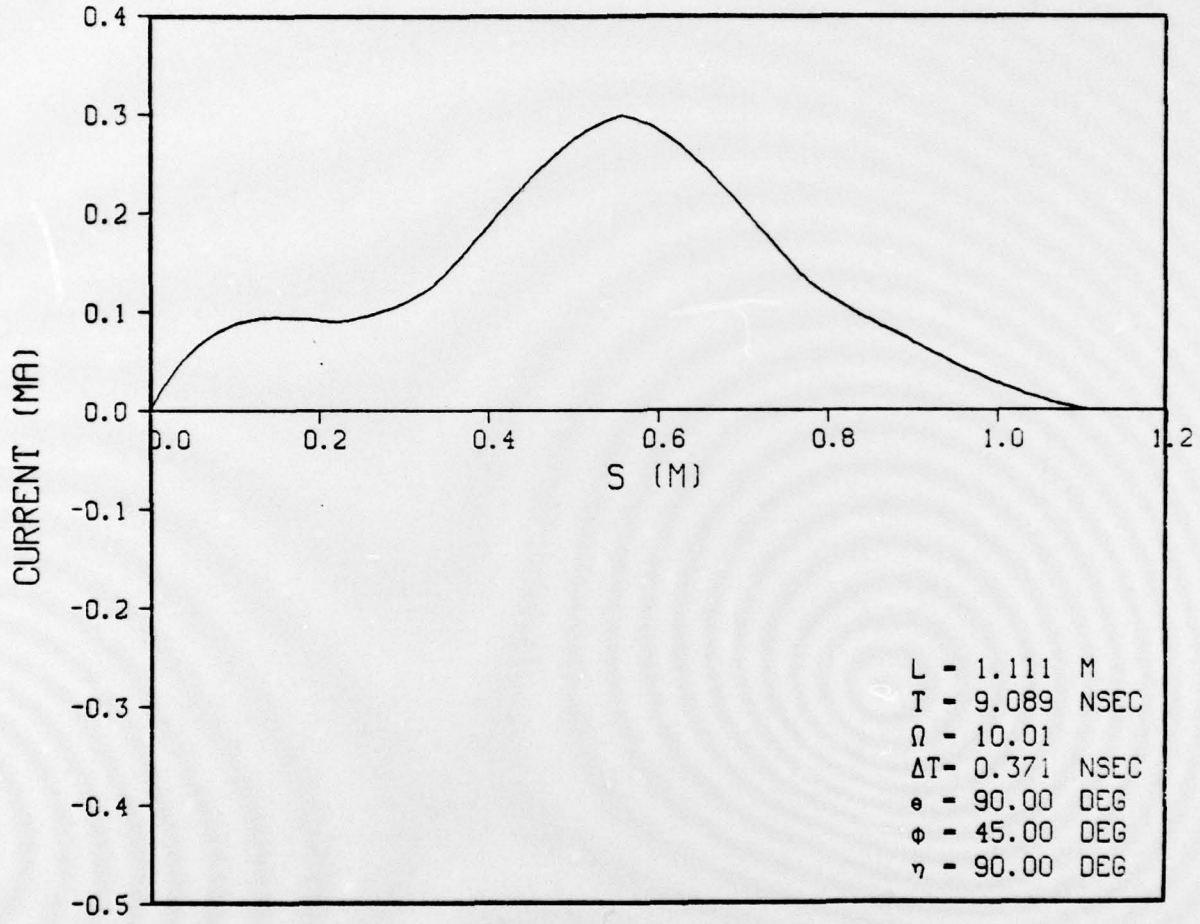

Figure 5-79. CURRENT DISTRIBUTION-GAUSSIAN PULSE

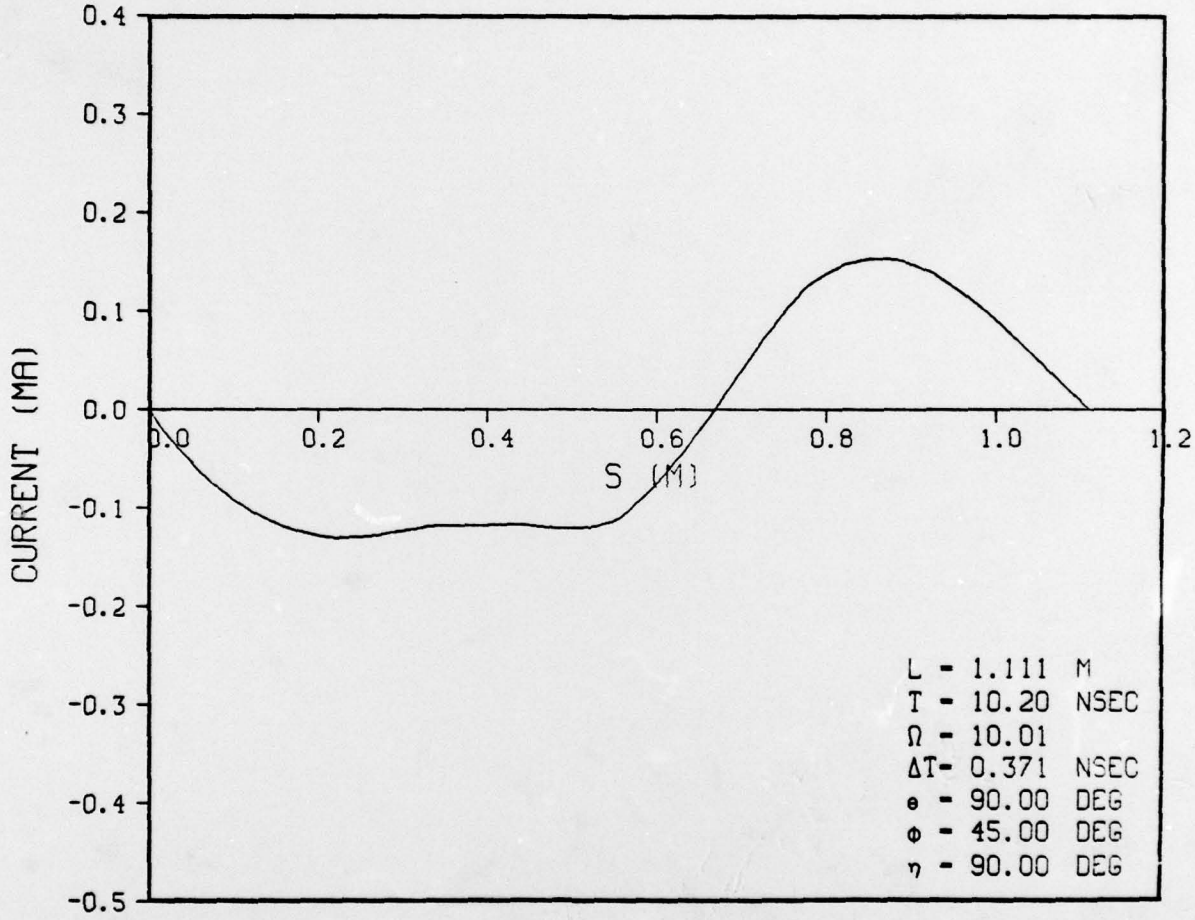

Figure 5-80. CURRENT DISTRIBUTION-GAUSSIAN PULSE

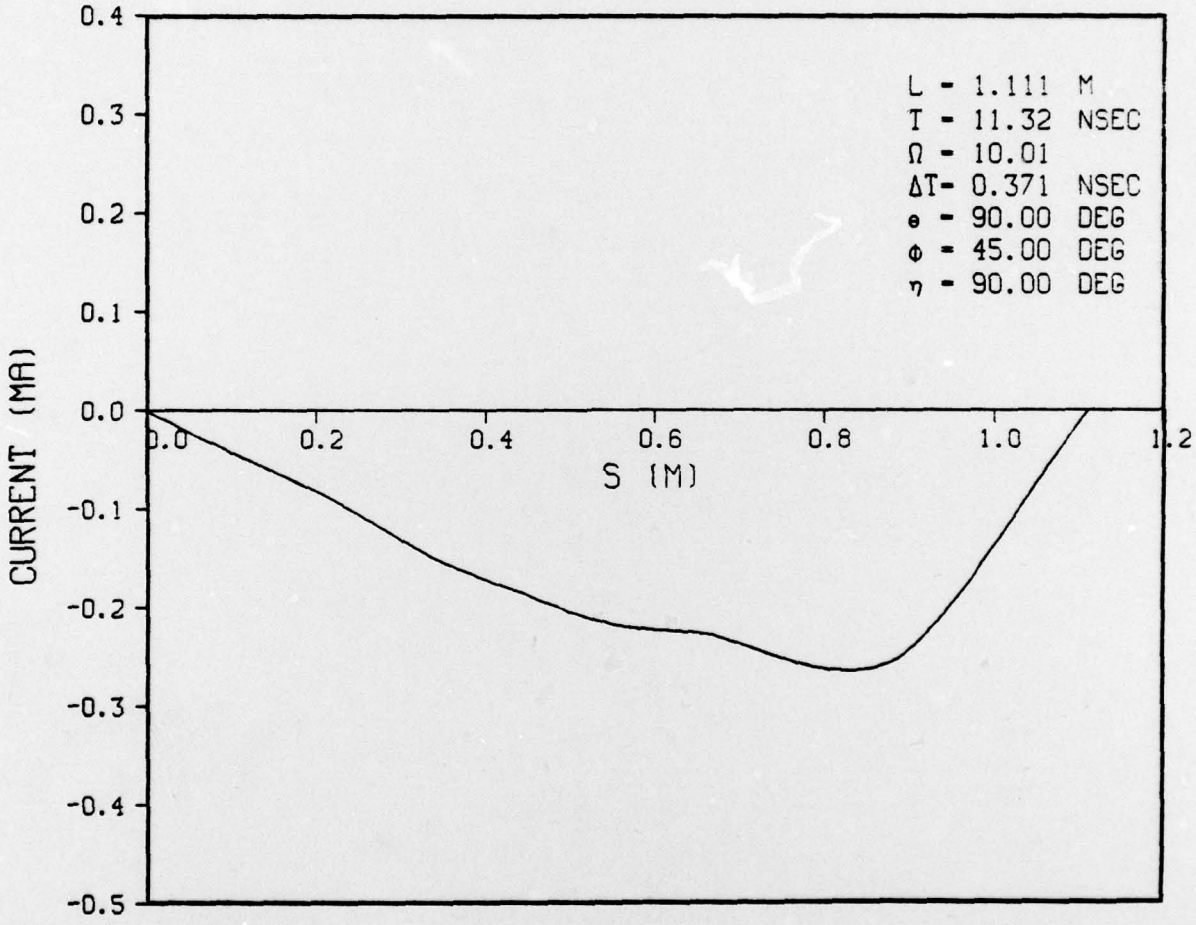

Figure 5-81. CURRENT DISTRIBUTION-GAUSSIAN PULSE

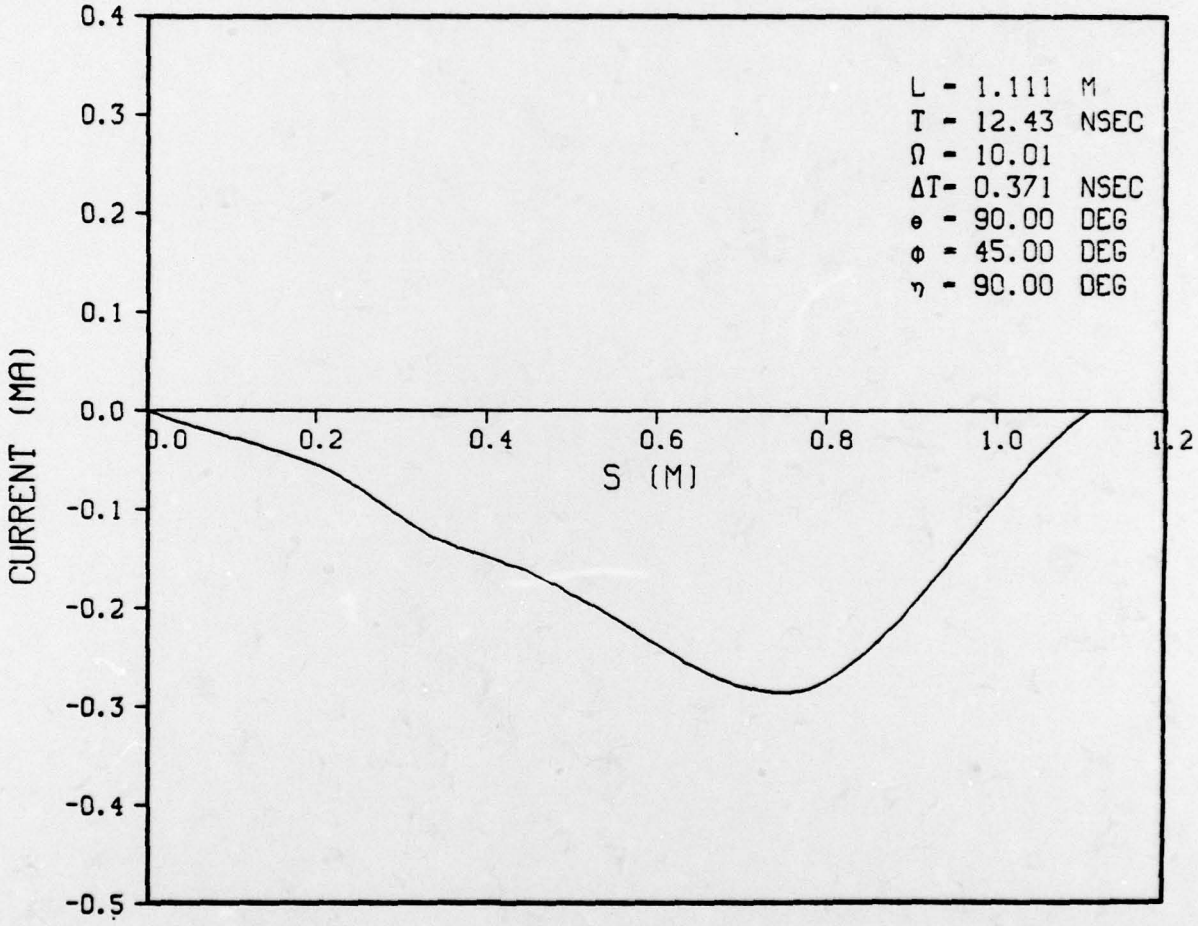

Figure 5-82. CURRENT DISTRIBUTION-GAUSSIAN PULSE

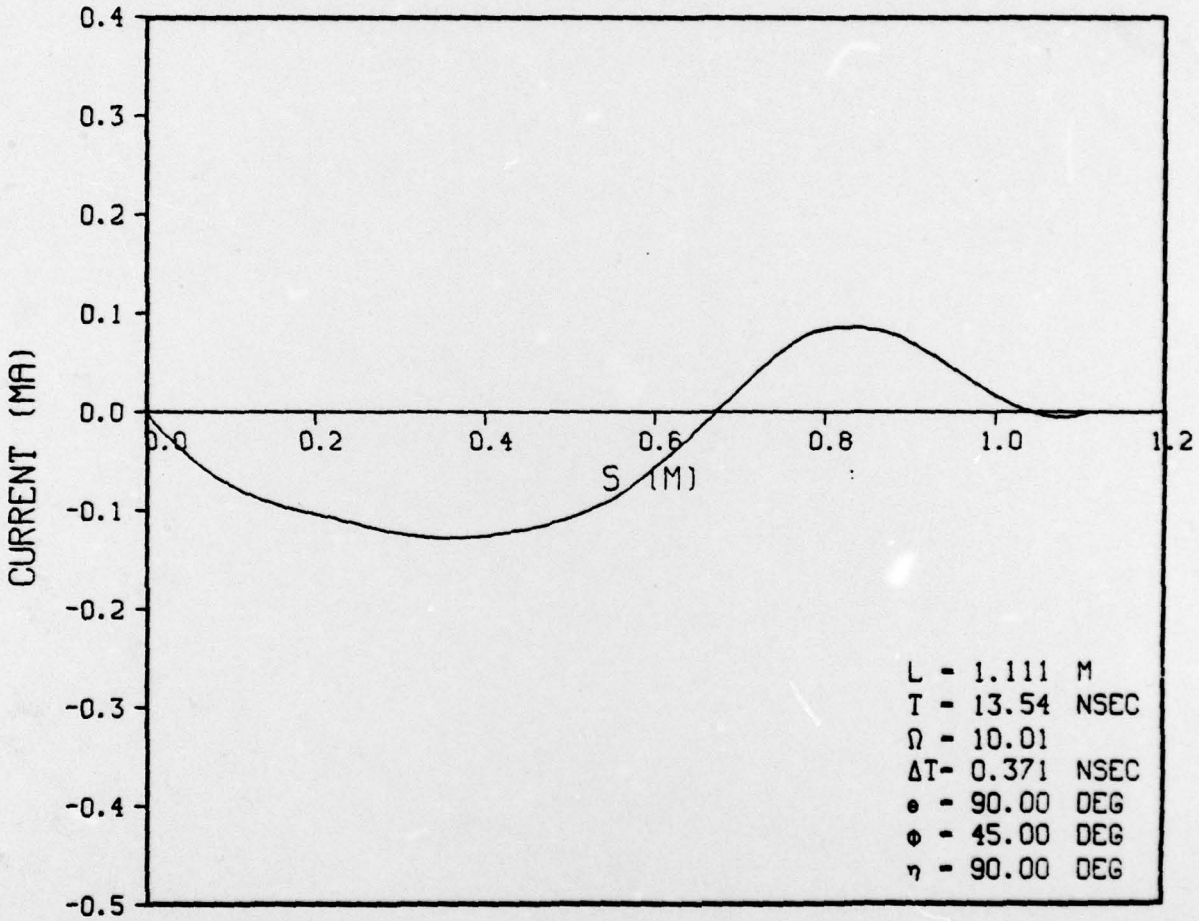

Figure 5-83. CURRENT DISTRIBUTION-GAUSSIAN PULSE

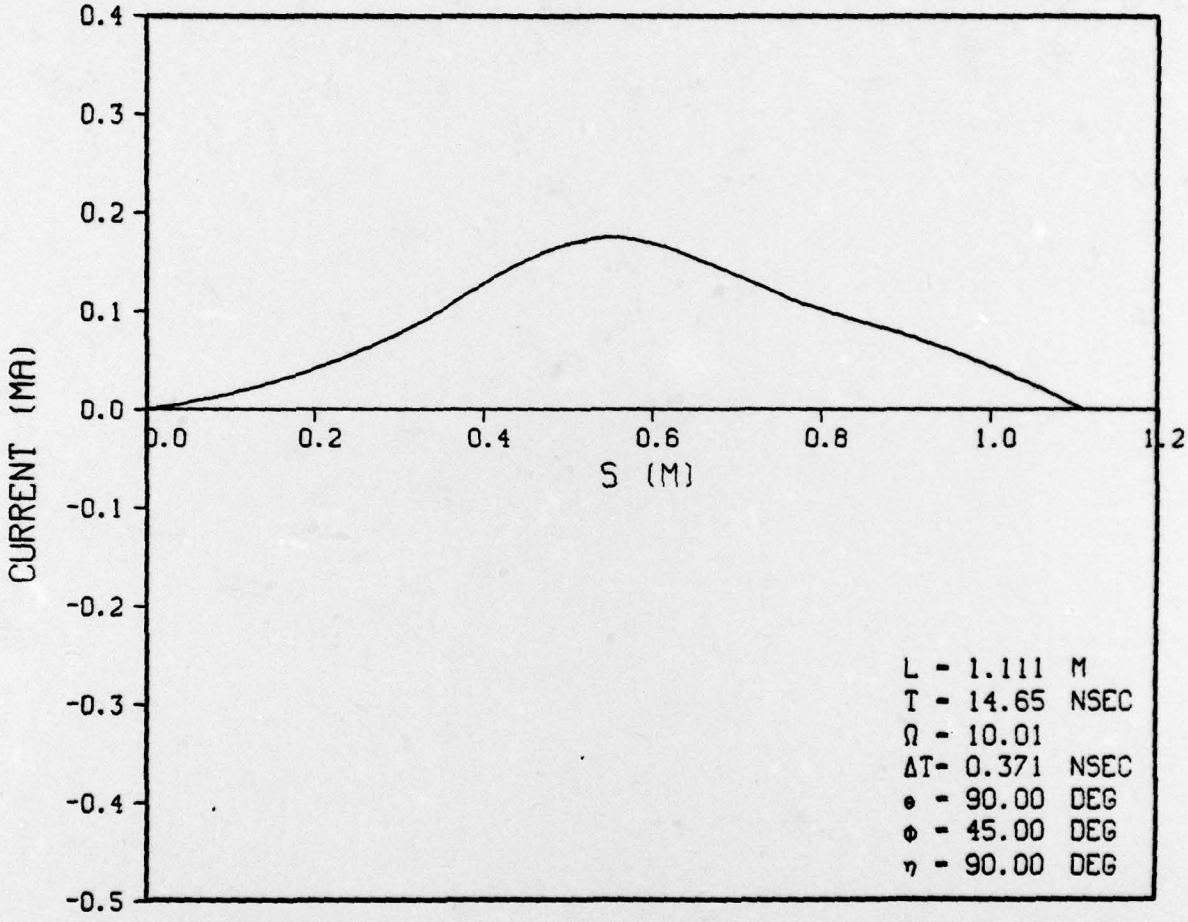

Figure 5-84. CURRENT DISTRIBUTION-GAUSSIAN PULSE

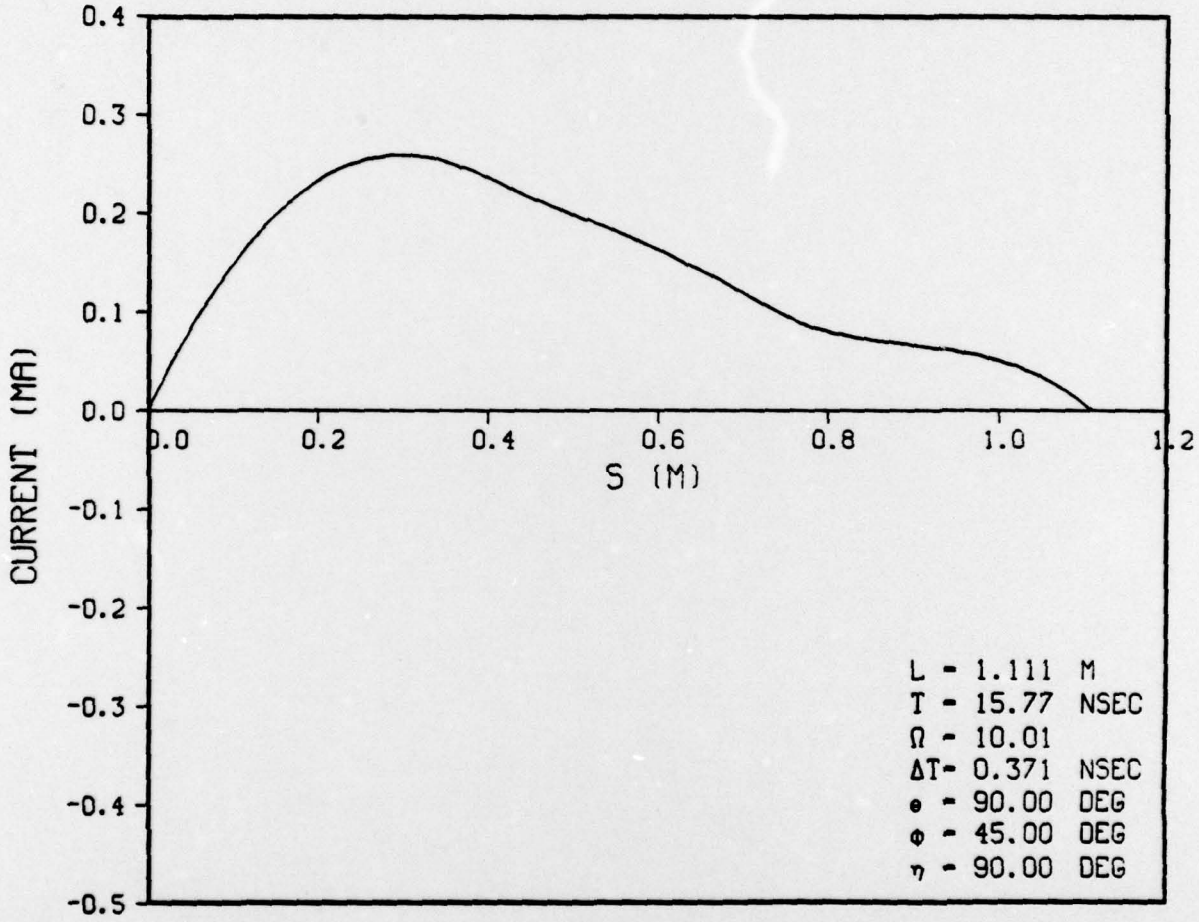

Figure 5-85. CURRENT DISTRIBUTION-GAUSSIAN PULSE

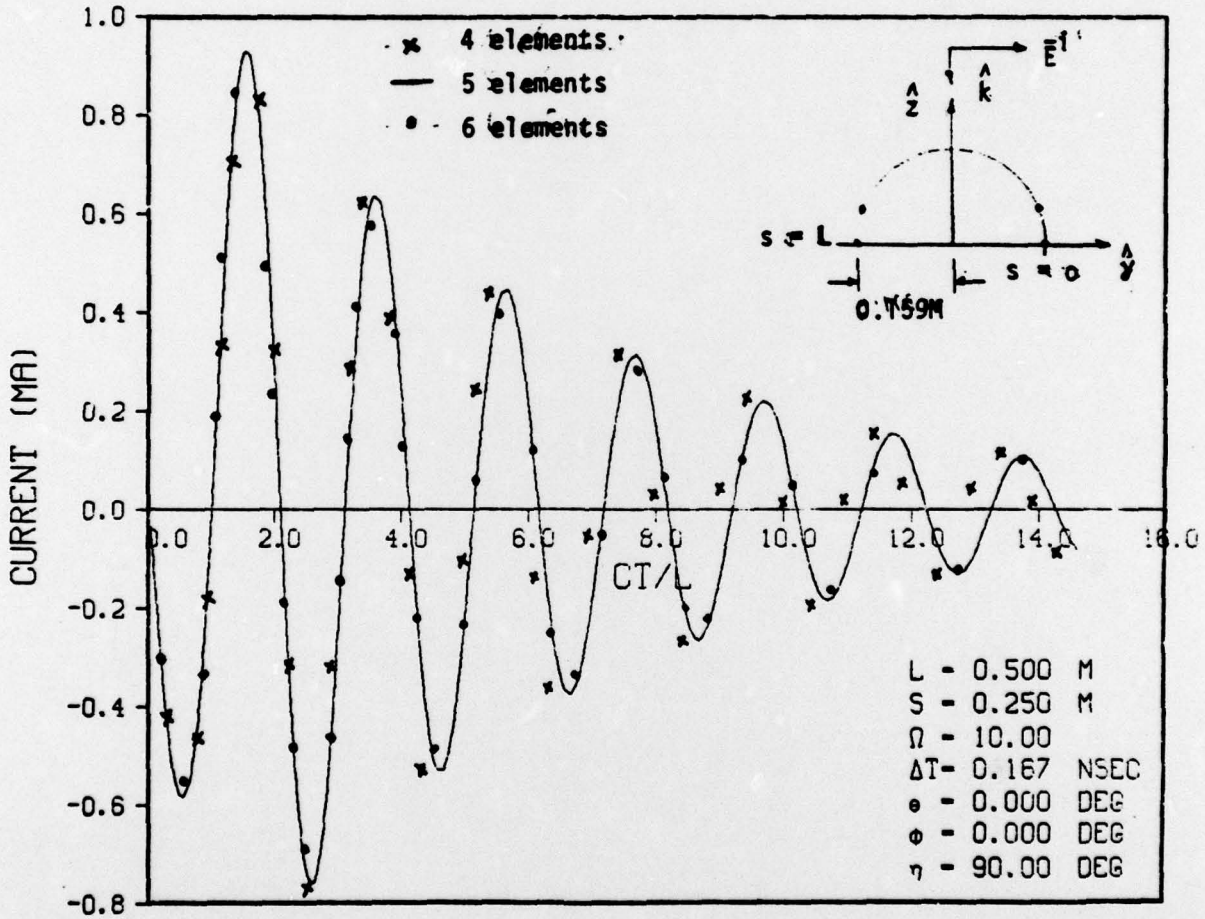

Figure 5-86. TRANSIENT CURRENT-GAUSSIAN PULSE

6. CONCLUSION

In this study the finite element method for electromagnetic techniques has been developed to solve transient scattering problems directly in the time domain. The problem is formulated in terms of a variational time-dependent integro-differential equation which is to be solved by a finite difference scheme in time and a finite element technique in space. Based on this approach a computer program is written to calculate the transient current on curved thin-wire scatterers when excited by an arbitrary plane wave pulse. Numerical results show good accuracy and convergence for the FEM approach. Thus, it transpires that the FEM can be a good numerical tool in solving transient electromagnetic problems. As a numerical method for solving electromagnetic scattering problems, the FEM offers the following advantages:

(1) Since the formulation is based on the variational principle, the solution is more stable and the error is minimized.

(2) Although the region is divided into finite elements, the whole domain remains as a continuum because of the imposed restriction on the continuity across element interfaces. This is contrary to the point-matching solution used in the method of moments where the true solution is valid only at the matching points in the whole domain.

(3) FEM approach is particularly useful in handling complex geometries.

In spite of its advantages, the FEM-based time-domain code developed here has two shortcomings from a numerical solution point of view. The shortcomings are:

(1) The mathematical and bookkeeping aspects of the FEM are involved, and

(2) The computational time seems to be longer as the code is not optimized.

It is therefore hoped that further research work in this area would alleviate these difficulties.

REFERENCES

[1] Wilson, E.L. and Nickell, R.E., "Application of Finite Element Method to Heat Conduction Analysis," Nucl. Eng. Des. 4 (1966) 1.

[2] Oden, T.J., "A General Theory of Finite Elements," Intl. J. Num. Methods 1 (1969) 247.

[3] Sankar, A. and Tong, T.C., "Current Computation on Complex Structures by Finite Element Method," Electronics Letters (London) 11 (1975) 481.

[4] Sankar, A. and Tong, T.C., "Current Computation by the Finite Element Method," NOSC Report. Performed under contract No. N00123-76-C-0729, APS/URSI Intl. Symposium Digest (1977).

[5] Melosh, R.J., "Basis of Derivatives of Matrices for Direct Stiffness Method," AIAA J. 1 (1963) 1631.

[6] Zienkiewicz, O.C., "The Finite Element Method in Engineering Science," McGraw Hill, London (1967).

[7] Irons, B., "Comments on Papers: Theoretical Foundations of the Finite Element Method," Int. J. Solids & Structures 6 (1970) 695.

[8] Landt, J.A. and Miller, E.K., "WT-MBA/LLL1B : A Computer Program for the Time Domain Electromagnetic Response of Thin Wire Structures," Lawrence Livermore Laboratory (1974).